

A Study into the Self-Assembly of Bioactive Peptide Amphiphiles

A thesis submitted for the degree of Doctor of Philosophy

Department of Chemistry

Steven Kirkham

November 2016

Declaration

I can confirm that this is my own work and the use of material from other sources has been properly and fully acknowledged.

Steven Kirkham

Acknowledgements

I would firstly like to thank Professor Ian Hamley for giving me the opportunity to do this PhD. From receiving my offer until submitting my thesis he has been a fantastic mentor and has enabled my PhD to be rewarding, productive and enjoyable. I would also like to thank Dr Valeria Castelletto for putting up with me bombarding her with questions every day, and her invaluable help and patience with me over the past three years. A massive thanks also goes to (now Dr) Ashkan Dehsorkhi who I took over from as the PhD student in Ian's lab. He set me up to cope with all of the new techniques and theories from going from a Bioscience background to a physical chemistry one, and was another who managed to put up with my daily barrage of questions. Thank you to Nick Spencer for help with x-ray techniques, but even more so for the catch-up football chats whenever I went down to the lab. I am grateful to Stan, Abdullah and Sarah for their help with the gel and cell studies, and Steve for his assistance when we visited ISIS for SANS. Emerson Da Silva for the help throughout his year in Reading, and the laughs he provided when we had beamtime. Thank you to all of the collaborators I have worked with over the past three years.

I would like to thank Sam for introducing me to squash, and for briefly making me think I had been calculating weight percentage wrong for two years. I would like to thank Jess for all her support and encouragement, and for making the final year of my PhD by far the best. Finally my mum, dad and brother for getting me this far and always being there for me.

Abstract

There are a vast array of different molecules which have shown the ability to self-assemble in solvent to form a range of nanostructures. Micelles are formed by surfactant-like molecules with hydrophobic and hydrophilic parts, and β -sheet fibrils are formed by peptide-based molecules. This self-assembly is driven through non-covalent interactions of the domains to form supramolecular assemblies. Peptide amphiphiles are one of these groups of self-assembling compounds. They can be purely peptidic (composed of hydrophobic and hydrophilic residues), or a combination of amino acids with hydrophobic lipid chains, hydrophilic polymers etc.

The first part of the thesis concerns three different lipopeptides comprised of the same peptide sequence attached to differing numbers of palmitoyl lipid chains. The compounds are found to form micellar or bilayer structures, with different morphology and secondary structure characteristics, which may explain their differing bioactivities. The second part leads on from this and investigated the comparison between the self-assembly of another lipopeptide and its constituent peptide. The peptide formed twisted tapes, compared with fascinating raft-like structures with the lipopeptide, which to our knowledge had not previously been seen before with this class of biomolecule. In chapter 4, a dipeptide attached to a bulky aromatic fluorophore is explored through its self-assembly, and cytotoxicity and cellular uptake. Large twisted nanotapes were observed above an experimentally determined aggregation concentration, and the compound was found to be non-toxic and taken up into perinuclear regions of cells. Chapter 5 describes the self-assembly properties of an antifungal compound, amphotericin B, at concentrations above an experimentally determined aggregation point. It was found that it had a time-dependent change in secondary structure and formation of a mixture of cylindrical micelles and very long twisting tapes. In chapter 6, the self-assembly of another drug, daptomycin, is examined with and without calcium ions. Calcium is believed to be necessary for assembly to occur. No differences were observed here however, with similar aggregation concentrations and structures formed in both conditions. The final chapter consists of a report on the self-assembly properties of three polymer-peptide conjugates with hydrophilic central blocks and hydrophobic tyrosine end-caps, as well as preliminary experiments into their cytocompatibility when incorporated into alginate-based hydrogels. They were shown to form fibrils with different morphologies and β -sheet content, and our study shows the effect on self-assembly of midblock length and polymer type.

Table of Contents

| | |
|--|----|
| Chapter 1 - Introduction | 1 |
| 1.1 Peptides..... | 1 |
| 1.1.1 Peptide self-assembly | 1 |
| 1.2 Peptide amphiphiles | 3 |
| 1.2.1 Peptide amphiphile self-assembly | 4 |
| 1.3 Lipopeptides..... | 8 |
| 1.3.1 Further uses of lipopeptides | 11 |
| 1.4 Toll-like receptor agonists..... | 11 |
| 1.4.1 TLR agonist agents in cancer treatment | 13 |
| 1.4.2 TLR agonist agents in non-cancer treatment | 14 |
| 1.5 Light, temperature and pH effect on PAs | 15 |
| 1.6 Hydrogels | 17 |
| 1.6.1 Natural and synthetic hydrogels | 18 |
| 1.6.2 Further applications of hydrogels | 21 |
| 1.6.3 Enzyme-responsive hydrogels..... | 22 |
| 1.6.4 Poly (ethylene glycol)-based hydrogels | 23 |
| 1.7 Methods of tagging in cell culture | 24 |
| 1.8 Aims..... | 25 |
| 1.9 References..... | 26 |

| | |
|---|----|
| Chapter 2 – The effect of lipid chain number on the self-assembly of Toll-like receptor agonist lipopeptides | 40 |
| 2.1 Introduction | 40 |
| 2.2 Materials & Methods | 43 |
| 2.2.1 Fluorescence Assays..... | 43 |
| 2.2.2 Circular Dichroism (CD) | 43 |
| 2.2.3 Small-Angle X-ray Scattering (SAXS)..... | 44 |
| 2.2.4 Cryo-Transmission electron microscopy (cryo-TEM) | 44 |
| 2.3 Results & Discussion..... | 45 |
| 2.4 References..... | 56 |
| | |
| Chapter 3 - Self-assembly of Macrophage-Activating Lipopeptide (MALP-2) | 59 |
| 3.1 Introduction | 59 |
| 3.2 Materials and methods | 61 |
| 3.2.1 Fluorescence Spectroscopy..... | 62 |
| 3.2.2 Fourier Transform Infra-Red (FTIR) Spectroscopy | 62 |
| 3.2.3 Circular Dichroism (CD) | 63 |
| 3.2.4 Small-Angle X-ray Scattering (SAXS)..... | 63 |
| 3.2.5 X-ray Diffraction (XRD) | 64 |
| 3.2.6 Cryogenic Transmission Electron Microscopy (Cryo-TEM) | 64 |
| 3.3 Results and discussion..... | 65 |
| 3.4 References..... | 75 |

| | |
|--|-----|
| Chapter 4 - Addition of dileucine motif to FITC fluorophore enables use in cell labelling | 78 |
| 4.1 Introduction | 78 |
| 4.2 Materials and methods | 81 |
| 4.2.1 Fluorescence Spectroscopy..... | 81 |
| 4.2.2 Circular Dichroism (CD) | 81 |
| 4.2.3 Fourier Transform Infra-red (FTIR) spectroscopy..... | 82 |
| 4.2.4 Cryo-Transmission electron microscopy (cryo-TEM) | 82 |
| 4.2.5 Human fibroblast cell culturing and cell viability and uptake assays..... | 83 |
| 4.3 Results and discussion..... | 84 |
| 4.3.1 Self-assembly studies | 84 |
| 4.3.2 Cell viability and compatibility studies..... | 89 |
| 4.4 References..... | 96 |
| | |
| Chapter 5- The self-assembly of commercially available anti-fungal drug Amphotericin B | 99 |
| 5.1 Introduction | 99 |
| 5.2 Materials and methods | 102 |
| 5.2.1 Pyrene fluorescence..... | 103 |
| 5.2.2 Cryo-TEM..... | 103 |
| 5.2.3 Small-angle X-ray scattering (SAXS) | 103 |
| 5.2.4 Circular Dichroism (CD) | 104 |
| 5.2.5 Fourier transform infrared spectroscopy (FTIR) | 104 |
| 5.2.6 Two-photon fluorescence lifetime imaging | 104 |

| | |
|--|------------|
| 5.3 Results and discussion..... | 105 |
| 5.4 References..... | 116 |
| | |
| Chapter 6 - Self-assembly of daptomycin, and comparison with and without calcium chloride | |
| | 119 |
| 6.1 Introduction | 119 |
| 6.2 Materials & Methods | 121 |
| 6.2.1 Fluorescence Assays..... | 122 |
| 6.2.2 Cryo-Transmission electron microscopy (cryo-TEM) | 122 |
| 6.2.3 Circular Dichroism (CD) | 122 |
| 6.2.4 Small-Angle X-ray Scattering (SAXS)..... | 123 |
| 6.2.5 Fourier transform infrared spectroscopy (FTIR) | 123 |
| 6.3 Results and discussion..... | 124 |
| 6.4 References..... | 134 |
| | |
| Chapter 7 - Self-assembly of custom-synthesised telechelic conjugates with | |
| PEO/poly(alanine) central blocks | 137 |
| 7.1 Introduction | 137 |
| 7.2 Materials & Methods | 139 |
| 7.2.1 NMR and FTIR Spectroscopy | 139 |
| 7.2.2 Sample Preparation..... | 140 |
| 7.2.3 Circular Dichroism (CD) | 140 |

| | |
|--|------------|
| 7.2.4 Fourier transform infrared spectroscopy (FTIR) | 140 |
| 7.2.5 X-ray Diffraction (XRD) | 141 |
| 7.2.6 Cryo-Transmission electron microscopy (cryo-TEM) | 141 |
| 7.2.7 Small-Angle X-ray Scattering (SAXS)..... | 142 |
| 7.2.8 Alginate hydrogel protocol..... | 142 |
| 7.3 Results and discussion..... | 143 |
| 7.4 References..... | 157 |
| | |
| Chapter 8 - General conclusions and future work..... | 162 |
| 8.1 References..... | 167 |
| List of publications | 168 |

Chapter 1 - Introduction

1.1 Peptides

Peptides consist of chains of two or more amino acids linked through covalent peptide bonds. These polypeptide chains are formed through reaction of the carboxyl group of one amino acid residue with the amine group of another. Literature varies in the exact number of residues, but a peptide is deemed to become classified as a protein when the number of monomers in the chain increases past a threshold of around 50 [1]. Polypeptide chains consist of the main body of repeating amino acids, the backbone, and branches consisting of differing residues [1]. There are 22 different amino acids found in organisms, with 20 of those split into essential and non-essential amino acids. The former includes 9 amino acids which humans are unable to synthesise naturally, and so which need to be ingested through diet. The non-essential amino acids are able to be synthesised by the human body, and the final two which do not fit into either category, selenocysteine and pyrrolysine, are produced through unique mechanisms [2]. There are also many other amino acids that have been discovered [3], however, they are unable to be incorporated into peptide chains. The names of the amino acids can be shortened to either one, or three letter abbreviations, to describe the sequence of peptides. Their variability in side chains is what differentiates them, and categories can be formed based on these side chain differences. These include hydrophobic, hydrophilic, aliphatic, aromatic, and based on charge; positive, negative or neutral.

1.1.1 Peptide self-assembly

Peptides have the ability to self-assemble into nanostructures based on the presence of different amino acids, and which order they are in. The primary structure is based on the sequence of the amino acids in the chain, which has an effect on the secondary structure,

formed from the polar carboxyl and amine groups binding through hydrogen bonds to other peptide chains [1]. Tertiary structure is similar to secondary structure in the sense that it is from interactions between chains, but differs through inclusion of non-covalent interactions, such as van der Waals forces and hydrogen bonding [1]. These self-assembling peptides can be used in the field of medicine, such as in drug delivery systems, or they can be harmful, for example as amyloid fibrils, a hallmark of Alzheimer's disease. This self-assembly can be due to the hydrophobic/hydrophilic nature of the peptide, as well as the charge of the amino acids. The β -sheet is a common secondary structure which arises from peptide self-assembly. It can be present in one of two forms, parallel and antiparallel, shown in figure 1. Antiparallel has been shown to be the most common form, which is explained through the higher stability compared to the parallel form [4]. β -sheets then may further assemble into nanotubes with a hollow centre, nanofibrils with a solid core, and tapes, among other structures [5].

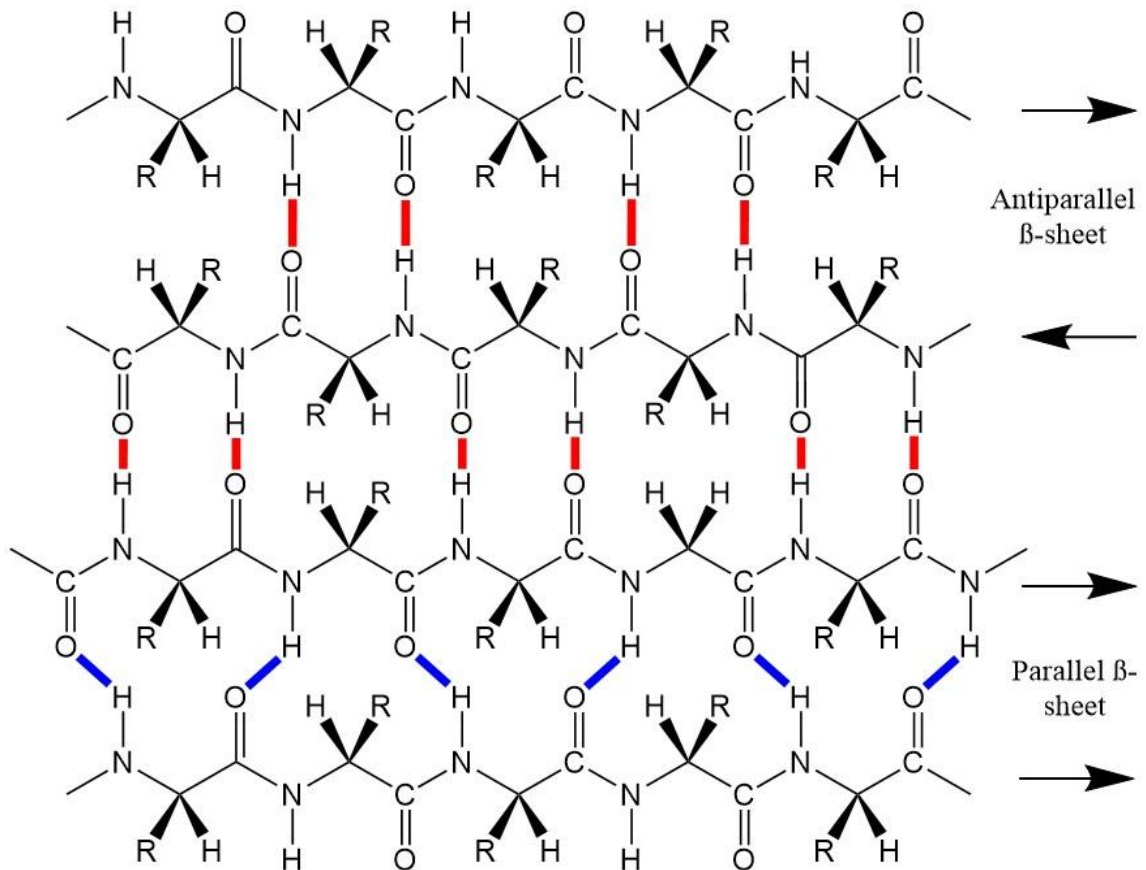


Figure 1 β -sheet structure and orientations. Red and blue lines show hydrogen bonding.

1.2 Peptide amphiphiles

Peptide amphiphiles (PAs) are compounds which have both hydrophilic and hydrophobic properties as a consequence of the presence of a lipid chain and order and binding of their amino acids. Their structure can be broken down into distinct parts, shown in figure 2. The first of these is a hydrophobic section, commonly a long alkyl tail. The second is a small chain of amino acids which gives rise to hydrogen bonding within the peptide. The third area is comprised of charged residues which increase the solubility of the peptide in water. Finally the fourth section is hydrophilic in nature and gives the peptide the ability to communicate with cells or other peptides and proteins [6, 7].

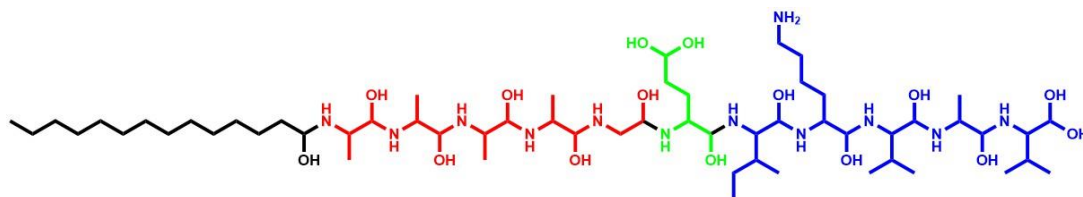


Figure 2 The different domains which make up a PA molecule; hydrophobic tail in black, β -sheet forming segment in red, charged groups in green, and bioactive epitope in blue. Adapted from [6].

Similar to other amphiphilic molecules, peptide amphiphiles also aggregate above a certain concentration threshold, the critical aggregation concentration (CAC). Fluorescence methods can be used to detect this point. Pyrene is a probe which fluoresces when in a hydrophobic environment, making it appropriate for use in determining the CAC of a range of amphiphiles [8, 9], including peptide amphiphiles [10, 11]. Another similar method is through use of Thioflavin T, which is able to detect CAC in amyloid-like structure, or β -sheet forming, peptides [12, 13]. The CAC of lipopeptides is also discoverable using this method [14-16]. 8-Anilino-naphthalene-1-sulfonic acid (ANS) is another compound used as a fluorescing molecular probe. One paper lists a number of different types of substance with which it has been used to show the CAC of [17], including protein aggregation and fibril formation [18].

1.2.1 Peptide amphiphile self-assembly

The self-assembly of peptide amphiphiles is driven through interactions of at least three of the sections shown in figure 2; interaction between hydrophobic tails, hydrogen bonding between the central peptide section, and electrostatic repulsions from the charged amino acids [6]. The ultimate structure formed through self-assembly is a balance between these three forces. Through molecular simulations, it was shown that a “pure” hydrophobic interaction would lead to formation of fine sized micelles, whereas a “pure” hydrogen bonding system would

lead to formation of a broad distribution of β -sheets [19]. In a system with relatively weak hydrogen bonding, spherical micelles are the dominant species, with β -sheets interspersed. Upon increasing hydrogen bonding, the spherical micelles are destabilised, leading to long cylindrical fibres [19]. The importance of amino acids in the peptide chain on self-assembly was also investigated [20]. Using a number of different modified PAs, this group found that the four amino acids present nearest to the nanofiber core were responsible for the hydrogen bond-forming β -sheets. Conversely, the amino acids further away from the core were found to be less important in stabilising the structure. If the hydrogen bonding of these four was disrupted, so too was the β -sheet formation, instead leading to the formation of spherical micelles. This implies that they are the most important amino acids in a self-assembled structure.

Surfactant-like peptides (SLPs) are an example of PA molecules which consist of a hydrophobic tail of at least four successive hydrophobic residues, with at least two charged residues forming the headgroup [7]. They have the ability to self-assemble due to their amphiphilic nature, which, when in aqueous solution, will generally lead to the hydrophobic tails grouping on the inside of the structure. This causes the hydrophilic headgroups to face outwards [6]. These headgroups often contain the epitope, the section of the peptide which interacts with other proteins and cellular components, and so the self-assembly is important for the functionality of the peptide [6]. Another structure which can be formed by self-assembly is the β -sheet, which is formed through an alternating pattern of hydrophobic and hydrophilic residues creating a sheet with one hydrophobic, and one hydrophilic side [21]. Self-assembly can lead to the formation of nanotubes, nanovesicles [22], sheets [23], and other structures, such as peptide bilayers [7]. In order for the structures to form, which is important in the design of PA molecules for therapeutic use, there must be a correct balance of hydrophobicity and hydrophilicity. Too much of the former will lead to the peptide precipitating out, whereas

too much of the latter will lead to dissolution, neither of which will lead to the formation of a nanostructure [23].

The ability of the molecules to assemble so that the epitopes are presented on the outside of the nanostructure, along with the biocompatibility that the hydrophobic tail provides, means that PA molecules can be exploited for medical purposes. They can be used as a drug delivery system, with the hydrophobic tail providing entry into the cell, and the epitope interacting with the target cellular component or protein to form a complex [24]. Their use in wound healing has also been proposed due to their ability to form sheets with bioactive epitopes presented at the surface [23, 25]. With a size on the nano-scale range, the PA molecules do sacrifice some drug delivery capacity compared with liposomes, but gain the ability to cross over cell membranes more easily [25]. There are further advantages, which include a lowered risk of being cleared from the body, and a higher surface area to volume ratio, giving higher solubility. However, smaller particle size has also been shown to result in a shorter circulation time, leading to the belief that 10-100 nm is the ideal diameter for drug delivery systems [1, 25].

The hydrophobic tail is vitally important in PAs as it contributes to the amphiphilicity of the molecule, thus allowing it to self-assemble. This causes the tails to sequester on the inside of the self-assembled structure, thus exposing the hydrophilic section on the outside. This is important when designing PAs to be used in a variety of purposes which require interaction from the bioactive epitope. The length of the alkyl chain has been found to be important in modulating self-assembly, and in the liability of being influenced by environmental factors [26]. The Stupp group used a molecule with a peptide sequence CCCCCGGG(SPO₄)RGD, with varying lengths of alkyl chain. (RGD is a tripeptide sequence, arginine-glycine-aspartic acid, which is able to mediate cell adhesion through recognition of cell adhesion molecules [27]). It was found that upon acidification, the longer alkyl chain molecules, with 10, 16 and 22

carbons, formed gels, whereas the smallest, below 6 carbons, did not. The smallest also needed high weight percentage in solution in order to form a precipitate, in contrast to the larger alkyl length molecules which were able to precipitate even at the lowest weight percentage used. The length of the alkyl chain has also been shown to have an effect on the thermal stability of structures formed through self-assembly [28, 29]. In these studies, two different length monoalkyl chains, C₆ and C₁₆, were found to form an α -helical structure in water compared with the peptide with no chain attached which had no discernible structure. The C₁₆ PA had higher thermal stability than the C₆ one, also seen with another 39-residue triple-helical model peptide tested. This work leads on from previous research which found the same increase in thermal stability with a longer dialkyl chain compared with the peptide without it [30].

The effect on self-assembly of the hydrophobic tail length of A₃K, A₆K, and A₉K was investigated [31]. A₃K was found to have no cac in this study, and was shown through atomic force microscopy (AFM) to form stacked bilayers. A₆K and A₉K did give cac values, with A₆K being higher than A₉K, and these peptides were found to assemble into long fibres/worm-like-micelles, and short narrow rods respectively. In contrast, other studies have found A₆K in fact forms nanotubes above a experimentally determined cac in one study [32], and above a 12 wt% threshold in another [33]. The length of the hydrophobic peptide chain in these peptides was investigated for its effect on antibacterial capacity [34]. Using both Gram-negative (*Escherichia coli*) and Gram-positive (*Staphylococcus aureus*) bacterial strains, A₃K was shown to give the weakest antibacterial activity, followed by A₆K, with A₉K giving the highest. The mode of antibacterial action has been proposed to be cell permeation, and thus was expected that smaller nanostructure objects would more readily pass through the bacterial cell membrane. This correlates with the results seen here as the thinner and smaller self-assembled A_nK structures, with the more hydrophobic tails, the higher the observed antibacterial efficiency.

1.3 Lipopeptides

Lipopeptides are a type of peptide amphiphile formed of two main parts; a hydrophobic alkyl/lipid chain, attached to a hydrophilic peptide section. They are one of the most popular biosurfactants (surfactants produced by bacteria, yeast or fungi) which are produced as a defence mechanism against other microorganisms [35, 36]. These lipopeptide producers include genera of fungi such as *Aspergillus*, and bacteria including *Streptomyces*, *Pseudomonas* and *Bacillus* [37]. *Bacillus subtilis* is the producer of what is believed to be the most active lipopeptide, surfactin [38, 39]. It has been suggested that some of the biological functions of surfactin, including its ability to form ionised pores in phospholipid bilayers, are due to it being an amphiphile [40]. Other potent lipopeptides include a group called polymyxins, produced by *Bacillus polymyxa* among others, which generally consist of a hydrophobic tail bound to a cyclic peptide [41, 42]. Polymyxin B and E (also known as colistin) both possess antibacterial activity versus a number of gram-negative bacteria [43]. Their cationic properties allow them to bind to the anionic bacterial outer membrane, causing membrane damage and leading to cytoplasmic leakage [41].

Daptomycin, produced by *Streptomyces roseosporus*, is a cyclic lipopeptide drug used in the treatment of life-threatening infections caused by Gram positive bacteria [44, 45]. The molecular structure is shown in figure 3. It is usually used when resistance to other drugs is seen, such as in methicillin-resistant *Staphylococcus aureus* (MRSA), and vancomycin-resistant Enterococci [44, 46]. Interestingly, daptomycin contains a non-natural amino acid, L-kynurenine, which is responsible for the lipopeptide's fluorescence properties with an emission peak at 460 nm [47, 48]. Daptomycin's suggested mechanism of action involves insertion of its hydrophobic decanoyl chain into the bacterial membrane [46, 48, 49]. This causes the outflow of potassium ions from the cell, leading to cell death [50]. There are studies

A group of cyclic lipopeptides under the name Iturins have a peptide motif attached via an amide bond to a β -amino fatty acid [35]. They include Iturin A, C, D and E, as well as bacillomycin D, F and L, bacillopeptin, and mycosubtilin [54]. They have a broad range of activity against yeasts and fungi, as well as a small number of bacteria [55]. Their method of action involves increasing the permeability of membranes, leading to K^+ ion leakage, and ultimately cell death [56]. This is through the formation of ion-conducting pores, dependent on the characteristics of the target membrane, as well as the peptide motif on the iturin [55]. Fengycin is a similar group to Iturin, with a cyclic peptide linked to a β -hydroxy lipid tail. They differ through their structures containing unusual amino acids, for example ornithine and allo-threonine [57]. The fengycin group includes fengycin A and B, and plipastatin A and B, which have been shown to give high antifungal activity, specifically against filamentous fungi [58]. The kurstakin group comprises the lowest molecular weight lipopeptides, produced by the Gram-positive subspecies *Bacillus thuringiensis kurstaki* HD-1 [35]. They differ through their lipid chain, whilst retaining the same amino acid sequence [59]. It has been suggested that the kurstakins are pore-forming, but have only limited spectrum of activity [59].

Amphotericin B, although not classified as a lipopeptide, is another well-characterised antifungal drug. Like daptomycin, it is produced by a *Streptomyces* species, in this case *Streptomyces nodosus*, and has been used against a range of fungal infections for over 50 years without resistance developing against it, in contrast to many other antifungals [60, 61]. One of the main disadvantages of amphotericin use is its high toxicity, leading to side effects including nausea, rigors, fever, and hypo/hypertension [62]. Its mechanism of action is believed to be through the formation of pores in the cell walls of fungi, with preferential selectivity for ergosterol, present in fungal cell membranes but not in those of humans [63]. Amphotericin binds in pairwise form with another amphotericin molecule at the hydrophobic polyene backbone, forming a dimer. It is suggested that this dimer over time forms into a tetramer, and that the toxicity of the drug is due to the dimer form [64, 65].

1.3.1 Further uses of lipopeptides

Lipopeptides also have applications in the cosmetic industry, notably in skincare in anti-wrinkle formulations. One of these is C₁₆-KTTKS, also known by the trade name Matrixyl [66, 67]. Many of the peptides used in skin care formulations are lipidated, often with palmitoyl chains, shown to increase permeability through the outer layer of skin [68, 69]. KTTKS is a pentapeptide sequence which has been shown to inhibit collagenases, and lead to an increase in extracellular matrix production (ECM) [70]. The latter is thought to be through a synergistic effect whereby the presence of KTTKS with transforming growth factor beta-1 (TGF- β1) leads to an increase in fibroblast activity, ultimately increasing ECM formation [67]. The Hamley group has undertaken considerable research into C₁₆-KTTKS and its self-assembly. They found it assembled into incredibly long tape like structures of micron length, with polydisperse width on the nanoscale [71]. Due to the presence of other surfactants in formulations of skin-care products, model surfactants were also tested for their influence on self-assembly of C₁₆-KTTKS. It was found that both sodium dodecyl sulphate (an anionic surfactant) [72], and Pluronic copolymer P123 (a non-ionic surfactant) [73] have an effect, changing from nanotapes to differing fibril structures. The same group also compared the self-assembly of C₁₆-KTTKS against two other cosmetically active PAs, C₁₆-GHK and C₁₆-KT [74]. The latter two were shown to form crystal-like aggregates with relatively lower β-sheet content than the C₁₆-KTTKS nanotapes. All 3 did however show bilayer structures through SAXS experiments, along with similar aggregation concentrations.

1.4 Toll-like receptor agonists

Lipopeptides have also been developed which act as toll-like receptor (TLR) agonists. Toll-like receptors are a class of transmembrane receptors involved in the innate immune system, and which make up an important group of pattern recognition receptors (PRRs) [75]. They are

composed of an N-terminal ligand recognition domain, with the cytoplasmic signalling section at the C-terminal end [76]. They are split between receptors that recognise bacterial and fungal-derived components, present on the surface of cells, and microbial and viral-derived components, present in intracellular membranes [77]. There are a number of different TLRs, numbered 1-13, although 12 and 13 are not found in humans [78]. TLR 1, 2, 4, 5 and 6 are found in the plasma membrane and in general are responsive to hydrophobic components, whereas TLR 3, 7, 8, 9 and 11 are located in the endosome and are usually responsive to hydrophilic residues [79-82]. When ligand binding to TLRs occurs, adaptor molecules are recruited in the cytoplasm, forming part of the signal transduction pathway [83]. This activates an immune response, releasing cytokines causing inflammation, as well as immune cells such as MHC and adhesion molecules [84].

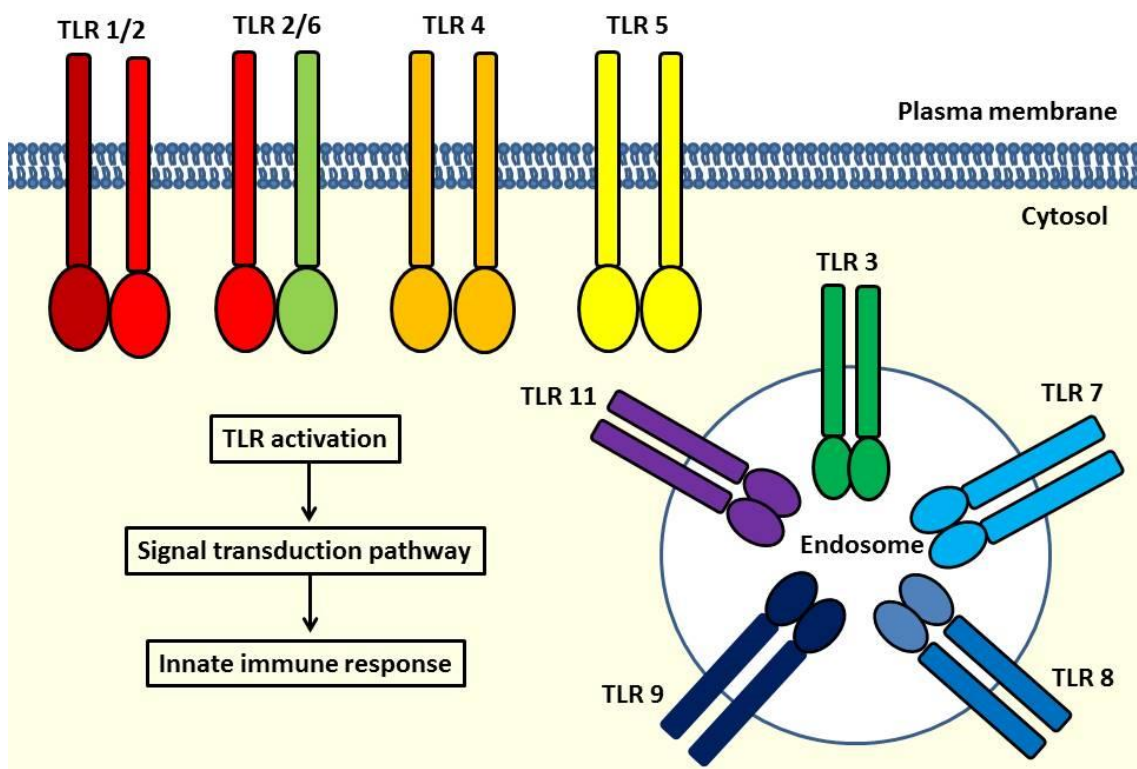


Figure 4 Cellular distribution of Toll-like receptors (TLRs). TLRs 1,2,4,5 and 6 are expressed on the cell surface, while TLRs 3, 7, 8, 9 and 11 are expressed intracellularly. Adapted from [162].

1.4.1 TLR agonist agents in cancer treatment

Due to activation of TLRs having such an important role in innate immune response, they have become a target for disease treatment. TLR agonists have been investigated for potential use in cancer treatment, with some mouse models showing reduced tumour growth, and destruction of established tumours when combined with other anti-cancer drugs [85-88]. The effect of different TLRs on different cancer types has been reviewed [89]. Here it is shown that in some cases, activation of TLRs on one type of cancer can induce cell death, whereas on another cancer cell type can induce cell survival, and even proliferation and promotion of resistant phenotypes. There are only 3 different TLR agonists that have been approved by the FDA as monotherapy treatments of cancer; BCG (Bacillus Calmette-Guerin), MPL (monophosphoryl lipid A), and imiquimod. Probably the most successful of these, BCG, is used in the treatment of bladder cancer [90]. It activates both TLR 2 and TLR 4 through the mycobacterial component, and also TLR 9 through its bacterial DNA [91, 92]. MPL is part of a broader group of lipid A molecules which stimulate TLR 4 and are often used as vaccine adjuvants [90]. It contains the lipid part of lipopolysaccharide (LPS), known to illicit a strong immune response in animals, but has been shown to be at least 100 times less toxic [93]. It has been safely used in vaccines for both hepatitis B, and human papillomavirus (HPV) [94]. Imiquimod is a target of TLR 7 and is used in the treatment of superficial basal cell carcinoma, but also in a wide range of other diseases including HPV-related warts [90]. Like imiquimod, another type of imidazoquinoline called resiquimod has potential to be used as a vaccine adjuvant, and in humans has been shown to activate both TLR 7 and 8 [95].

As previously mentioned, TLR agonists have potential to be used in combination with other conventional anti-cancer treatments. They can augment chemotherapy, ionising radiation or monoclonal antibodies [90]. Studies have shown that when an agonist of TLR 2 and 4 is added alongside chemotherapy, tumour progression is reduced, and survival is prolonged in liver or lung metastases [96]. This is through the controlled release of tumour necrosis factor-alpha

(TNF- α) which causes easier passage into tumour vessels for anti-cancer drugs. This leads to arresting of tumour-related angiogenesis [97]. The TLR agonists also activate a signalling pathway which leads to increased expression of inducible nitric oxide synthase (iNOS), helping apoptosis in chemotherapy-resistant tumour cells [98]. Alongside the studies into liver and lung cancers, TLR agonists have also been shown to work alongside other conventional treatments against sarcoma, mammary carcinoma, and lymphoma [99, 100]. Mouse models were used to show CpG oligodeoxynucleotides (ODNs), synthetic DNA sequences that have immunostimulatory effects, act upon TLR 9 present on dendritic and B cells, enhancing the effects of radiotherapy. Further research has shown the same using CpG in initial tests in patients with malignant glioma and non-Hodgkin lymphoma [101, 102]. Ultimately, the future of TLR agonist use in cancer treatment is believed to be when used in combination with other anti-cancer agents, rather than as a singular medication.

1.4.2 TLR agonist agents in non-cancer treatment

Although cancer is a large target for TLRs used in therapy, TLR agonists may have already shown, or have the potential, to be used in a number of other ways. Macrophage-activating lipopeptide 2 (MALP-2) was originally isolated from *Mycoplasma fermentans*, and as its name suggests is a potent stimulator of macrophages, as well as monocytes [103]. It binds to TLR 2 and 6 in epithelial cells, which leads to a signalling cascade causing activation of NF- κ B [104]. In murine models, this has been shown to occur in the lungs and leads to a decrease in bacterial burden when used against *Streptococcus pneumoniae* [105]. There is also a related synthetic analog of MALP-2, Pam₂Cys, which has been used as a vaccine adjuvant candidate in a number of cases [106-108]. A PEGylated version of the compound has been tested without the presence of antigen in a mouse model [109]. PEG-Pam₂Cys was intranasally introduced to the mice, causing an influx of neutrophils and macrophages. This was shown to increase

resistance to the influenza A virus, as well as reduce the risk of transmission. Another positive from this case was that the compound didn't completely prevent infection, allowing the production of memory T cells, and thus protection against further infection.

As well as showing potential in cancer treatment, CpG-ODN has also been used against a number of different infections. In one case it showed both protective immunity, and was curative, against *Leishmania major* infection in mice [110]. Protection and cure were both also found by a different group against herpes simplex virus type 2 (HSV-2) when CpG-ODN was given mucosally in mice [111]. Another study found that bacterial DNA containing unmethylated CpG motifs gave mice protection against otherwise lethal doses of both *Francisella tularensis* and *Listeria monocytogenes* [112]. Jiang et al. investigated the efficacy of a modified version of CpG-ODN, 1826, against the H1N1 strain of influenza which had caused a pandemic in 2009 [113]. Using a mouse model, it was shown that injection of the synthetic compound prior to introduction of H1N1 lead to inhibition of virus replication in the lungs, reduced lesions, and prevented mortality. Using a combination of another CpG-ODN, and Pam2CSK4, a diacylated lipopeptide, a high resistance to a variety of lung infections was found when tested synergistically in mice [114]. The combination of the two allowed for activation of TLR 2 and 6 (Pam2CSK4) and TLR 9 (CpG-ODN), which showed survival against otherwise lethal doses of both Gram positive, *Streptococcus pneumoniae*, and Gram negative, *Pseudomonas aeruginosa*, infections in mice. In vitro, the combination also showed reduction in bacterial cells of *Bacillus anthracis*.

1.5 Light, temperature and pH effect on PAs

PAs can be manipulated by altering their local environment, allowing for another level of control for their design in different applications. There are a number of factors which can have

an effect on the self-assembly of PAs. These include the use of UV light, altering of pH and temperature, and the use of enzymes in enzyme-responsive systems.

One group has been particularly involved in the manipulation of peptides, including using UV light [115]. They had already shown that introducing hydrophobic tails to peptides which have the ability to form fibrils stabilises the structures and allows them to more easily be manipulated [116, 117]. In ref. [115], they investigated the disassembly of peptide aggregate fibres through manipulation of hydrophobicity by attaching a UV-sensitive cleavable hydrophobic alkyl chain to a hexapeptide. Upon treatment with UV light, the linker was cleaved, which led to the dissociation of the fibres. This was determined by CD, which showed a transformation from a β -sheet to a random coil. Another example of UV light being used to manipulate peptide self-assembly was investigated by another group [118]. Similarly to the previous paper, an alkyl chain was used, this time with a UV-sensitive 2-nitrobenzyl group, which was linked to the hydrophilic peptide chain RGDS. Light exposure caused a change in structure from nanospheres to nanofibers, also causing a transition from a solution to a gel. Another paper by the Stupp group used the same 2-nitrobenzyl cleavable linker, this time attached to a $GV_3A_3E_3$ peptide [119]. The effect of light exposure here caused a transformation of quadruple helices to single fibres upon cleavage of the photo-sensitive linker. Light-sensitive linkers have also been used in cell culturing [120]. In this case, another nitrobenzyl linker was used and enabled an RGDS cell adhesion epitope to be removed from the PA upon exposure to light, allowing for more control over the spreading of cells. This time however, the self-assembled nanofiber structures were not transformed, and stayed the same.

Temperature can also have an effect on the self-assembly and conformation of peptide amphiphiles, seen also by past and present members of our group [121-123]. These investigations initially centred around C_{16} -KTTKS, which is known to simulate collagen production [67]. It was found that at 20°C, a β -sheet structure was present, and upon heating

above 55°C, a transformation into a random coil arrangement was seen. This was confirmed through CD, which also found that upon cooling back down to 20°C, over time it reassembled into a β -sheet [122]. Another peptide, C₁₆-KKFFVLK, underwent the same heating and cooling regime and was found to transition from a mixture of helical ribbons and nanotubes to twisted tapes above 55°C [123]. Like with the previous PA, the structural change was shown to be reversible upon cooling.

The self-assembly of PAs can also be affected by pH changes. The PA, C₁₆-KTTKS, was also investigated at a range of pHs, from pH 2-7 [124]. The PA has applications in skin care as an anti-wrinkle formula, and so pHs 4-7 were chosen to cover the range found in skin. It was found that at pH 7, tape-like structures are seen, at pH 4 they become twisted right handed structures, pH 3 they were flat and tape-like, and at pH 2 spherical micelles were seen. Another paper discussed a PA with a C₁₆ alkyl tail, this time with an RGD cell adhesion motif attached [26]. It was found that fibres are formed at pH 4 and disassemble at higher pH, and that these states are reversible.

1.6 Hydrogels

Hydrogels are often networks of polymers (natural or synthetic), as well as small molecules, which have the ability to absorb large amounts of water or other biological fluids [125, 126]. Their networks can be formed from a range of different types, including covalent bonds between monomers, cross-links, and intermolecular interactions such as hydrogen bonding and van der Waals forces [125]. Hydrogels can be categorised into a range of different types based on their characteristics, one of which is their subunits. Homopolymer gels are ones which consist of only one monomeric subunit type, copolymers of two or more different types, and interpenetrating polymeric networks which are formed of entangling non-covalent bonds between two or more different networks [125]. Hydrogels may also be distinguished by their

ionic charges as neutral, anionic, cationic, or ampholytic, meaning they carry both a positive and negative charge. Finally, their physical architecture may be termed amorphous with random chain organisation, semicrystalline with compact ordered chains, or hydrogen-bonded giving a 3-dimensional structure to the network [125].

Environmental factors such as pH, temperature, etc., can have an effect on the structure and swelling of hydrogels sensitive to them, making them ideal drug delivery systems due to the control over when the drug is released based on these factors [125]. Only hydrogel networks which have either acidic or basic units or both are sensitive to changes in pH [125]. When these groups are ionised by a change of pH, the network's swelling force is increased due to the development of fixed charges throughout. Temperature-sensitive hydrogels generally have increased solubility at lower temperatures that leads to swelling. At higher temperatures, the hydrophobicity of the compound increases and this leads to precipitation [125].

1.6.1 Natural and synthetic hydrogels

Naturally-derived and synthetic polymers differ in many ways when incorporated as hydrogels. Biocompatibility is generally higher in natural polymers than synthetic ones, with the latter having a higher instance of causing negative bodily responses [127]. This is due to the recognition of the naturally-derived materials by the surrounding environment of the body, although this may lead to an immune reaction which is a larger concern with protein-based polymers. Synthetic polymers however are more likely to be recognised by the body as foreign, which can lead to inflammatory responses, problems with clearance of the hydrogel, and toxicity [127]. Conversely, due to the body's recognition of natural polymers, they may be more easily cleared through enzymatic or hydrolytic degradation, which is an advantage for hydrogels which are only in place for a short-term specified time, although this obviously represents a problem for more permanent placements. Synthetic polymers have some

advantages over natural ones due to their simplicity of structure, which often makes chemical modifications much easier, and also provide a greater control over structure and mass [127].

The most common naturally-derived polymer in animals is collagen, due to its presence in a large number of different human tissues [127]. Collagens are easily degraded and cleared by enzymes which recognise them, and they allow a range of cell types to attach. The disadvantages of collagen-based hydrogels are that they are expensive, can cause immunogenic reactions, and, even when cross-linked with other compounds, can lack strength [128]. Gelatin is another common polymer, and closely-resembles collagen in that it is formed through the breakage of the collagen's triple helix, leaving the three separate coils [127]. Tissue engineering is one of its main areas of use due to high biocompatibility, the ability to easily form a gel, and the ability to control gelation through temperature. Other examples of natural polymers used for the production of hydrogels include hyaluronate, fibrin, alginate (shown in figure 5), agarose and chitosan, which each have differing advantages and disadvantages in tissue engineering [129].

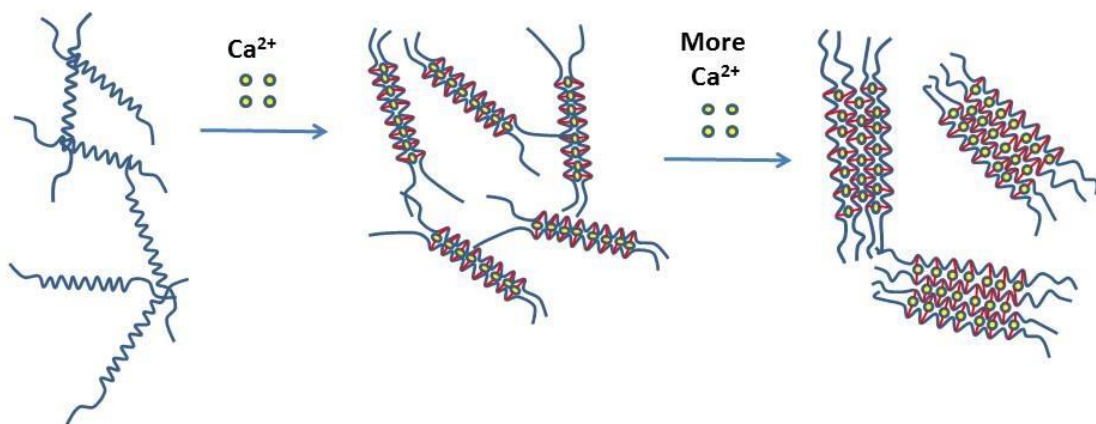


Figure 5 Cross-linking of sodium alginate with calcium ions.

One of the most commonly investigated synthetic polymers is poly (2-hydroxyethyl methacrylate), or poly (HEMA) [127, 130]. The properties of poly (HEMA) hydrogels are dependent on what other molecules or compounds they are cross-linked with [127]. Due to their inability to be degraded in the environment of the body, a new type incorporating dextran into the structure was produced, which was enzyme-degradable through cross-link hydrolysis [131]. Other poly (acrylic) synthetic polymers include poly (N-isopropylacrylamide), which has the benefit of having a lower critical solution temperature (LCST) of around 32 °C. This means that the polymer containing a drug can be injected into the body in a hydrated state, and then at body temperature, a volume transition phase occurs which shrinks it down, reducing its size dramatically and releasing the drug [127]. However, hydrogels of this polymer suffer setbacks commonly seen with synthetic polymers through a lack of degradation of cross-links, although, as with poly (HEMA), this can be rectified through incorporation of dextran [132], which also solves some of the toxicity issues.

Another synthetic polymer, poly (ethylene oxide), or PEO, does not suffer from toxicity issues in its native form, and still maintains a high biocompatibility [127]. Its poor degradability under physiological conditions can be alleviated through addition of degradable units such as esters or Ala-Pro-Gly-Leu chains, which also makes such copolymers suitable in tissue engineering [133]. Copolymers of PEO, such as triblock copolymers with poly (propylene oxide), or PPO, sandwiched between two PEO molecules, also have interesting properties. PEO-PPO-PEO is able to form a hydrogel through control of temperature, but without permanent cross-link formation [134]. This triblock copolymer again has the issue of lack of degradation however, and so copolymers with poly (lactic acid), or PLA, have been developed, with existing proof of the safety of PLA [135]. Other synthetic polymers include poly (vinyl alcohol) used as a long-term structure for cell culturing due to its physiological degradation issues, polyphosphazene, and synthetically prepared proteins designed to mimic natural proteins, which have issues due to the complexity of their production [127, 128].

1.6.2 Further applications of hydrogels

The use of hydrogels in contact lenses was one of the first biomedical uses due to their permeability to oxygen, material properties (being both soft enough as to not irritate the eyeball, but strong enough to withstand eye movement), and their surface hydrophilicity which enables sustained contact to the eyeball through their wetting ability [136]. This is an example of a use of the synthetic polymer, poly (HEMA) [137].

As previously mentioned, hydrogels can also be used in the delivery of drugs. Along with the factors aforementioned, hydrogels are also suited through their ability to protect the drug from environments which would otherwise damage the drug on the way to its designated site, such as acidic pH in the stomach and enzyme degradation [138]. They can also be synthesised separately from the drug itself, with the drug later added to the self-assembling system [25]. The property of hydrogels to absorb large amounts of water allows them to become ideal candidates to mimic the environment of tissues, which themselves are heavily hydrated, and to be used for the delivery of drugs and in wound healing. The β -sheet structure, which is very stable in water, can become the scaffolding which allows cells to attach to and culture on [21, 139]. Hydrogels provide a three dimensional scaffold for cell culturing, which has both advantages and disadvantages over two dimensional monolayer cell culturing. Three dimensional cell culturing more accurately mimics the natural environment of cells in tissues, influencing spatial organisation, as well as well as interactions with other cells [140, 141]. However, two dimensional cultures have easier environmental control, observation of cells, measurement and manipulation [140]. A problem associated with normal cell culturing is the use of proteases such as trypsin to detach cells from dishes or flasks as they can cause damage to the cells. Culturing cells on temperature-responsive hydrogels like poly (N-isopropylacrylamide) enables them to be detached easily by lowering the temperature [142].

1.6.3 Enzyme-responsive hydrogels

Enzyme-responsive hydrogels change their functionality based on interaction with enzymes [143], similar to the temperature, pH etc., sensitive hydrogels mentioned before. These hydrogels present a unique concept in medical applications as the targets of the hydrogels for medical applications, i.e. humans, require enzymes for all of their physiological processes. The major advantages are that due to the specificity of enzymes for substrates, hydrogels can be designed to target certain areas before being activated/changed, and their efficiency as a catalyst means enzyme-responsive hydrogels can be fast acting [143]. In the design of these hydrogels, they must fit within certain criteria. Firstly, there must be an active site on the material similar to the substrate with which the enzymes react. There must also be a translation of the effect at the active site throughout the entirety of the hydrogel, followed by a change in the properties of it [143]. With enzyme-sensitive peptide-based hydrogels, naturally they will largely be targeted by proteases, of which there are many. Here, the proteases have the potential to either degrade or functionalise the hydrogel [143].

Enzyme-responsive hydrogels may be used in cell culturing. They can be functionalised with peptides, such as the short sequence Arg-Gly-Asp, or RGD [144], which leads to certain cell types attaching through integrins [145]. Ile-Lys-Val-Ala-Val (IKVAV) is another peptide sequence that can be incorporated into hydrogels in order to signal neuronal cell differentiation from stem cell progenitors [146]. Heparin is a biological molecule with one of its functions being that it binds to pro-angiogenic growth factors such as vascular endothelial growth factor (VEGF) [147, 148]. It was shown to give higher neovascularization when incorporated into a hydrogel and inserted into a pocket near a rat cornea [149]. The use of these hydrogels in the repairing of tissue damage has also been proposed in the form of an injectable scaffold [150]. This idea has led to two different proposed models of action. The first is that the cells are allowed to grow in a culture, and then mature on the hydrogel before then being implanted into the wound. The second is the hydrogel is implanted into the wound, and

the native cells surrounding the structure are allowed to grow and mature onto it, forming the tissue. For both strategies, adhesion peptides, such as RGD mentioned before, would need to be incorporated into the hydrogel, along with other bioactive molecules such as growth factors and matrix metalloproteinases (MMPs) [150]. MMPs are responsible for degrading various ECM components, which when normally regulated, is important in development, tissue repair etc. [151].

Enzyme-responsive hydrogels have also been discussed as having potential applications in diagnostics [152]. The amount of enzyme activity that is under investigation may be quantified through the observation of gel phase conversion from a solid to a gel. This change can be seen without the need for expensive specialised equipment, and so represents a cheaper alternative to other diagnostics. If higher sensitivities are required, fluorophores which can be cleaved by enzymes specific to the area under investigation may be used, with high levels of fluorescence indicating high enzyme activity [153]. Colour change assays can also be used to give a higher sensitivity than through observation of phase transition into hydrogels [152].

1.6.4 Poly (ethylene glycol)-based hydrogels

PEG-based block copolymers bound to other peptide fragments also have been used in hydrogels. Often, the peptide will form the inner section, or core, of the nanostructure, and PEG will form the outside, as a shell [154]. PEG has been shown to form different structures when combined with different peptides, as when bound to β A β AKLVFF micelles are formed [154], whereas fibril structures have been seen when bound to other peptides such as FFKLVFF [155]. One advantage of PEG-based hydrogels is that they can be engineered to melt at approximately body temperature [156], and when bound to a matching substrate, they can also be degraded by enzymes [157]. PEG itself as a molecule is suited to hydrogel applications due to its inertness, low cost, biocompatibility, water solubility, and low immunogenicity [158,

159]. Due to the expanding knowledge of characteristics of PEG and its conjugates, it is becoming an increasingly viable compound in the field of biotechnology.

1.7 Methods of tagging in cell culture

There are a number of different ways molecules may be tagged when used in cell culturing. One of the most common methods is by using a fluorescent tag in the form of a fluorophore attached covalently to a functional group on the molecule. A common fluorophore used is fluorescein, along with some of its derivatives such as fluorescein isothiocyanate (FITC), which are engineered for different purposes [160]. Another method of tagging used in cell culturing is isotopic labelling [161]. This involves the use of an isotope which has the same characteristics as the normal atom and which will not interfere with normal processes. It is tracked as it undergoes reactions, or for its presence in certain parts of a cell, through the difference in mass, vibrations or radioactive decay when compared with the normally present atom. Deuterium oxide, or heavy water, is an example of an isotopic label where the hydrogen atoms are replaced with an isotope, deuterium, giving D₂O.

1.8 Aims

The overarching aim of the research discussed in this thesis is to investigate further into the self-assembly of peptide amphiphiles. This will include a range of different PAs, from short peptide sequences, to large, polyethylene oxide-containing molecules, to lipopeptide drugs.

Specifically, the aims are:

- To investigate the self-assembly of the Toll-like receptor agonists PamCSK₄, Pam₂CSK₄, and Pam₃CSK₄, and to compare the effects of the number of palmitoyl chains.
- To compare the self-assembly of the TLR-agonist MALP-2 with its constituent peptide to determine the effects of the attached lipid chains.
- To determine whether the fluorophore FITC, when bound to a dileucine peptide motif, is able to be uptaken into cells, and to determine the self-assembled structure of the molecule above its cac.
- To investigate the morphology of the self-assembled structure of the polyene antifungal drug amphotericin B.
- To further research into the cyclic lipopeptide daptomycin, showing the morphology of daptomycin self-assembled structures, and investigating the proposed link between CaCl₂ presence and micellization.
- To investigate the self-assembly of three custom-synthesised telechelic tyrosine conjugates (with PEG or poly (alanine) midblocks), to determine the effect of the short peptide end caps and size of the central polymer block.

1.9 References

- [1] J. Berg, J. Tymoczko and L. Stryer, *Protein Structure and Function*, New York: W.H Freeman, 2002, pp. 117-118.
- [2] M. Rother and J. Krzycki, "Selenocysteine, Pyrrolysine, and the Unique Energy Metabolism of Methanogenic Archaea," *Archaea*, vol. 2010, p. 453642, 2010.
- [3] I. Wagner and H. Musso, "New Naturally-Occuring Amino Acids," *Angewandte Chemie-Internation Edition in English*, vol. 22, no. 11, pp. 816-828, 1983.
- [4] Y. Zhao and Y. Wu, "A theoretical study of beta-sheet models: is the formation of hydrogen-bond networks cooperative?," *Journal of the American Chemical Society*, vol. 124, no. 8, pp. 1570-1571, 2002.
- [5] M. Krysmann, V. Castelletto, J. McKendrick, L. Clifton, I. Hamley, P. Harris and S. King, "Self-assembly of peptide nanotubes in an organic solvent," *Langmuir*, vol. 24, no. 15, pp. 8158-8162, 2008.
- [6] H. Cui, M. Webber and S. Stupp, "Self-Assembly of Peptide Amphiphiles: From Molecules to Nanostructures," *Biopolymers*, vol. 94, no. 1, pp. 1-18, 2010.
- [7] I. Hamley, "Self-assembly of amphiphilic peptides," *Soft Matter*, vol. 7, no. 9, pp. 4122-4138, 2011.
- [8] K. Kalyanasundaram and J. Thomas, "Environmental effects on vibronic band intensities in pyrene monomer fluorescence and their application in studies of micellar systems," *Journal of the American Chemical Society*, vol. 99, no. 7, pp. 2039-2044, 1977.
- [9] F. Winnik, "Photophysics of preassociated pyrenes in aqueous polymer-solutions and in other organized media," *Chemical Reviews*, vol. 93, no. 2, pp. 587-614, 1993.
- [10] M. Guler, R. Claussen and S. Stupp, "Encapsulation of pyrene within self-assembled peptide amphiphile nanofibers," *Journal of materials chemistry*, vol. 15, no. 42, pp. 4507-4512, 2005.
- [11] R. Jones, V. Castelletto, C. Connon and I. Hamley, "Collagen stimulating effect of peptide amphiphile C16-KTTKS on human fibroblasts," *Molecular Pharmaceuticals*, vol. 10, no. 3, pp. 1063-1069, 2013.
- [12] H. LeVine, "Thioflavine T interaction with synthetic Alzheimer's disease β -amyloid peptides: detection of amyloid aggregation in solution," *Protein Science*, vol. 2, no. 3, pp. 404-410, 1993.

- [13] H. LeVine, "Quantification of beta-sheet amyloid fibril structures with thioflavin T," in *Methods in Enzymology*, San Diego, Academic Press, 1999, pp. 274-284.
- [14] V. Castelletto, G. Cheng, B. Greenland and I. Hamley, "Tuning the self-assembly of the bioactive dipeptide L-carnosine by incorporation of a bulky aromatic substituent," *Langmuir*, vol. 27, no. 6, pp. 2980-1988, 2011.
- [15] I. Hamley, A. Dehsorkhi and V. Castelletto, "Coassembly in binary mixtures of peptide amphiphiles containing oppositely charged residues," *Langmuir*, vol. 29, no. 16, pp. 5050-5059, 2013.
- [16] V. Castelletto, R. Gouveia, C. Connon, I. Hamley, J. Seitsonen, A. Nykanen and J. Ruokolainen, "Alanine-rich amphiphilic peptide containing the RGD cell adhesion motif: a coating material for human fibroblast attachment and culture," *Biomaterials Science*, vol. 2, no. 3, pp. 362-369, 2014.
- [17] R. Latypov, D. Liu, K. Gunasekaran, T. Harvey, V. Razinkov and A. Raibekas, "Structural and thermodynamic effects of ANS binding to human interleukin-1 receptor antagonist," *Protein Science*, vol. 17, no. 4, pp. 652-663, 2008.
- [18] T. Scheibel and L. Serpell, "Physical methods for studies of fiber formation and structure," in *Protein Folding Handbook*, Weinheim, Germany, Wiley-VCH, 2005, pp. 197-253.
- [19] Y. Velichko, S. Stupp and M. de la Cruz, "Molecular Simulation Study of Peptide Amphiphile Self-Assembly," *The Journal of Physical Chemistry B*, vol. 112, no. 8, pp. 2326-2334, 2008.
- [20] S. Paramonov, H. Jun and J. Hartgerink, "Self-assembly of peptide-amphiphile nanofibers: the roles of hydrogen bonding and amphiphilic packing," *Journal of the American Chemical Society*, vol. 128, no. 22, pp. 7291-7298, 2006.
- [21] S. Vauthey, S. Santoso, H. Gong, N. Watson and S. Zhang, "Molecular self-assembly of surfactant-like peptides to form nanotubes and nanovesicles," *Proceedings of the National Academy of Sciences of the United States of America*, vol. 99, no. 8, pp. 5255-5360, 2002.
- [22] X. Zhao, "Design of self-assembling surfactant-like peptides and their applications," *Current Opinion in Colloid & Interface Science*, vol. 14, no. 5, pp. 340-348, 2009.
- [23] S. Son, M. Brimble, S. Yang, P. Harris, T. Reddingius, B. Muir, O. Hutt, L. Waddington, J. Guan and G. Savage, "Synthesis and Self-Assembly of a Peptide-Amphiphile as a Drug Delivery Vehicle," *Australian Journal of Chemistry*, vol. 66, no. 1, pp. 23-29, 2013.
- [24] D. Leite, E. Barbu, G. Pilkington and A. Lalatsa, "Peptide Self-Assemblies for Drug Delivery," *Current Topics in Medicinal Chemistry*, vol. 15, no. 22, pp. 2277-2289, 2015.

- [25] M. Goldberg, R. Langer and X. Jia, "Nanostructured materials for applications in drug delivery and tissue engineering," *Journal of Biomaterials Science-Polymer Edition*, vol. 18, no. 3, pp. 241-269, 2007.
- [26] J. Hartgerink, E. Beniash and S. Stupp, "Peptide-amphiphile nanofibers: a versatile scaffold for the preparation of self-assembling materials," *Proceedings of the National Academy of Sciences of the United States of America*, vol. 99, no. 8, pp. 5133-5138, 2001.
- [27] S. D'Souza, M. Ginsberg and E. Plow, "Arginyl-glycyl-aspartic acid (RGD): a cell adhesion motif," *Trends in Biochemical Sciences*, vol. 16, no. 7, pp. 246-250, 1991.
- [28] Y. Yu, M. Tirrell and G. Fields, "Minimal Lipidation Stabilizes Protein-Like Molecular Architecture," *Journal of the American Chemical Society*, vol. 120, no. 39, pp. 9979-9987, 1998.
- [29] P. Forns, J. Lauer-Fields, S. Gao and G. Fields, "Induction of protein-like molecular architecture by monoalkyl hydrocarbon chains," *Biopolymers*, vol. 54, no. 7, pp. 531-546, 2000.
- [30] Y. Yu, P. Berndt, M. Tirrell and G. Fields, "Self-Assembling Amphiphiles for Construction of Protein Molecular Architecture," *Journal of the American Chemical Society*, vol. 118, no. 50, pp. 12515-12520, 1996.
- [31] X. H., J. Wang, S. Han, J. Wang, D. Yu, H. Zhang, D. Xia, X. Zhao, T. Waigh and J. Lu, "Hydrophobic-Region-Induced Transitions in Self-Assembled Peptide Nanostructures," *Langmuir*, vol. 25, no. 7, pp. 4115-4123, 2009.
- [32] A. Nagai, Y. Nagai, H. Qu and S. Zhang, "Dynamic behaviors of lipid-like self-assembling peptide A6D and A6K nanotubes," *Journal of Nanoscience and Nanotechnology*, vol. 7, no. 7, pp. 2246-2252, 2007.
- [33] S. Bucak, C. Cenker, I. Nasir, U. Olsson and M. Zackrisson, "Peptide Nanotube Nematic Phase," *Langmuir*, vol. 25, no. 8, pp. 4262-4265, 2009.
- [34] C. Chen, F. Pan, S. Zhang, J. Hu, M. Cao, H. Xu, X. Zhao and J. Lu, "Antibacterial Activities of Short Designer Peptides: a Link between Propensity for Nanostructuring and Capacity for Membrane Destabilization," *Biomacromolecules*, vol. 11, no. 2, pp. 402-411, 2010.
- [35] I. Mnif and D. Ghribi, "Review lipopeptides biosurfactants: Mean classes and new insights for industrial, biomedical, and environmental applications," *Peptide science*, vol. 104, no. 3, pp. 129-147, 2015.
- [36] I. Hamley, "Lipopeptides: From Self-assembly to Bioactivity," *Chemical Communications*, vol. 51, no. 41, pp. 8574-8583, 2015.
- [37] J. Raaijmakers, I. De Bruijn, O. Nybroe and M. Ongena, "Natural functions of lipopeptides

- from *Bacillus* and *Pseudomonas*: more than surfactants and antibiotics," *FEMS Microbiology Reviews*, vol. 34, no. 6, pp. 1037-1062, 2010.
- [38] D. Cooper, S. Liss, R. Longay and J. Zajic, "Surface Activity of *Mycobacterium* and *Pseudomonas*," *Journal of fermentation technology*, vol. 59, no. 2, pp. 97-101, 1989.
- [39] F. Peypoux, J. Bonmatin and J. Wallach, "Recent trends in the biochemistry of surfactin," *Applied microbiology and biotechnology*, vol. 51, no. 5, pp. 553-563, 1999.
- [40] A. Grau, J. Gomez-Fernandez, F. Peypoux and A. Ortiz, "A study on the interactions of surfactin with phospholipid vesicles," *Biochimica et biophysica acta*, vol. 1418, no. 2, pp. 307-319, 1999.
- [41] D. Landman, C. Georgescu, D. Martin and J. Quale, "Polymyxins Revisited," *Clinical microbiology reviews*, vol. 21, no. 3, pp. 449-465, 2008.
- [42] T. Suzuki, K. Tanaka, J. Matsubara and S. Kimoshita, "Trehalose lipid and branched-b-hydroxy fatty acids formed by bacteria grown on n-alkanes," *Agricultural and biological chemistry*, vol. 33, no. 11, pp. 1619-1625, 1969.
- [43] A. Kucers, S. Crowe, M. Grayson and J. Hoy, "The Use of Antibiotics," in *Polymyxins*, Oxford, Butterworth-Heinemann, 1997, pp. 667-675.
- [44] J. Woodworth, E. J. Nyhart, G. Brier, J. Wolny and H. Black, "Single-Dose Pharmacokinetics and Antibacterial Activity of," *Antimicrobial agents and chemotherapy*, vol. 36, no. 2, pp. 318-325, 1992.
- [45] R. Baltz, V. Miao and S. Wrigley, "Natural products to drugs: daptomycin and related lipopeptide antibiotics," *Natural product reports*, vol. 22, no. 6, pp. 717-741, 2005.
- [46] D. Jung, A. Rozek, M. Okon and R. Hancock, "Structural transitions as determinants of the action of the calcium-dependent antibiotic daptomycin," *Chemistry & biology*, vol. 11, no. 7, pp. 949-957, 2004.
- [47] J. Muraih and M. Palmer, "Estimation of the subunit stoichiometry of the membrane-associated daptomycin oligomer by FRET.," *Biochimica et biophysica acta*, vol. 18, no. 7, pp. 1642-1647, 2012.
- [48] J. Qiu and L. Kirsch, "Evaluation of lipopeptide (daptomycin) aggregation using fluorescence, light scattering, and nuclear magnetic resonance spectroscopy.," *Journal of Pharmaceutical sciences*, vol. 103, no. 3, pp. 853-61, 2014.
- [49] T. Zhang, J. Muraih, B. MacCormick, J. Silverman and M. Palmer, "Daptomycin forms cation- and size-selective pores in model membranes.," *Biochimica et biophysica acta*, vol. 1838, no. 10, pp. 2425-2430, 2014.

- [50] J. Silverman, N. Perlmutter and H. Shapiro, "Correlation of Daptomycin Bactericidal Activity and Membrane Depolarization in *Staphylococcus aureus*," *Antimicrobial agents and chemotherapy*, vol. 47, no. 8, pp. 2538-2544, 2003.
- [51] W. Scott, S. Baek, D. Jung, R. Hancock and S. Straus, "NMR structural studies of the antibiotic lipopeptide daptomycin in DHPC micelles," *Biochimica et biophysica acta*, vol. 1768, no. 12, pp. 3116-3126, 2007.
- [52] D. Denning, "Echinocandin antifungal drugs," *The Lancet*, vol. 362, no. 9390, pp. 1142-1151, 2003.
- [53] A. Sucher, E. Chahine and H. Balcer, "Echinocandins: the newest class of antifungals," *Annals of Pharmacotherapy*, vol. 43, no. 10, pp. 1647-1657, 2009.
- [54] P. Jacques, "Surfactin and Other Lipopeptides from *Bacillus* spp.," *Biosurfactants*, vol. 20, pp. 57-91, 2010.
- [55] M. Ongena and P. Jacques, "Bacillus lipopeptides: versatile weapons for plant disease biocontrol," *Trends in Microbiology*, vol. 16, no. 3, pp. 115-125, 2008.
- [56] R. Maget-Dana and F. Peypoux, "Iturins, a special class of pore-forming lipopeptides: biological and physicochemical properties.," *Toxicology*, vol. 87, no. 1-3, pp. 151-174, 1994.
- [57] A. Moyne, R. Shelby, T. Cleveland and S. Tuzun, "Bacillomycin D: an iturin with antifungal activity against *Aspergillus flavus*," *Journal of Applied Microbiology*, vol. 90, no. 4, pp. 622-629, 2001.
- [58] N. Vanittanakom, W. Loeffler, U. Koch and G. Jung, "Fengycin--a novel antifungal lipopeptide antibiotic produced by *Bacillus subtilis* F-29-3.," *The Journal of Antibiotics*, vol. 39, no. 7, pp. 888-901, 1986.
- [59] M. Bechet, T. Carade, W. Hussein, A. Abderrahmani, M. Chollet, V. Leclere, T. Dubois, D. Lereclus, M. Pupind and P. Jacques, "Structure, biosynthesis, and properties of kurstakins, nonribosomal lipopeptides from *Bacillus* spp.," *Applied Microbiology and Biotechnology*, vol. 95, no. 3, pp. 593-600, 2012.
- [60] B. Matthew and M. Nath, "Recent approaches to antifungal therapy for invasive mycoses," *ChemMedChem*, vol. 4, no. 3, pp. 310-323, 2009.
- [61] O. Cornely, J. Vehreschild and A. Ullmann, "Is there a role for polyenes in treating invasive mycoses?," *Current Opinion in Infectious Diseases*, vol. 19, no. 6, pp. 565-570, 2006.
- [62] R. Laniado-Laborin and M. Cabrales-Vargas, "Amphotericin B: side effects and toxicity," *Revista Iberoamericana de Micrologia*, vol. 26, no. 4, pp. 223-227, 2009.

- [63] J. Milhaud, V. Ponsinet, M. Takashi and B. Michels, "Interactions of the drug amphotericin B with phospholipid membranes containing or not ergosterol: new insight into the role of ergosterol.," *Biochimica et Biophysica Acta*, vol. 1558, no. 2, pp. 95-108, 2002.
- [64] J. Torrado, R. Espada, M. Ballesteros and S. Torrado-Santiago, "Amphotericin B formulations and drug targeting," *Journal of Pharmaceutical Sciences*, vol. 97, no. 7, pp. 2405-2425, 2008.
- [65] J. Starzyk, M. Gruszecki, K. Tutaj, R. Luchowski, R. Szlajak, P. Wasko, W. Grudzinski, J. Czub and W. Guszecki, "Self-association of amphotericin B: spontaneous formation of molecular structures responsible for the toxic side effects of the antibiotic.," *The Journal of Physical Chemistry B*, vol. 118, no. 48, pp. 13821-13832, 2014.
- [66] K. Lintner, "Cosmetic or Dermopharmaceutical Use of Peptides for Healing, Hydrating and Improving Skin Appearance During Natural or Induced Aging". France Patent US6620419 B1, September 2003.
- [67] K. Katayama, J. Armendariz-Borunda, R. Raghov, A. Kang and J. Seyer, "A pentapeptide from type I procollagen promotes extracellular matrix production," *The Journal of Biological Chemistry*, vol. 268, no. 14, pp. 9941-9944, 1993.
- [68] C. Choi and D. Berson, "Cosmeceuticals," *Seminars in Cutaneous Medicine and Surgery*, vol. 25, no. 3, pp. 163-168, 2006.
- [69] N. Abu Samah and C. Heard, "Topically applied KTTKS: a review," *International Journal of Cosmetic Science*, vol. 33, no. 6, pp. 483-490, 2011.
- [70] M. Lupo and A. Cole, "Cosmeceutical peptides," *Dermatologic Therapy*, vol. 20, no. 5, pp. 343-349, 2007.
- [71] V. Castelletto, I. Hamley, J. Perez, L. Abezgauz and D. Danino, "Fibrillar superstructure from extended nanotapes formed by a collagen-stimulating peptide," *Chemical Communications*, vol. 46, no. 48, pp. 9185-9187, 2010.
- [72] V. Castelletto, I. Hamley, J. Adamcik, R. Mezzenga and J. Gummel, "Modulating self-assembly of a nanotape-forming peptide amphiphile with an oppositely charged surfactant," *Soft Matter*, vol. 8, no. 1, pp. 217-226, 2012.
- [73] A. Dehsorkhi, V. Castelletto, I. Hamley and P. Linder, "Influence of a non-ionic amphiphilic copolymer on the self-assembly of a peptide amphiphile that forms nanotapes," *Soft Matter*, vol. 8, no. 33, pp. 8608-8615, 2012.
- [74] V. Castelletto, I. Hamley, C. Whitehouse, P. Matts, R. Osbourne and E. Baker, "Self-Assembly of Palmitoyl Lipopeptides Used in Skin Care Products," *Langmuir*, vol. 29, no. 29, pp. 9149-9155, 2013.

- [75] N. Gay and M. Gangloff, "Structure and Function of Toll Receptors and Their Ligands," *Annual Review of Biochemistry*, vol. 76, pp. 141-165, 2007.
- [76] J. Bell, G. Mullen, C. Leifer, A. Mazzone, D. Davies and D. Segal, "Leucine-rich repeats and pathogen recognition in Toll-like receptors.," *Trends in Immunology*, vol. 24, no. 10, pp. 528-533, 2003.
- [77] E. Hennessey, A. Parker and L. O'Neill, "Targeting Toll-like receptors: emerging therapeutics?," *Nature Reviews. Drug discovery*, vol. 9, no. 4, pp. 293-307, 2010.
- [78] R. Mahla, M. Reddy, D. Prasad and H. Kumar, "Sweeten PAMPs: Role of Sugar Complexed PAMPs in Innate Immunity and Vaccine Biology.," *Frontiers in Immunology*, vol. 4, p. 248, 2013.
- [79] S. Kumar, H. Ingle, D. Prasad and H. Kumar, "Recognition of bacterial infection by innate immune sensors.," *Critical Reviews in Microbiology*, vol. 39, no. 3, pp. 229-246, 2013.
- [80] T. Kawai and S. Akira, "The role of pattern-recognition receptors in innate immunity: update on Toll-like receptors," *Nature Immunology*, vol. 11, no. 5, pp. 373-384, 2010.
- [81] K. Lim and L. Straudt, "Toll-like receptor signaling," *Cold Spring Harbor Perspectives in Biology*, vol. 5, no. 1, 2013.
- [82] L. O'Neill, D. Goldenbock and A. Bowie, "The history of Toll-like receptors – redefining innate immunity," *Nature Reviews Immunology*, vol. 13, no. 6, pp. 453-460, 2013.
- [83] M. Gilliet, W. Cao and Y. Liu, "Plasmacytoid dendritic cells: sensing nucleic acids in viral infection and autoimmune diseases.," *Nature Reviews. Immunology*, vol. 8, no. 8, pp. 594-606, 2008.
- [84] N. Bhardwaj, "TLR Agonists: Are They Good Adjuvants?," *Cancer J*, vol. 16, no. 4, pp. 382-391, 2011.
- [85] F. Rudilla, C. Fayolle, N. Casares, M. Durantez, L. Arribillaga, T. Lozano, L. Villanueva, R. Pio, P. Sarobe, C. Leclerc, J. Prieto and J. Lasarte, "Combination of a TLR4 ligand and anaphylatoxin C5a for the induction of antigen-specific cytotoxic T cell responses," *Vaccine*, vol. 30, no. 18, pp. 2848-2858, 2012.
- [86] G. Stone, S. Barzee, V. Snarsky, C. Santucci, B. Tran, R. Langer, G. Zugates, D. Anderson and R. Kornbluth, "Nanoparticle-delivered multimeric soluble CD40L DNA combined with Toll-Like Receptor agonists as a treatment for melanoma.," *PLoS One*, vol. 4, no. 10, p. e7334, 2009.
- [87] C. Schneider, T. Schmidt, C. Ziske, K. Tiemann, K. Lee, V. Uhlinsky, P. Behrens, T. Sauerbruch, I. Schmidt-Wolf, P. Muhlrath, J. Schmidt and A. Marten, "Tumour suppression induced by the macrophage activating lipopeptide MALP-2 in an ultrasound

- guided pancreatic carcinoma mouse model.," *Gut*, vol. 53, no. 3, pp. 355-361, 2004.
- [88] M. Davis, D. Vasquez-Dunddel, J. Fu, E. Albesiano, D. Pardoli and Y. Kim, "Intratumoral administration of TLR4 agonist absorbed into a cellular vector improves antitumor responses.," *Clinical Cancer Research*, vol. 17, no. 12, pp. 3984-3992, 2011.
- [89] S. Kaczanowska, A. Joesph and E. Davila, "TLR agonists: our best frenemy in cancer immunotherapy," *Journal of Leukocyte Biology*, vol. 93, no. 6, pp. 847-863, 2013.
- [90] S. Adams, "Toll-like receptor agonists in cancer therapy," *Immunotherapy*, vol. 1, no. 6, pp. 949-964, 2009.
- [91] S. Tsuji, M. Matsuomo, O. Takeuchi, S. Akira, I. Azuma, A. Hayashi, K. Toyoshima and T. Seya, "Maturation of human dendritic cells by cell wall skeleton of *Mycobacterium bovis* bacillus Calmette-Guérin: involvement of toll-like receptors.," *Infection and Immunity*, vol. 68, no. 12, pp. 6883-6890, 2000.
- [92] J. Uehori, M. Matsumoto, S. Tsuji, T. Akazawa, O. Takeuchi, S. Akira, T. Kawata, I. Azuma, K. Toyoshima and T. Seya, "Simultaneous Blocking of Human Toll-Like Receptors 2 and 4 Suppresses Myeloid Dendritic Cell Activation Induced by *Mycobacterium bovis* Bacillus Calmette-Guérin Peptidoglycan," *Infection and Immunity*, vol. 71, no. 8, pp. 4238-4249, 2003.
- [93] J. Ulrich, K. Masihi and W. Lange, "Mechanisms of nonspecific resistance to microbial infections induced by trehalose dimycolate (TDM) and monophosphoryl lipid A (MPL)," in *Advances in the biosciences*, Oxford, United Kingdom, Pergamon Journals Ltd, 1988, pp. 167-178.
- [94] N. Garcon, D. Descamps, M. Leyssen, M. Stoffel and A. Pasquale, "Designing Vaccines against Human Papillomavirus and Hepatitis B Virus: Similarities and Differences for Preventable Viral Infections and role of AS04 Adjuvant System in Addressing Specific Challenges," *Journal of Vaccines and Vaccination*, vol. 3, no. 130, pp. 1-12, 2012.
- [95] M. Tomai, R. Miller, K. Lipson, W. Kieper, I. Zarraga and J. Vasilakos, "Resiquimod and other immune response modifiers as vaccine adjuvants," *Expert Review of Vaccines*, vol. 6, no. 5, pp. 835-847, 2007.
- [96] R. Garay, P. Viens, J. Bauer, G. Normier, M. Bardou, J. Jeannin and C. Chiavaroli, "Cancer relapse under chemotherapy: Why TLR2/4 receptor agonists can help," *European Journal of Pharmacology*, vol. 563, no. 1-3, pp. 1-17, 2007.
- [97] C. Ruegg, A. Yilmaz, G. Bieler, J. Bamat, P. Chaubert and F. Lejeune, "Evidence for the involvement of endothelial cell integrin α V β 3 in the disruption of the tumor vasculature induced by TNF and IFN- γ ," *Nature Medicine*, vol. 4, no. 4, pp. 408-414, 1998.

- [98] F. Re and J. Strominger, "Heterogeneity of TLR-induced responses in dendritic cells: from innate to adaptive immunity," *Immunobiology*, vol. 209, no. 1-2, pp. 191-198, 2004.
- [99] L. Milas, K. Mason, H. Ariga, N. Hunter, R. Neal, D. Valdecanas, A. Krieg and J. Whisnant, "CpG Oligodeoxynucleotide Enhances Tumor Response to Radiation," *Cancer Research*, vol. 64, no. 15, pp. 5074-5077, 2004.
- [100] K. Mason, H. Ariga, R. Neal, D. Valdecanas, N. Hunter, A. Krieg, J. Whisnant and L. Milas, "Targeting Toll-like Receptor 9 with CpG Oligodeoxynucleotides Enhances Tumor Response to Fractionated Radiotherapy," *Cancer Research*, vol. 11, no. 1, pp. 361-369, 2005.
- [101] A. Salazar, H. Levy, S. Ondra, M. Kende, B. Scherokman, D. Brown, H. Mena, N. Martin, K. Schwab, D. Donovan, D. Dougherty, M. Pulliam, M. Ippolito, M. Graves, H. Brown and A. Ommaya, "Long-term treatment of malignant gliomas with intramuscularly administered polyinosinic-polycytidylic acid stabilized with polylysine and carboxymethylcellulose: an open pilot study.," *Neurosurgery*, vol. 38, no. 6, pp. 1103-1104, 1996.
- [102] J. Friedberg, H. Kim, M. McCauley, E. Hessel, P. Sims, D. Fisher, L. Nadler, R. Coffman and A. Freedman, "Combination immunotherapy with a CpG oligonucleotide (1018 ISS) and rituximab in patients with non-Hodgkin lymphoma: increased interferon- α/β -inducible gene expression, without significant toxicity," *Blood*, vol. 105, no. 2, pp. 489-495, 2005.
- [103] C. Link, R. Gavioli, T. Ebensen, A. Canella, E. Reinhard and C. Guzman, "The Toll-like receptor ligand MALP-2 stimulates dendritic cell maturation and modulates proteasome composition and activity," *European Journal of Immunology*, vol. 34, no. 3, pp. 899-907, 2004.
- [104] O. Takeuchi, A. Kaufmann, K. grote, T. Kawai, K. Hoshino, M. Morr, P. Muhlradt and S. Akira, "Cutting Edge: preferentially the R-stereoisomer of the mycoplasmal lipopeptide macrophage-activating lipopeptide -2 activates immune cells through a toll-like receptor 2- and MyD88-dependent signalling pathway," *Journal of Immunology*, vol. 164, no. 2, pp. 554-557, 2000.
- [105] K. Reppe, T. L. A. Tschernig, V. van Laak, K. Grote, M. Zemlin, B. Gutbier, H. Muller, M. Kursar, H. Schutte, S. Rosseau, R. Pabst, N. Suttorp and M. Witzenrath, "Immuno-stimulation with macrophage-activating lipopeptide-2 increased survival in murine pneumonia," *American Journal of Respiratory Cell and Molecular Biology*, vol. 40, no. 4, pp. 474-481, 2009.
- [106] W. Zeng, S. Ghosh, Y. Lau, L. Brown and D. Jackson, "Highly immunogenic and totally synthetic lipopeptides as self-adjuvanting immunocontraceptive vaccines," *Journal of Immunology*, vol. 169, no. 9, pp. 4905-4912, 2002.
- [107] D. Jackson, Y. Lau, T. Le, A. Suhrbier, G. Deliyannis, C. Cheers, C. Smith, W. Zeng and L. Brown, "A totally synthetic vaccine of generic structure that targets Toll-like receptor 2

- on dendritic cells and promotes antibody or cytotoxic T cell responses," *Proceedings of the National Academy of Sciences of the United States of America*, vol. 101, no. 43, pp. 15440-15445, 2004.
- [108] B. Chua, W. Zeng and D. Jackson, "Synthesis of Toll-like receptor-2 targeting lipopeptides as self-adjvanting vaccines," *Methods in Molecular Biology*, vol. 494, pp. 247-261, 2008.
- [109] A. Tan, E. Mifsud, W. Zeng, K. Edenborough, J. Mcvernon, L. Brown and D. Jackson, "Intranasal administration of the TLR2 agonist Pam2Cys provides rapid protection against influenza in mice," *Molecular Pharmaceutics*, vol. 9, no. 9, pp. 2710-2718, 2012.
- [110] S. Zimmerman, O. Egeter, S. Hausmann, G. Lipford, M. Rocken, H. Wagner and K. Heeg, "Cutting edge: CpG oligodeoxynucleotides trigger protective and curative Th1 responses in lethal murine leishmaniasis," *Journal of Immunology*, vol. 160, no. 8, pp. 3627-3630, 1998.
- [111] A. Harandi, K. Eriksson and J. Holmgren, "A protective role of locally administered immunostimulatory CpG oligodeoxynucleotide in a mouse model of genital herpes infection," *Journal of Virology*, vol. 77, no. 2, pp. 953-962, 2003.
- [112] K. Elkins, T. Rhinehart-Jones, S. Stibitz, J. Conover and D. Klinman, "Bacterial DNA containing CpG motifs stimulates lymphocyte-dependent protection of mice against lethal infection with intracellular bacteria," *Journal of Immunology*, vol. 162, no. 4, pp. 2291-2298, 1999.
- [113] T. Jiang, H. Zhai, X. Li, Y. Deng, J. Liu, L. Xu, J. Han, R. Cao, E. Qin and C. Qin, "CpG oligodeoxynucleotides protect against the 2009 H1N1 pandemic influenza virus infection in a murine model," *Antiviral Research*, vol. 89, no. 1, pp. 124-126, 2011.
- [114] J. Duggan, D. You, J. Cleaver, D. Larson, R. Garza, F. Guzman Pruneda, M. Tuvim, J. Zhang, B. Dickey and S. Evans, "Synergistic interactions of TLR2/6 and TLR9 induce a high level of resistance to lung infection in mice," *Journal of Immunology*, vol. 186, no. 10, pp. 5916-5926, 2011.
- [115] J. Meijer, M. Henckens, D. Löwik and J. van Hest, "Disassembling peptide-based fibres by switching the hydrophobic–hydrophilic balance," *Soft Matter*, no. 9, pp. 1135-1137, 2007.
- [116] D. Löwik, I. Shklyarevskiy, L. Ruizendaal, P. Christianen, J. Maan and J. van Hest, "A highly ordered material from magnetically aligned peptide amphiphile nanofiber assemblies," *Advanced Materials*, vol. 19, no. 9, pp. 1191-1195, 2007.
- [117] J. Meijer, M. Roeters, V. Viola, D. Löwik, G. Vriend and J. van Hest, "Stabilization of peptide fibrils by hydrophobic interaction," *Langmuir*, vol. 23, no. 4, pp. 2058-2063, 2007.

- [118] T. Muraoka, C.-Y. Koh, H. Cui and S. Stupp, "Light-triggered bioactivity in three dimensions," *Angewandte Chemie*, vol. 48, no. 32, pp. 5946-5949, 2009.
- [119] T. Muraoka, H. Cui and S. Stupp, "Quadruple helix formation of a photoresponsive peptide amphiphile and its light-triggered dissociation into single fibers," *Journal of the American Chemical Society*, vol. 130, no. 10, pp. 2946-2947, 2008.
- [120] S. Sur, J. Matson, M. Webber, C. Newcomb and S. Stupp, "Photodynamic control of bioactivity in a nanofiber matrix," *ACS nano*, vol. 6, no. 12, pp. 10776-10785, 2012.
- [121] J. Miravet, B. Escuder, M. Segarra-Maset, M. Tena-Solsona, I. Hamley, A. Dehsorkhi and V. Castelletto, "Self-assembly of a peptide amphiphile: transition from nanotape fibrils to micelles," *Soft Matter*, vol. 9, no. 13, pp. 3558-3564, 2013.
- [122] P. Palladino, V. Castelletto, A. Dehsorkhi, D. Stensenko and I. Hamley, "Conformation and Self-Association of Peptide Amphiphiles Based on the KTTKS Collagen Sequence," *Langmuir*, vol. 28, no. 33, pp. 12209-12215, 2012.
- [123] I. Hamley, A. Dehsorkhi, V. Castelletto, S. Fuzeland, S. Atkins, J. Seitsonen and J. Ruokolainen, "Reversible helical ribbon unwinding transition of a self-assembling peptide amphiphile," *Soft Matter*, vol. 9, no. 39, pp. 9290-9293, 2013.
- [124] A. Dehsorkhi, V. Castelletto, I. Hamley, J. Adamcik and R. Mezzenga, "The effect of pH on the self-assembly of a collagen derived peptide amphiphile," *Soft Matter*, vol. 9, no. 26, pp. 6033-6036, 2013.
- [125] N. Peppas, "Preparation methods and structure of hydrogels," *Biomaterials Science*, vol. 2, no. 25, pp. 35-37, 2003.
- [126] N. Peppas, P. Bures, W. Leobandung and H. Ichikawa, "Hydrogels in pharmaceutical formulations," *European Journal of Pharmaceutics and Biopharmaceutics*, vol. 50, no. 1, pp. 27-46, 2000.
- [127] K. Lee and D. Mooney, "Hydrogels for tissue engineering," *Chemical Reviews*, vol. 101, no. 7, pp. 1869-1879, 2001.
- [128] S. Pulpura and J. Kohn, "Trends in the development of bioresorbable polymers for medical applications," *Journal of Biomaterials Applications*, vol. 6, no. 3, pp. 216-250, 1992.
- [129] M. Tibbitt and K. Anseth, "Hydrogels as Extracellular Matrix Mimics for 3D Cell Culture," *Biotechnology and Bioengineering*, vol. 103, no. 4, pp. 655-663, 2009.
- [130] O. Wichterle and D. Lim, "Hydrophilic gels for biological use," *Nature*, vol. 185, no. 1, pp. 117-118, 1960.

- [131] T. Meyvis, S. De Smedt, J. Demeester and W. Hennink, "Influence of the degradation mechanism of hydrogels on their elastic and swelling properties during degradation," *Macromolecules*, vol. 33, no. 13, pp. 4717-4725, 2000.
- [132] K. Huh, J. Hashi, T. Ooya and N. Yui, "Synthesis and characterization of dextran grafted with poly(N-isopropylacrylamide-co-N,N-dimethyl-acrylamide)," *Macromolecular Chemistry*, vol. 201, no. 5, pp. 613-619, 2000.
- [133] J. West and J. Hubbell, "Polymeric biomaterials with degradation sites for proteases involved in cell migration," *Macromolecules*, vol. 32, no. 1, pp. 241-244, 1999.
- [134] P. Alexandridis, D. Z Zhou and A. Khan, "Lyotropic liquid crystallinity in amphiphilic block copolymers: Temperature effects on phase behaviour and structure for poly(ethylene oxide)-b-poly(propylene oxide)-b-poly(ethylene oxide) copolymers o," *Langmuir*, vol. 12, no. 11, pp. 2690-2700, 1996.
- [135] K. Huh and Y. Bae, "Synthesis and characterization of poly(ethylene glycol)/poly(L-lactic acid) alternating multiblock copolymers," *Polymer*, vol. 40, no. 22, pp. 6147-6155, 1999.
- [136] B. Tighe, "The design of polymers for contact lens applications," *Polymer International*, vol. 8, no. 3, pp. 71-77, 1976.
- [137] A. Kidane, J. Szabocsik and K. Park, "Accelerated study on lysozyme deposition on poly(HEMA) conact lenses," *Biomaterials*, vol. 19, no. 22, pp. 2051-2055, 1998.
- [138] Y. Qiu and K. Park, "Environment-sensitive hydrogels for drug delivery," *Advanced Drug Delivery Reviews*, vol. 64, no. 1, pp. 49-60, 2012.
- [139] B. Ratner and S. Bryant, "Biomaterials: Where we have been and where we are going," *Annual Review of Biomedical Engineering*, vol. 6, no. 1, pp. 41-75, 2004.
- [140] R. Edmonson, J. Broglie, A. Adcock and L. Yang, "Three-dimensional cell culture systems and their applications in drug discovery and cell-based biosensors," *Assay and Drug Development Technologies*, vol. 12, no. 4, pp. 207-218, 2014.
- [141] F. Pampaloni, E. Reynaud and E. Stelzer, "The third dimension bridges the gap between cell culture and live tissue," *Nature Reviews, Molecular Cell Biology*, vol. 8, no. 10, pp. 839-845, 2007.
- [142] O. Kwon, A. Kikuchi, M. Yamato, Y. Sakurai and T. Okano, "Rapid cell sheet detachment from poly(N-isopropylacrylamide)-grafted porous cell culture membranes," *Journal of Biomedical Materials Research*, vol. 50, no. 1, pp. 82-89, 2000.
- [143] M. Zelzer, S. Todd, A. Hirst, T. McDonald and R. Ulijn, "Enzyme responsive materials: design strategies and future developments," *Biomaterials Science*, vol. 1, no. 1, pp. 11-39, 2013.

- [144] R. Ulijn, N. Bibi, V. Jayawarna, P. Thornton, S. Todd, R. Mart, A. Smith and J. Gough, "Bioresponsive hydrogels," *Materials Today*, vol. 10, no. 4, pp. 40-48, 2007.
- [145] B. Jeschke, J. Meyer, A. Jonczyk, H. Kessler, P. Adamietz, N. Meenen, M. Kantlehner, C. Goepfert and B. Nies, "RGD-peptides for tissue engineering of articular cartilage," *Biomaterials*, vol. 23, no. 16, pp. 3455-3463, 2002.
- [146] G. Silva, C. Czeisler, K. Niece, E. Beniash, D. Harrington, J. Kessler and S. Stupp, "Selective differentiation of neural progenitor cells by high-epitope density," *Science*, vol. 303, no. 5662, pp. 1352-1355, 2004.
- [147] J. Rak and J. Weitz, "Heparin and angiogenesis," *Arteriosclerosis Thrombosis and Vascular Biology*, vol. 23, no. 11, pp. 1954-1955, 2003.
- [148] K. Ranjagam, H. Behanna, M. Hui, X. Han, J. Hulvat, J. Lomasney and S. Stupp, "Heparin binding nanostructures to promote growth of blood vessels," *Nano Letters*, vol. 6, no. 9, pp. 2086-2090, 2006.
- [149] S. Amano, R. Rohan, M. Kuroki, M. Tolentino and A. Adamis, "Requirement for vascular endothelial growth factor in wound- and inflammation-related corneal neovascularization," *Investigative Ophthalmology & Visual Science*, vol. 39, no. 1, pp. 18-22, 1998.
- [150] Q. P. Hou, P. De Bank and K. Shakesheff, "Injectable scaffolds for tissue regeneration," *Journal of Materials Chemistry*, vol. 14, no. 13, pp. 1915-1923, 2004.
- [151] H. Nagase, R. Visse and G. Murphy, "Structure and function of matrix metalloproteinases and TIMPs," *Cardiovascular Research*, vol. 69, no. 3, pp. 562-573, 2006.
- [152] R. Ulijn, "Enzyme-responsive materials: a new class of smart biomaterials," *Journal of Materials Chemistry*, vol. 16, no. 23, pp. 2217-2225, 2006.
- [153] S. Kiyonaka, K. Sada, I. Yoshimura, S. Shinkai, N. Kato and I. Hamachi, "Semi-wet peptide/protein array using supramolecular hydrogel," *Nature Materials*, vol. 3, no. 1, pp. 58-64, 2004.
- [154] V. Castelletto, J. McKendrick, I. Hamley, U. Olsson and C. Cenker, "PEGylated Amyloid Peptide Nanocontainer Delivery and Release System," *Langmuir*, vol. 26, no. 14, pp. 11624-11627, 2010.
- [155] I. Hamley, M. Krysmann, V. Castelletto and L. Noirez, "Multiple Lyotropic Polymorphism of a Poly(ethylene glycol)-Peptide Conjugate in Aqueous Solution," *Advanced Materials*, vol. 20, no. 23, pp. 4394-4397, 2008.
- [156] I. Hamley, G. Cheng and V. Castelletto, "A Thermoresponsive Hydrogel Based on Telechelic PEG End-Capped with Hydrophobic Dipeptides," *Macromolecular Bioscience*,

- vol. 11, no. 8, pp. 1068-1078, 2011.
- [157] V. Castelletto, G. Newby, Z. Zhu, I. Hamley and L. Noirez, "Self-assembly of PEGylated peptide conjugates containing a modified amyloid beta-peptide fragment," *Langmuir*, vol. 26, no. 12, pp. 9986-9996, 2010.
- [158] S. Ryan, G. Mantovani, X. Wang, D. Haddleton and D. Brayden, "Advances in PEGylation of important molecules: delivery aspects," *Expert Opinion on Drug Delivery*, vol. 5, no. 4, pp. 371-383, 2008.
- [159] I. Hamley, "PEG-Peptide Conjugates," *Biomacromolecules*, vol. 15, no. 5, pp. 1543-1559, 2014.
- [160] M. Edidin, "Fluorescent Labeling of Cell Surfaces," in *Methods in Cell Biology*, NJ, USA, Academic Press, 1989, pp. 88-93.
- [161] A. Chokkathukalam, D. Kim, M. Barrett, R. Breitling and D. Creek, "Stable isotope-labeling studies in metabolomics: new insights into structure and dynamics of metabolic networks," *Bioanalysis*, vol. 6, no. 4, pp. 511-524, 2014.
- [162] R. Pandey, F. Yu and A. Kumar, "Targeting Toll-like receptor signaling as a novel approach to prevent ocular infectious diseases," *Indian Journal of Medical Research*, vol. 138, no. 5, pp. 609-619, 2013.

Chapter 2 – The effect of lipid chain number on the self-assembly of Toll-like receptor agonist lipopeptides

2.1 Introduction

The innate immune system is a defence system and the first line against invading pathogens. In response to these pathogens, a range of pro-inflammatory mediators are released, simultaneously mobilising the adaptive immune system [1]. Toll-like receptors are a type of transmembrane receptor heavily involved in the innate immune response, found in a number of different organisms [2, 3]. They are expressed on the membranes of a number of different leukocytes, such as dendritic cells, monocytes and macrophages [4]. They detect lipoproteins found in bacteria, and trigger an immune reaction in response. There are a number of different TLRs which each detect different lipopeptides, and are located in different parts of the cell. Due to their importance in the innate immune response, TLR agonists have been labelled as an important therapeutic target, leading to the development of synthetic TLR agonists [5]. TLR2, activated by a large number of different bacteria, has been found to be unique in that it has been shown require assistance from TLR1 and 6 in order to initiate the majority of its cell signalling [1], (signalling through TLR2 alone has however also been reported [6]). It has also been found, through experimentation with macrophages from TLR-deficient mice, that TLR2 dimerised with TLR1 and TLR6 mediate responses to different lipopeptides. Studies have shown that TLR1 largely recognises triacylated lipopeptides, compared with TLR6 which recognises diacylated [7-9].

As part of the research into TLR agonists, it was found that lipopeptides N-acetylated via glycerol-linked cysteines are good stimulators of TLRs, especially TLR2 [10]. Based on Braun's lipoprotein, found abundantly in the cell membrane of many gram-negative bacteria, a

synthetic analog was produced. This was tripalmitoyl-S-glycerol-cysteine, or Pam3Cys, used for the purpose of boosting immunogenicity from influenza when bound to an MHC (major histocompatibility complex) epitope [11]. Using this as a starting point, a group of compounds were developed with differing numbers of palmitoyl lipid chains, 1, 2 and 3, attached to a CSK₄ peptide sequence, shortened to PamCSK₄, Pam₂CSK₄, and Pam₃CSK₄. Studies specifically investigating this group of compounds have shown binding of Pam₃CSK₄ to the TLR1/2 heterodimer induces the dimer into an “m” shape (shown in figure 1) due to the presence of an amide-bound lipid chain [12]. This extra lipid chain isn’t present on Pam₂CSK₄ and other diacylated peptides, and they therefore have a lower affinity for TLR1/2 due to an inability to induce a stable heterodimer. Another study revealed the reduced affinity the TLR2/6 complex has for triacylated peptides due to lack of binding site for the third lipid chain [13]. The lipid channel in TLR6 was shown through crystal structure experimentation to be blocked by two phenylalanines. In the case of diacylated peptides on the other hand, the heterodimerization of TLR2/6 gives an increased hydrophobic area in between the TLRs, which compensates for the lack of extra amide-bound lipid chain binding seen in the triacylated peptide-TLR1/2 complex.

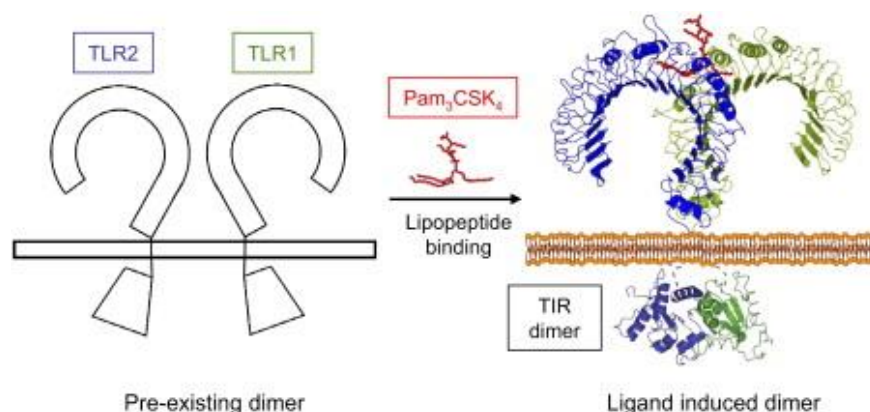


Figure 1 A model of ligand-induced heterodimerization of TLR1 and TLR2. Produced by Jin et al. [12].

Pam₃CSK₄, when bound to peptides, has previously been shown to induce CD8⁺ T-cells (cytotoxic T-cells which make up part of the immune system) at a greater rate than an adjuvant containing the Pam₃CSK₄ and peptide unbound to each other [14]. The effect of isomers on the compound's ability to generate an immune reaction was also investigated, using two different isomers around C-2 on the glycerol moiety, termed Pam-R and Pam-S. It was found that the R-Pam epimer induced greater interleukin-12 (IL-12) secretion than the S-Pam epimer, implying a higher degree of dendritic cell activation [15]. Despite the research into the binding conformations and immune response effects of the compounds, to our knowledge the self-assembly had not yet been investigated. The purpose of this chapter therefore is to shed light on the nature of their aggregation to suggest whether this may have an effect on their differing bioactivity.

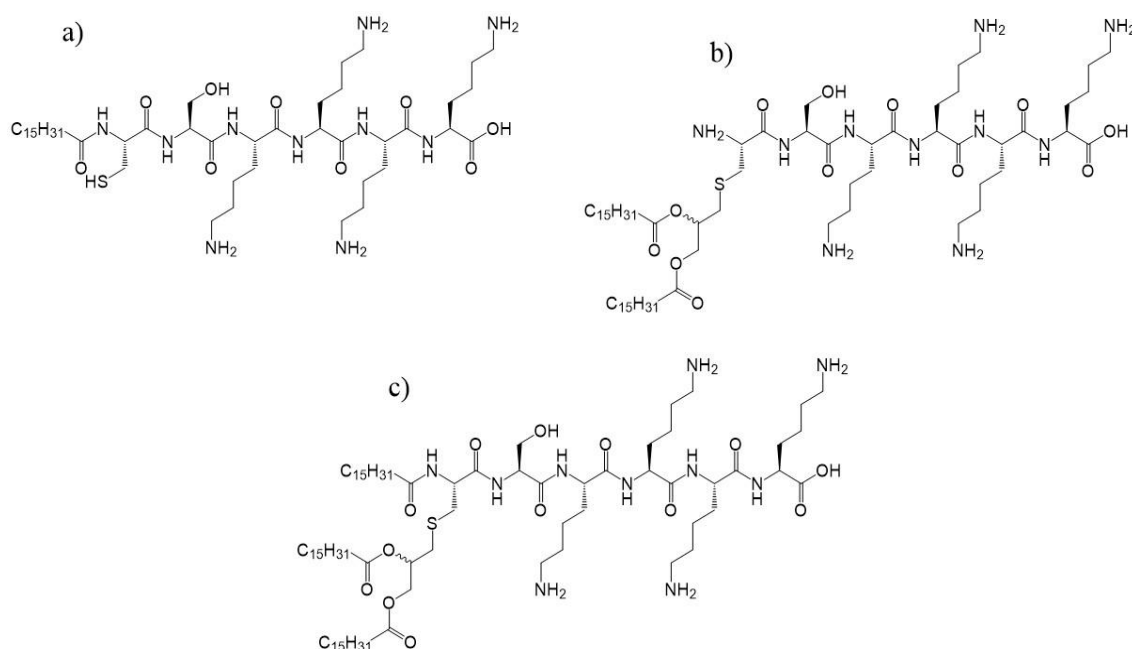


Figure 2 The molecular structures of each of the lipopeptides: a) PamCSK₄, b) Pam₂CSK₄, c) Pam₃CSK₄.

2.2 Materials & Methods

Pam₂CSK₄ and Pam₃CSK₄ were supplied as lyophilized powders by Invivogen, both as an HCl salt. Other Pam₃CSK₄, and PamCSK₄ samples were supplied as a TFA salt, and were purchased from EMC Microcollections (Tübingen, Germany). These powders were dissolved in provided limulus amoebocyte lysate (LAL) buffer solution to 0.5 wt%. LAL buffer solution is used in conjunction with these lipopeptides in standard bacterial endotoxin assays. The buffer contains different ionic species owing to the presence of extracts from horseshoe crab blood cells.

2.2.1 Fluorescence Assays

Fluorescence spectra were recorded with a Varian Cary Eclipse Fluorescence Spectrometer with samples in 4 mm inner width quartz cuvettes. The assays were performed using 1.3×10^{-3} – 0.13 wt% of the lipopeptides in 2.3×10^{-5} wt% pyrene solution. The samples were excited at $\lambda_{\text{ex}}=339$ nm, and the fluorescence emission was measured for $\lambda=(360-500$ nm).

2.2.2 Circular Dichroism (CD)

CD spectra were recorded using a Chirascan spectropolarimeter (Applied Photophysics, UK). Each sample (0.5 wt% lipopeptide) was placed in a cover slip cuvette (0.1 mm thick). Spectra are presented with absorbance $A < 2$ at any measured point with a 0.5 nm step, 1 nm bandwidth, and 1 second collection time per step in the range 20 °C – 60 °C with 10 °C steps on heating and 5 min equilibration at each temperature. Samples were then cooled to 20 °C and after a further 5 min equilibration, spectra were measured. The CD signal from the LAL water was subtracted from the CD data of the Pam solutions.

2.2.3 Small-Angle X-ray Scattering (SAXS)

Experiments were performed on beamline BM29 at the ESRF (Grenoble, France). A few microliters of samples were injected via an automated sample exchanger at a slow and very reproducible flux into a quartz capillary (1.8 mm internal diameter), which was then placed in front of the X-ray beam. The quartz capillary was enclosed in a vacuum chamber in order to avoid parasitic scattering. After the sample was injected in the capillary and reached the X-ray beam, the flow was stopped during the SAXS data acquisition. The sample was thermostated throughout its entire travel from the injector to the quartz capillary. SAXS experiments were performed at 20 °C. The $q = 4\pi\sin\theta/\lambda$ range is approximately 0.04-5 nm⁻¹, with $\lambda = 1.03 \text{ \AA}$ (12 keV) and a 2.87 m sample-detector distance. The images were captured using a PILATUS 1M detector. Data processing (background subtraction, radial averaging) was performed using dedicated beamline software ISPYB.

2.2.4 Cryo-Transmission electron microscopy (cryo-TEM)

Experiments were carried out at the laboratories of our collaborators at Aalto University in Finland using a field emission cryo-electron microscopy (JEOL JEM-3200FSC) operating at 200 kV. Images were taken using bright-field mode and zero loss energy filtering (omega type) with a slit width 20 eV. Micrographs were recorded using a Gatan UltraScan 4000 CCD camera. The specimen temperature was maintained at -187 °C during the imaging. Vitrified specimens were prepared using an automated FEI Vitrobot device using Quantifoil 3.5/1 holey carbon copper grids with 3.5 μm hole sizes. Grids were cleaned using a Gatan Solarus 9500 plasma cleaner just prior to use and then transferred into the environmental chamber of FEI Vitrobot at room temperature and 100% humidity. Thereafter, 3 μl of sample solution at 2 wt% concentration was applied on the grid, blotted once for 1 second and then vitrified in a 1/1

mixture of liquid ethane and propane at $-180\text{ }^{\circ}\text{C}$. Grids with vitrified sample solutions were maintained in a liquid nitrogen atmosphere and then cryo-transferred into the microscope.

2.3 Results & Discussion

The first experiment undertaken was to determine the cac of each of the three lipopeptides using the pyrene fluorescence technique, also used for a number of similar lipopeptide compounds [16, 17]. Seen in figure 3, this clearly showed that the number of lipid chains had an effect on the aggregation point. PamCSK₄ had a cac of $0.12 (\pm 0.02)$ wt%, Pam₂CSK₄ had a cac of $0.035 (\pm 0.003)$ wt%, and Pam₃CSK₄ had a cac of $0.003 (\pm 0.001)$ wt%.

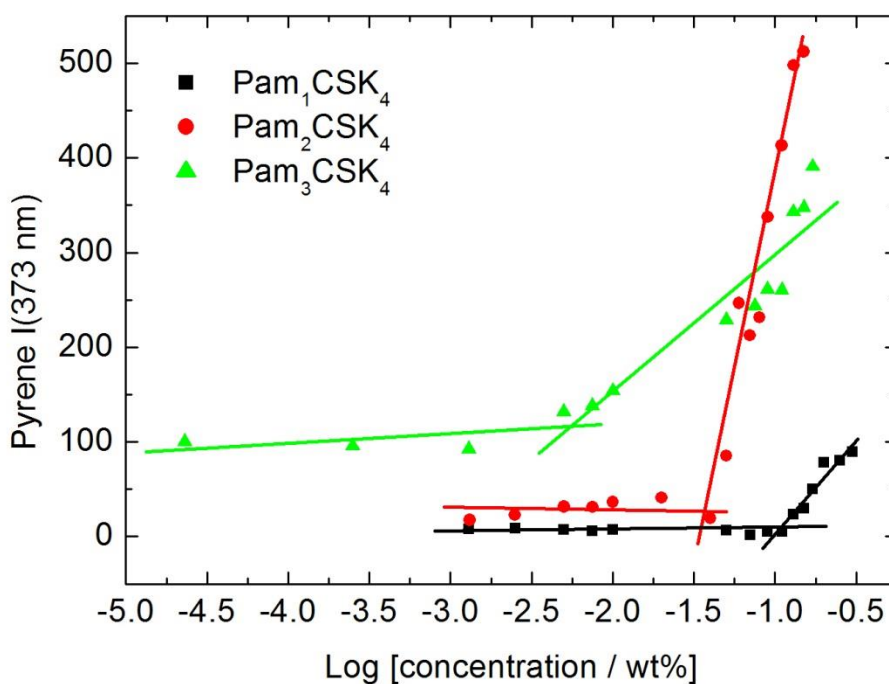


Figure 3 Critical aggregation concentrations of all three lipopeptides, indicated at the intersections of the lines. Concentration dependence of pyrene fluorescence at 373 nm.

The secondary structure of the lipopeptides was then examined using CD (figure 4), which again showed differences between the compounds. PamCSK₄ and Pam₂CSK₄ showed spectra which have previously been attributed to disordered conformations, with a minimum peak below 200 nm [18, 19]. Pam₂CSK₄ showed lower intensity, however, when compared with PamCSK₄. These two are in contrast to the spectra from Pam₃CSK₄, which is attributed to β -sheet secondary structure formation [18, 19]. This is due to the minimum peak seen at around 217 nm, followed by a maximum at around 200 nm.

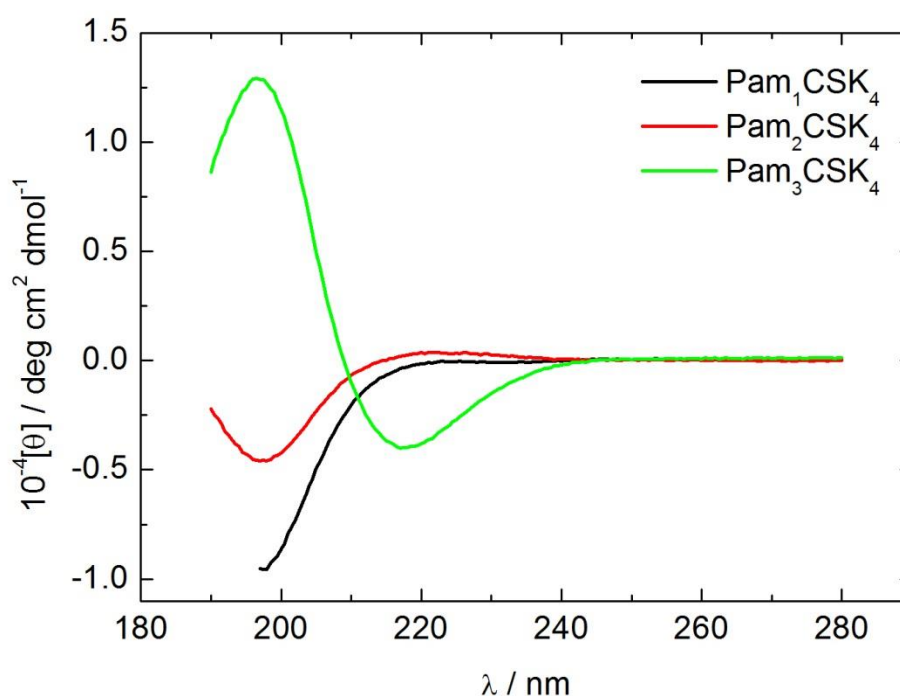


Figure 4 CD data of all three lipopeptides at 0.5 wt% taken at room temperature.

Representative cryo-TEM images were obtained of all 3 lipopeptides, shown in figure 5. Here Pam₃CSK₄ was found to differ from the other 2 again as it was shown to form a population of worm-like micelles in amongst spherical micelles. PamCSK₄ and Pam₂CSK₄ in contrast showed only spherical micelle formation. These results were used as a basis to complement our SAXS

results (figure 6). Spherical shell form factors were used for PamCSK₄ and Pam₂CSK₄, whereas Pam₃CSK₄ was fitted to a bilayer structure. The diameter of the spherical micelles observed in cryo-TEM images was consistent with those which fit the SAXS data. For the Pam₃CSK₄ compound, the bilayer thickness of 5.3 nm found through SAXS fitting implies interlocking of lipid chains. This is due to the known length of hexadecyl lipid chain being in the region of 1.6 nm, combined with the β -sheet forming hexapeptide headgroup of 6 lots of 0.33 nm, adding up to a total of 3.6 nm. This interdigitation of lipid chains has also previously been seen for other lipopeptides [16, 17]. The specific properties and dimensions of the structures these were fitted to are listed in table 1.

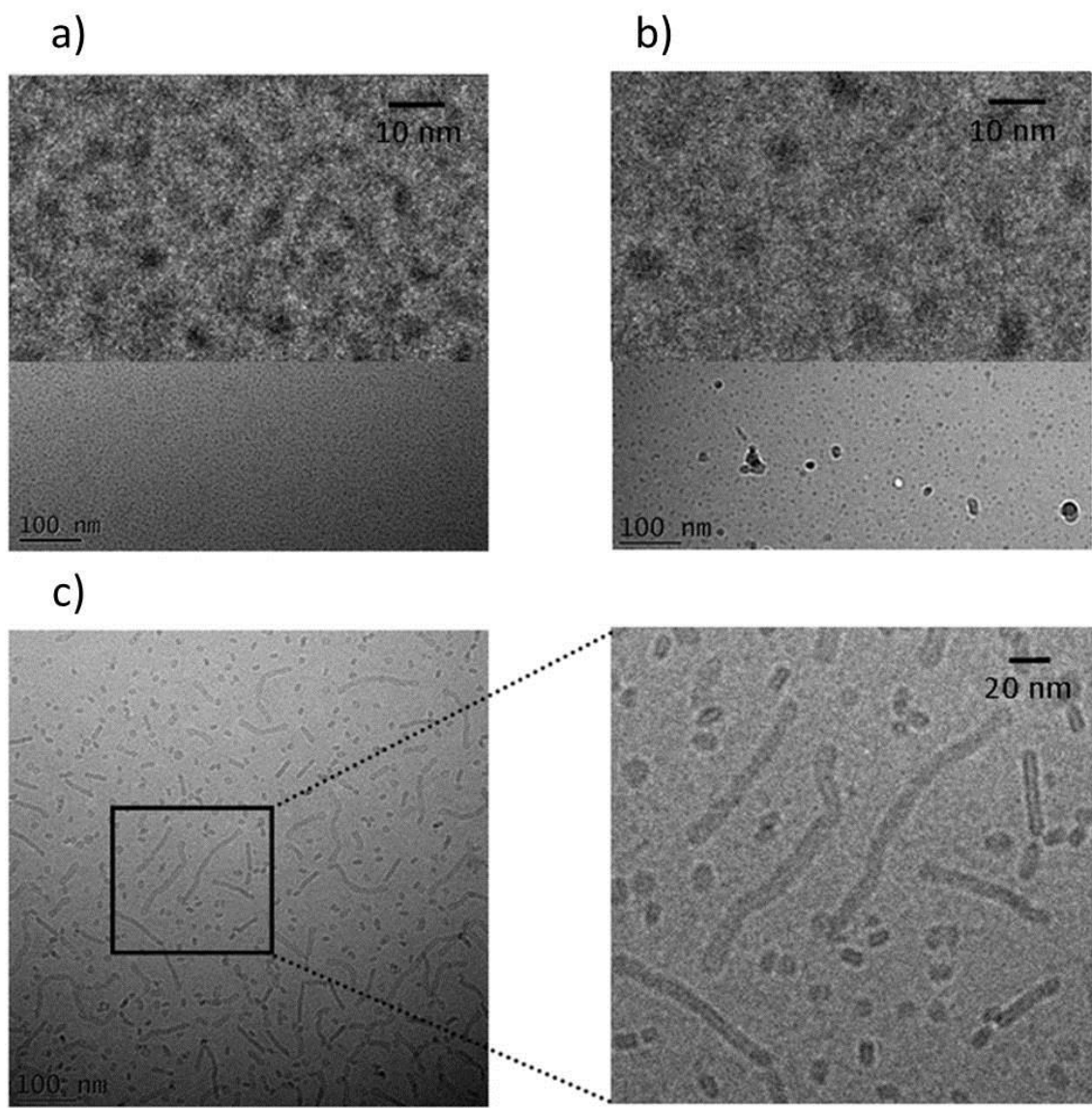


Figure 5 Representative cryo-TEM images of a) PamCSK₄, b) Pam₂CSK₄, and c) Pam₃CSK₄.
Figure courtesy of I.W. Hamley.

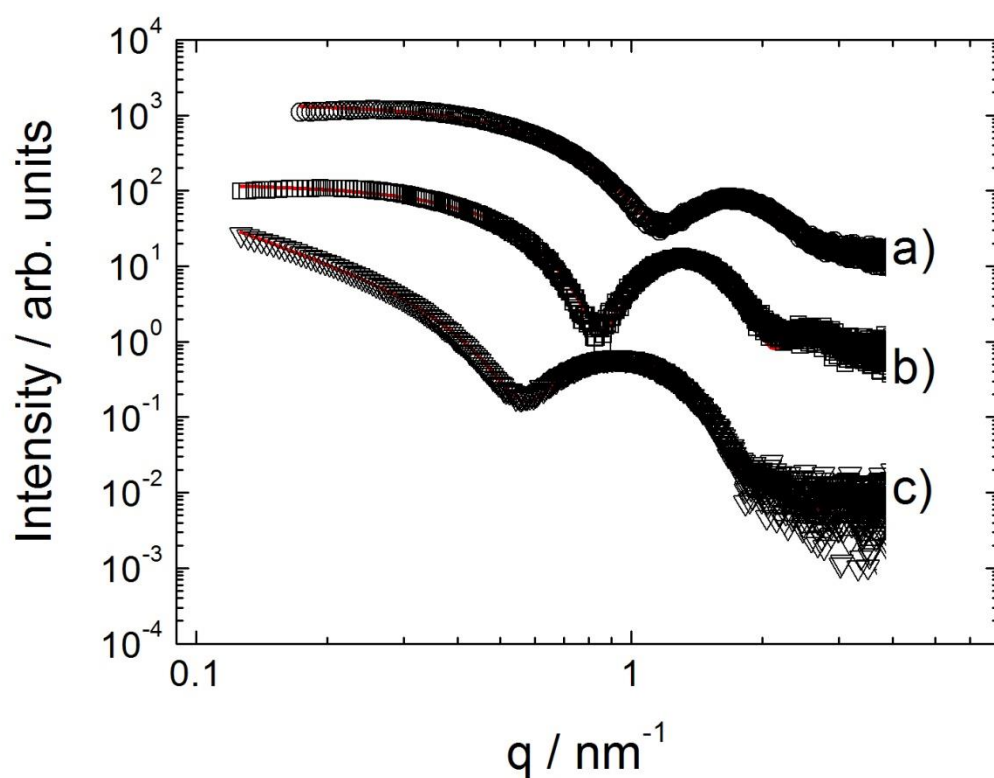


Figure 6 SAXS data with form factor models described in text for a) PamCSK₄, b) Pam₂CSK₄, c) Pam₃CSK₄. The open symbols are the experimental data, the solid red lines are the model form factor fits described in the text, with parameters shown in figure 6. Figure courtesy of I.W. Hamley.

| Spherical Micelle Form Factor | | | | | | |
|--------------------------------------|---------------------------|---|--------------------|-------------------|--|-------------------------|
| Sample | R(outer) ^a /nm | R(inner) ^b /nm | μ^c | v^d | Gaussian polydispersity parameters [R(outer)] ^c | Background ^f |
| PamCSK ₄ | 2.23 | 1.63 | -0.42 | 0.69 | N=1, $\sigma=0.625$ | 10 |
| Pam ₂ CSK ₄ | 3.30 | 2.42 | -0.67 | 0.033 | N=1, $\sigma=0.54$ | 0.08 |
| Gaussian Bilayer Form Factor | | | | | | |
| Sample | t/ ^g nm | $\sigma(\text{core}), \sigma(\text{out})^h$ /nm | $v(\text{core})^i$ | $v(\text{out})^j$ | Gaussian polydispersity parameters (t) ^k | Background ^l |
| Pam ₃ CSK ₄ | 5.33 | 3.89, 0.82 | -0.004 | 0.02 | N=0.17, $\sigma=0.71$ | 5.19 |

Table 1 Parameters for SAXS fitting form factor models using SASfit software, with corresponding equations available online in the SASfit manual.

^a Radius of outer core of micelle

^b Radius of inner core micelle

^c Ratio of core/shell scattering contrasts

^d Shell/solvent scattering contrast (arbitrary units)

^e Gaussian peak height N and half-width σ

^f Constant background term

^g Bilayer thickness

^h Width for core (lipid chain) electron density, σ_{core} , and outer (peptide) electron density, σ_{out} , Gaussian functions

ⁱ Scattering contrast of lipid core of bilayer (with respect to solvent) (arbitrary units)

^j Scattering contrast of peptide units at bilayer surface (with respect to solvent) (arbitrary units)

^k Gaussian peak height N and half-width σ

^l As well as the constant background, the radius of the bilayer objects was fixed at 500 nm. Since this is much larger than t, it does not influence the shape of the scattering profile.

Due to the purchasing of the lipopeptides from different sources, they were present as either hydrochloride or TFA salts. It was therefore necessary to determine whether these states had any effect on the self-assembly observed. Pam₃CSK₄, with both salts, was investigated through cryo-TEM and SAXS. This lipopeptide showed the formation of the previously mentioned worm-like micelles when in both states, as shown in figure 7. The same was seen in SAXS fitting (figure 8), where the same form factor model was used for both salt types, with very similar parameters.

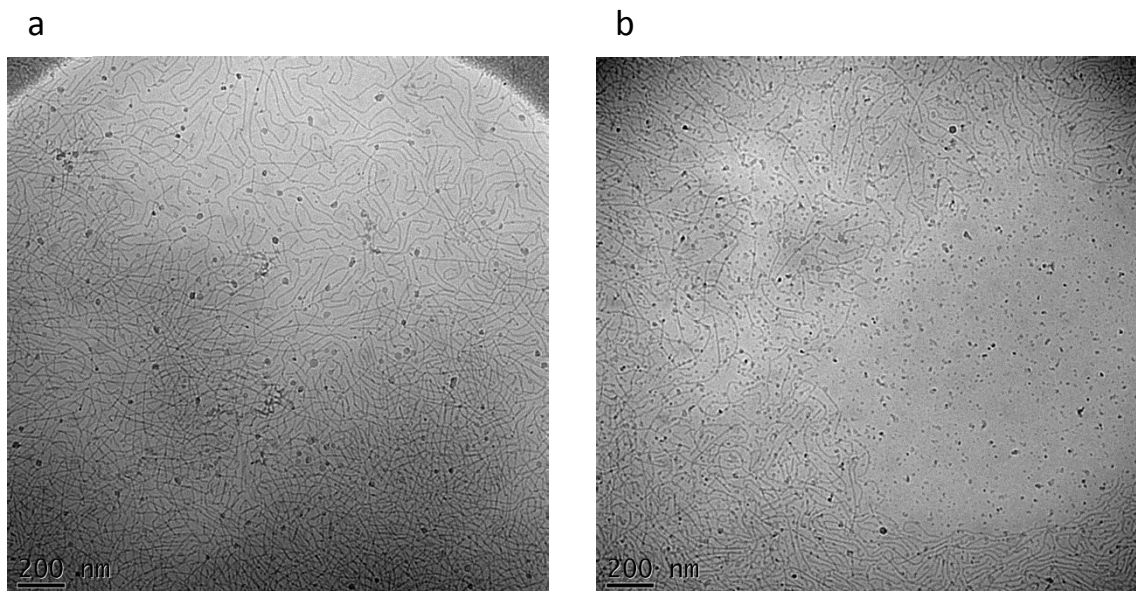


Figure 7 Representative cryo-TEM images of Pam₃CSK₄ salts; a) TFA, b) HCl.

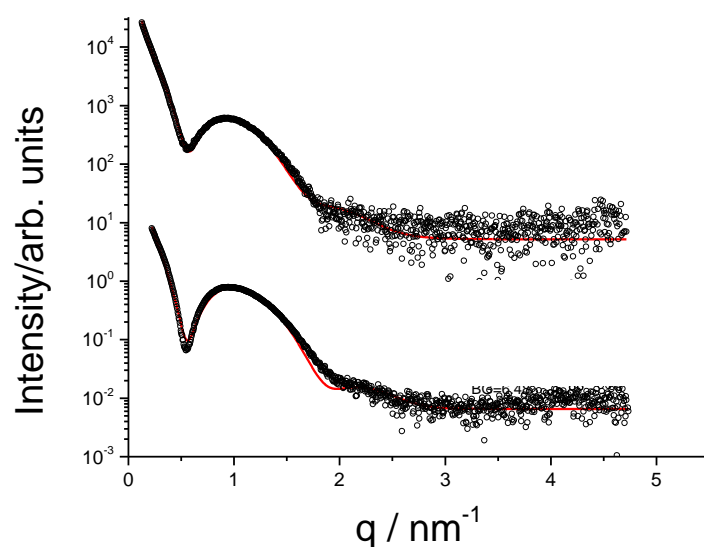


Figure 8 SAXS data for Pam_3CSK_4 salt, TFA at the top, HCl at the bottom. Figure courtesy of I.W. Hamley.

Based on the aforementioned results into self-assembly of the 3 lipopeptides, schematics are presented in figure 9. For PamCSK_4 and Pam_2CSK_4 , cryo-TEM and SAXS data clearly showed the presence of small spherical micelles, with the small radius consistent with disordered conformation shown through CD data. The radii of the self-assembled structures (2.2 nm for PamCSK_4 and 3.3 nm for Pam_2CSK_4) are explained by the extra lipid chain in the latter leading to a greater physical space being used. This sequestering of the lipid chains on the inside thus means that the charged KKKK sequence is present on the outside, with the CS linker in between separating from the hydrophobic centre. The Pam_3CSK_4 model is based on the presence of worm-like micelles and the successful fitting of the SAXS data to a bilayer structure. These structures are rare compared with the longer twisted nanotapes usually seen with other lipopeptides [20]. They have however been seen by another group which used a peptide amphiphile containing 13 alanine residues (chosen for their tendency towards α -helix formation) with 3 lysine residues interspersed to increase water solubility, attached to a singular 16 carbon chain [21]. The schematic of Pam_3CSK_4 was chosen based on the bilayer

SAXS and β -sheet CD data, showing a packed bilayer arrangement. It is assumed that the reason Pam₃CSK₄ did not form spherical micelles like the other 2 lipopeptides is the extra lipid chain constraining the packing, thus leading to the bilayer structure. As mentioned in the SAXS data discussion, a narrow width distribution was observed, incorporated into the proposed model, differing from the large distribution usually seen with nanotapes formed by lipopeptides.

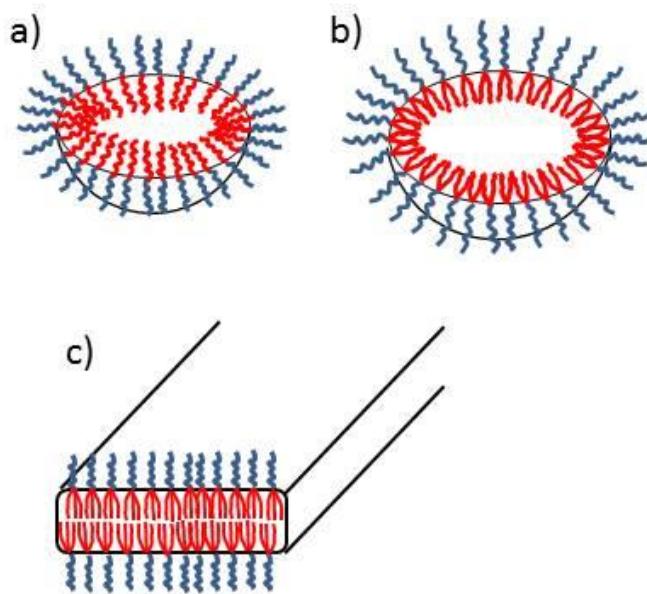


Figure 9 Proposed schematics of self-assembled structures of a) PamCSK₄, b) Pam₂CSK₄, c) Pam₃CSK₄.

The effect of temperature on the lipopeptides using temperature-dependent CD was investigated (figure 10). Previous studies into C₁₆ containing lipopeptides showed a change in structure at around 40 °C, also leading to a phase state change from gel to sol. We took spectra from each of the three lipopeptides at 10 °C increments from 20 – 60 °C, and then dropped the temperature back down to 20 °C for another measurement to determine whether any changes were reversible. The range 20 – 60 °C was chosen due to previous

research into palmitoyl-containing lipopeptides showing it to be the chain melting temperature range [22]. No significant changes were found upon heating and cooling PamCSK₄ and Pam₂CSK₄, but were for Pam₃CSK₄. The latter shows a change occurring between 30 and 40 °C, starting with β -sheet spectra and transitioning into a disordered structure at the higher temperatures. Upon cooling, this change was shown to be partially reversible, showing a return to β -sheet conformation, albeit at much lower intensity. Further investigation into whether the lipid chain melting may drive a change in the morphology of the self-assembled structures is a future area to target.

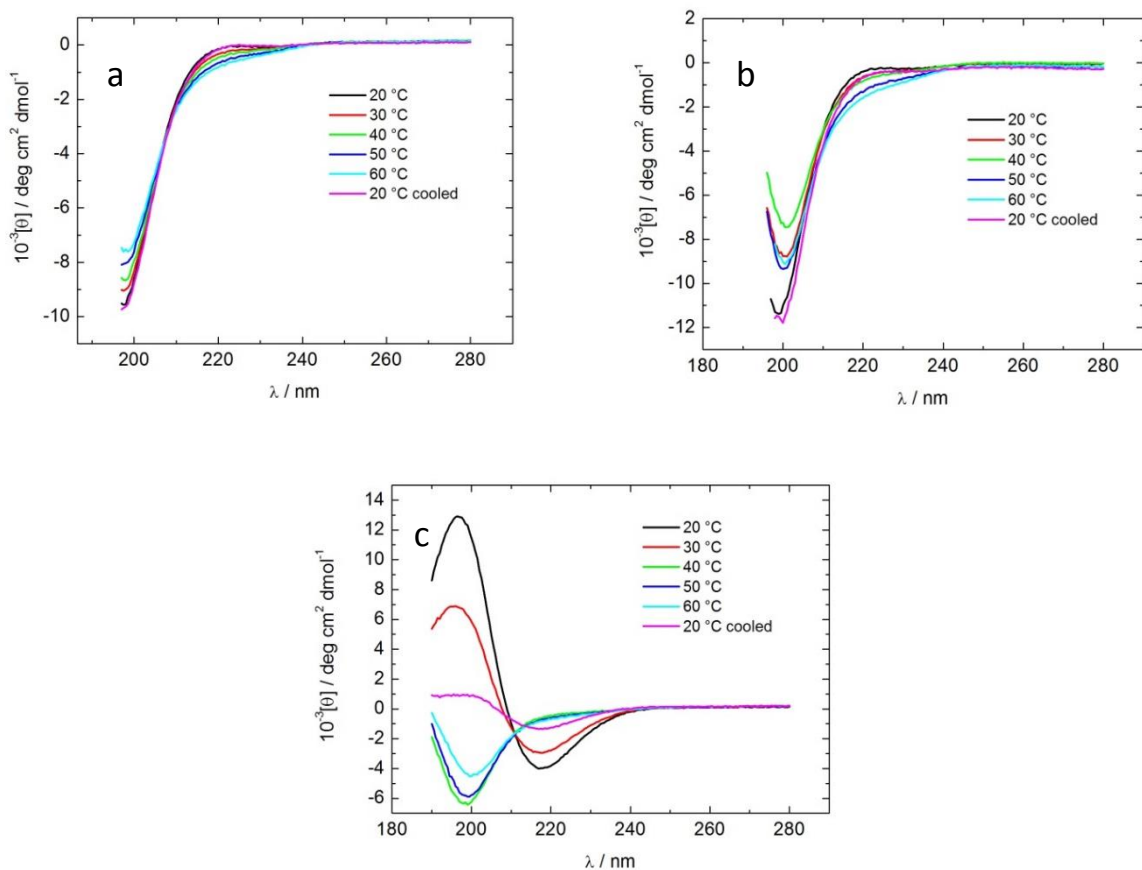


Figure 10 Temperature dependant CD spectra for a) PamCSK₄, b) Pam₂CSK₄, c) Pam₃CSK₄.

X-ray diffraction was attempted on the three lipopeptides through a previously used method of preparing higher concentration solutions, suspending a drop of the solution between two wax beads, and then allowing the solution to dry, ultimately forming a stalk to be analysed [23, 24]. However, despite following this protocol we were unable to develop stalks. Due to time constraints and technical issues, we were also unable to analyse the compounds through FTIR to confirm the secondary structures we had also seen through CD.

The purpose of this chapter was to investigate the effect that the number of lipid chains attached to a peptide can have on self-assembly. In this case we found that there is a difference when one and two chains are attached when compared with three. This may relate to the bioactivity of these compounds as, as previously mentioned, there is a difference in activation of different TLRs between the lipopeptides used in this study. To our knowledge, this link has not previously been made. This should therefore spark further research in the area of determining whether the self-assembled nanostructures have an effect on TLRs, and if so, by what mechanism. In the case of these particular lipopeptides, the presence of the cysteine linker residue as part of the peptide sequence may also be of interest, potentially to be used in the creation of cross-linked structures.

2.4 References

- [1] K. Omueti, J. Beyer, C. Johnson, E. Lyle and R. Tapping, "Domain exchange between human toll-like receptors 1 and 6 reveals a region required for lipopeptide discrimination.," *The Journal of Biological Chemistry*, vol. 280, no. 44, pp. 36616-36625, 2005.
- [2] E. Eriksson and D. Jackson, "Recent Advances with TLR2-Targeting Lipopeptide-Based Vaccines," *Current Protein & Peptide Science*, vol. 8, no. 4, pp. 412-417, 2007.
- [3] R. Thwaites, G. Chamberlain and S. Sacre, "Emerging role of endosomal toll-like receptors in rheumatoid arthritis," *Frontiers in Immunology*, vol. 5, pp. 1-10, 2014.
- [4] Y. Delneste, C. Beauvillain and P. Jeannin, "Innate immunity: structure and function of TLRs," *Medecine sciences*, vol. 23, no. 1, pp. 67-73, 2007.
- [5] T. Wright, A. Brooks, A. Didsbury, G. Williams, P. Harris, P. Dunbar and M. Brimble, "Direct peptide lipidation through thiol-ene coupling enables rapid synthesis and evaluation of self-adjuvanting vaccine candidates.," *Angewandte Chemie*, vol. 52, no. 40, pp. 10616-10619, 2013.
- [6] K. Farhat, S. Riekenberg, H. Heine, J. Debarry, R. Lang, J. Mages, U. Buwitt-Beckmann, K. Roschmann, G. Jung, K. Wiesmuller and A. Ulmer, "Heterodimerization of TLR2 with TLR1 or TLR6 expands the ligand spectrum but does not lead to differential signaling," *Journal of Leukocyte Biology*, vol. 83, no. 3, pp. 692-701, 2008.
- [7] O. Takeuchi, T. Kawai, P. Muhlrardt, M. Morr, J. Radolf, A. Zychlinsky, K. Takeda and S. Akira, "Discrimination of bacterial lipoproteins by Toll-like receptor 6," *International Immunology*, vol. 13, no. 7, pp. 933-940, 2001.
- [8] O. Takeuchi, S. Sato, T. Horiuchi, K. Hoshino, K. Takeda, Z. Dong, R. Modlin and S. Akira, "Cutting edge: role of Toll-like receptor 1 in mediating immune response to microbial lipoproteins," *Journal of Immunology*, vol. 169, no. 1, pp. 10-14, 2002.
- [9] L. Alexopoulou, V. Thomas, M. Schnare, Y. Lobet, J. Anquita, R. Schoen, R. Medzhitov, E. Fikrig and R. Flavell, "Hyporesponsiveness to vaccination with *Borrelia burgdorferi* OspA in humans and in TLR1- and TLR2-deficient mice," *Nature Medicine*, vol. 8, no. 8, pp. 878-884, 2002.
- [10] M. Zaman and I. Toth, "Immunostimulation by synthetic lipopeptide-based vaccine candidates: structure-activity relationships," *Frontiers in Immunology*, vol. 4, p. 318, 2013.
- [11] E. Borges, K. Wiesmuller, G. Jung and P. Walden, "Efficacy of synthetic vaccines in the induction of cytotoxic T lymphocytes. Comparison of the costimulating support provided by helper T cells and lipoamino acid," *Journal of Immunological Methods*, vol. 173, no. 2, pp. 253-263, 1994.
- [12] M. Jin, S. Kim, J. Heo, M. Lee, H. Kim, S. Paik, H. Lee and J. Lee, "Crystal structure of the TLR1-TLR2 heterodimer induced by binding of a tri-acylated lipopeptide," *Cell*, vol. 130,

no. 6, pp. 1071-1082, 2007.

- [13] J. Kang, X. Nan, M. Jin, S. Youn, S. Mah, S. Han, H. Lee, S. Paik and J. Lee, "Recognition of lipopeptide patterns by Toll-like receptor 2-Toll-like receptor 6 heterodimer," *Immunity*, vol. 31, no. 6, pp. 873-884, 2009.
- [14] S. Khan, M. Bijker, J. Weterings, H. Tanke, G. Adema, H. van, J. Drijfhout, C. Melief, H. Overkleeft, G. van der Marel, D. Filippov, S. van der Burg and F. Ossendorp, "Distinct uptake mechanisms but similar intracellular processing of two different toll-like receptor ligand-peptide conjugates in dendritic cells," *The Journal of Biological Chemistry*, vol. 282, pp. 21145-21159, 2007.
- [15] S. Khan, J. Weterings, C. Britten, A. de Jong, D. Graafland, C. Melief, S. van der Burg, G. van der Marel, H. Overkleeft, D. Filippov and F. Ossendorp, "Chirality of TLR-2 ligand Pam3CysSK4 in fully synthetic peptide conjugates critically influences the induction of specific CD8+ T-cells," *Molecular Immunology*, vol. 46, no. 6, pp. 1084-1091, 2009.
- [16] V. Castelletto, G. Cheng, C. Stain, C. Connon and I. Hamley, "Self-assembly of a peptide amphiphile containing L-carnosine and its mixtures with a multilamellar vesicle forming lipid," *Langmuir*, vol. 28, no. 31, pp. 11599-11608, 2012.
- [17] V. Castelletto, R. Gouveia, C. Connon and I. Hamley, "New RGD-peptide amphiphile mixtures containing a negatively charged diluent," *Faraday Discussions*, vol. 166, pp. 381-397, 2013.
- [18] C. Toniolo, F. Formaggio and R. Woody, "Electronic Circular Dichroism of Peptides," in *Comprehensive Chiroptical Spectroscopy: Applications in Stereochemical Analysis of Synthetic Compounds, Natural Products, and Biomolecules, Volume 2*, New York, Wiley-Blackwell, 2012.
- [19] B. Norden, A. Rodger and T. Dafforn, *Linear Dichroism and Circular Dichroism: A Textbook on Polarized-Light Spectroscopy*, Royal Society of Chemistry, 2010.
- [20] H. Cui, T. Muraoka, A. Cheetham and S. Stupp, "Self-assembly of giant peptide nanobelts," *Nano Letters*, vol. 9, no. 3, pp. 945-951, 2009.
- [21] T. Shimada, N. Sakamoto, R. Motokawa, S. Koizumi and M. Tirrell, "Self-assembly process of peptide amphiphile worm-like micelles," *The Journal of Physical Chemistry B*, vol. 116, no. 1, pp. 240-243, 2012.
- [22] D. Casey, K. Charalambous, A. Gee, R. Law and O. Ces, "Amphiphilic drug interactions with model cellular membranes are influenced by lipid chain-melting temperature," *Journal of the Royal Society*, vol. 11, no. 94, 2014.
- [23] A. Dehsorkhi, V. Castelletto and I. Hamley, "Influence of a non-ionic amphiphilic copolymer on the self-assembly of a peptide amphiphile that forms nanotapes," *Soft Matter*, vol. 8, no. 33, pp. 8608-8615, 2012.
- [24] A. Dehsorkhi, R. Gouveia, A. Smith, I. Hamley, V. Castelletto, C. Connon, M. Reza and J. Ruokolainen, "Self-assembly of a dual functional bioactive peptide amphiphile incorporating both matrix metalloprotease substrate and cell adhesion motifs," *Soft*

Matter, vol. 11, no. 16, pp. 3115-3124, 2015.

Chapter 3 - Self-assembly of Macrophage-Activating Lipopeptide (MALP-2)

3.1 Introduction

As previously mentioned in chapter 2, Toll-like receptors (TLRs) are a type of membrane receptor that play an important role in the conditioning of responses to bacterial lipopeptides, and creating a consequential immune response. Like the Pam_nCSK₄ samples investigated there, macrophage activating lipopeptide 2 (MALP-2) is another agonist of TLRs. Its molecular construction, shown in figure 1, consists of a GNNDESNISFKEK peptide sequence, bonded to a (2R)-3-((2-amino-3-oxobutyl)thio)propane-1,2-diyl dipalmitate lipid chain [1]. The “2” in the name MALP-2 relates to the 2 kDa weight of the lipopeptide. Lipidation of peptide chains leads to the compound having increased amphiphilicity, and subsequently self-assembly [2]. The self-assembly of the TLR agonist class and how it relates to bioactivity has not widely been investigated thus far. Lipopolysaccharide (LPS) and its lipid component, Lipid A, is one which has had some attention. One study found that when Lipid A aggregates, it has a greater bioactivity than in the monomeric state [3]. With LPS, there are varying results, with one group reporting increased activity when in aggregated state compared with monomeric [4], but with another finding monomeric to have higher activity [5].

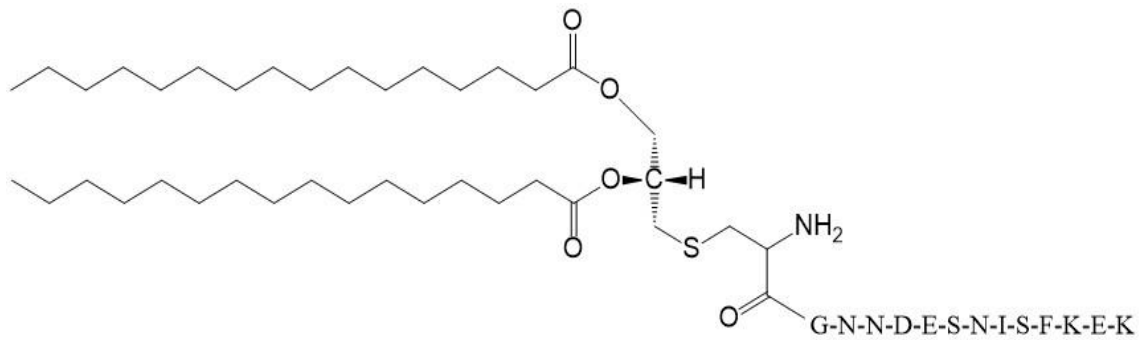


Figure 1 The molecular structure of MALP-2.

MALP-2, derived from *Mycoplasma fermentans* but now available synthetically, has been shown to exhibit stimulatory effects on macrophages and monocytes [6]. Using CD36, cluster of differentiation 36, (a cell surface receptor) as a co-receptor, it binds to the TLR2/6 heterodimer [7]. As mentioned in the previous chapter, this is due to MALP-2 being a diacylated peptide [8]. Through *in vivo* studies, its binding to TLR2/6 has then been shown to cause a cascade, increasing pro-inflammatory cytokines and chemokines, along with an increase in infiltration by neutrophils and lymphocytes [9, 10]. It has been found that there are two different stereoisomers of MALP-2, with the R isomer found to be 100 times more potent than the S isomer [11].

MALP-2 has been shown to have a variety of different applications. One study revealed an increase in leukocyte numbers and consequent suppression of early lung metastasis in mice [12]. Using a mouse model again, it was shown that MALP-2 was able to be used to improve the wound healing process through stimulation of mediators involved in early inflammation [13]. Another group found that in reconstructive surgery, MALP-2 could be applied to a porous polyethylene biomaterial used as a scaffolding to ease incorporation into the wound [14]. Rharbaoui et al. found that it stimulated a strong immune response in animals, highlighting the potential for it to be used as a vaccine adjuvant [15]. When MALP-2 was administered to

mice 24 hours before infection with *Streptococcus pneumoniae*, many of the clinical signs of infection were reduced and survival rates increased when compared with mice untreated with the compound [9]. Reppe et al. also found local pulmonary administration of MALP-2 in mice infected with influenza virus significantly reduced the level of bacteria in the lungs, a common complication of infection by the virus [16].

As with the Pam_nCSK₄ samples, to our knowledge the self-assembly of MALP-2 has not yet been characterised. In this chapter, the self-assembly of MALP-2 will be examined, and compared with that of the constituent peptide sequence GNNDESNISFKEK. The purpose will be to evaluate and compare the effects the peptide and lipid chain components have on the nature of the structures formed.

3.2 Materials and methods

MALP-2 was custom synthesised by Peptide Synthetics (UK). The average molecular mass was 2137.2 g mol⁻¹ (expected 2135.2 g mol⁻¹) with a purity >95%, as determined by analytical HPLC. The synthesis of this material is described elsewhere [1], although Peptide Synthetics have followed prior literature reports [17] to synthesise the lipid chain to which the peptide has been added by conventional stepwise solid phase peptide synthesis techniques. The starting material is an epoxide, (S)-(-)-glycidol (Sigma-Aldrich). Samples were dissolved in water, and all data are presented for samples at 0.5 wt% MALP-2 in water unless stated. The peptide GNNDESNISFKEK was custom synthesised by Peptide Synthetics. The average molecular mass was 1481.52 g mol⁻¹ (expected 1481.54 g mol⁻¹) with purity >95% as determined from analytical HPLC.

3.2.1 Fluorescence Spectroscopy

ANS (8-anilo-1-naphthalenesulfonic acid) and Thioflavin T (ThT) fluorescence were used in order to determine the cac. Spectra were recorded with a Varian Cary Eclipse fluorescence spectrophotometer with samples in 4 mm inner width quartz cuvettes. Pyrene assays were conducted using 1.3×10^{-3} – 0.13 wt% of MALP-2 in 2.3×10^{-5} wt% pyrene solution. The sample was excited at $\lambda_{\text{ex}}=339$ nm, and the fluorescence emission was measured for $\lambda= 360$ -500 nm. ANS, a fluorophore, is a probe sensitive to hydrophobic environments and so is suitable for these cac experiments [18]. Samples were excited at $\lambda_{\text{ex}}=356$ nm, and the fluorescence emission was measured for $\lambda= 400$ -670 nm, using a 74 μM ANS solution to solubilise the peptide. ThT is used in cac assays in order to detect formation of amyloid-like structures such as β -sheets, and thus is used in cac assays for amyloid fibril-forming peptides [19]. Samples were excited at $\lambda_{\text{ex}}=440$ nm, and the fluorescence emission was measured for $\lambda= 460$ -600 nm, and the peptide dissolved in a 5.0×10^{-3} wt% ThT solution.

3.2.2 Fourier Transform Infra-Red (FTIR) Spectroscopy

Variable temperature FTIR experiments for MALP-2 and GNNDESNIKFKEK were performed using a PerkinElmer Spectrum II FTIR spectrometer. Solutions in D_2O were sandwiched between two CaF_2 plate windows, with a 0.0533 mm thick Teflon spacer. The plate sandwich was heated and cooled using a Specac 4000 series high stability heating controller, and a Specac electrical heating jacket. Experiments were performed by increasing the temperature from 25 to 60 °C with a 5 °C step at a rate ~ 1 °C/min. The temperature was then reduced to 25 °C at a rate ~ 2 °C/3 min. A D_2O background spectrum was subtracted from the spectrum of each sample. For temperature-dependent FTIR, the D_2O spectra was measured as a function of the temperature and subtracted from the FTIR of the sample at the corresponding

temperature. After D₂O subtraction, a constant baseline of 0.013 and -0.003 was subtracted from the spectra for MALP-2 and GNNDESNISFKEK respectively.

3.2.3 Circular Dichroism (CD)

CD spectra were recorded using a Chirascan spectropolarimeter (Applied Photophysics, UK). Each sample was placed in a cover slip cuvette (0.1 mm thick). Spectra are presented with absorbance $A < 2$ at any measured point with a 0.5 nm step, 1 nm bandwidth, and 1 second collection time per step. For MALP-2, samples were measured in the range 25 °C – 70 °C with 10 °C steps on heating and 2 min equilibration at each temperature. 0.5 wt% MALP-2 was used. For GNNDESNISFKEK, solutions were measured using parallel plaques (0.01 mm gap) for concentrations 0.5-2 wt% and a quartz cuvette (1 mm thick) for 0.008 wt%. The CD spectra for 0.008-1 wt% were smoothed using the Chirascan software, confirming that the residual trace shows only noise randomly distributed about zero.

3.2.4 Small-Angle X-ray Scattering (SAXS)

SAXS experiments were performed on beamline B21 at Diamond (Harwell, UK) using a BioSAXS robot. Solutions were loaded into the 96-well plate of an EMBL BioSAXS robot and then injected via an automated sample exchanger into a quartz capillary (1.8 mm internal diameter) in the X-ray beam. The quartz capillary was enclosed in a vacuum chamber, in order to avoid parasitic scattering. After the sample was injected into the capillary and had reached the X-ray beam, the flow was stopped during the SAXS data acquisition. B21 operated with a fixed camera length (3.9 m) and fixed energy (12.4 keV). The images were captured using a Pilatus 2 M detector. Data processing, including background subtraction and radial averaging, was performed using the dedicated software Scatter.

3.2.5 X-ray Diffraction (XRD)

XRD was performed on a peptide stalk prepared by drawing a fiber of a 1 or 10 wt% peptide solution between the ends of wax-coated capillaries. After separation of the capillaries and drying, a stalk was left on the end of one capillary. MALP-2 stalks were mounted vertically onto the goniometer of an Oxford Instruments Gemini X-ray diffractometer, equipped with a Sapphire 3 CCD detector. The sample-to-detector distance was 45 mm. GNNDESNISFKEK stalks were mounted vertically onto the four axis goniometer of a RAXIS IV++ X-ray diffractometer (Rigaku) equipped with a rotating anode generator, while the XRD data was collected using a Saturn 992 CCD camera. The sample-to-detector distance was 50 mm. CLEARER software [20] was used to reduce the 2D data to a one-dimensional intensity profile.

3.2.6 Cryogenic Transmission Electron Microscopy (Cryo-TEM)

Experiments were carried out at the laboratories of our collaborators at Aalto University in Finland using a field emission cryo-electron microscopy (JEOL JEM-3200FSC) operating at 300 kV. Images were taken using bright-field mode and zero loss energy filtering (omega type) with a slit width 20 eV. Micrographs were recorded using a Gatan UltraScan 4000 CCD camera. The specimen temperature was maintained at -187 °C during the imaging. Vitrified specimens were prepared using an automated FEI Vitrobot device using Quantifoil 3.5/1 holey carbon copper grids with 3.5 µm hole sizes. Grids were cleaned using a Gatan Solarus 9500 plasma cleaner just prior to use and then transferred into the environmental chamber of FEI Vitrobot at room temperature and 100% humidity. Thereafter, 3 µl of sample solution at 0.5 wt% concentration was applied on the grid, blotted once for 1 second, and then vitrified in a 1/1 mixture of liquid ethane and propane at -180 °C. Grids with vitrified sample solutions were maintained in a liquid nitrogen atmosphere and then cryo-transferred into the microscope.

3.3 Results and discussion

Firstly, the cac of MALP-2 was determined using pyrene fluorescence assay, described in more detail in chapter 2. Figure 2 shows the experimentally determined cac, giving a value of 5.7×10^{-2} (± 0.02) wt%.

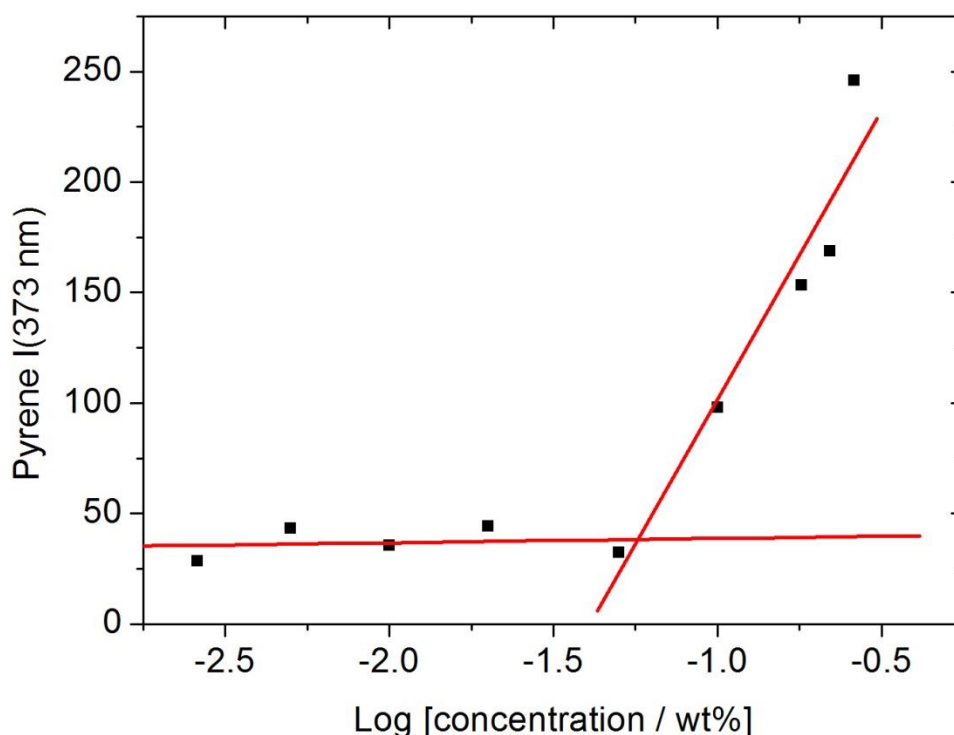


Figure 2 Critical aggregation concentrations of MALP-2 through pyrene fluorescence, indicated at the intersections of the lines. Concentration dependence of pyrene fluorescence at 373 nm.

The secondary structure of MALP-2 was then probed through a combination of CD and FTIR spectroscopy, and using temperature dependence as in chapter 2 to determine whether there was any lipid chain melting. CD was first to be measured over a range of temperatures from 20 °C to 60 °C and then after cooling back down to 20 °C to determine whether any change was reversible. The results, shown in figure 3, clearly show a β -sheet spectrum based on the

minimum at 220 nm and a maximum at around 200 nm [21, 22]. There is no significant change in structure upon heating, aside from a slight reduction in molar ellipticity around the 200 nm maxima peak.

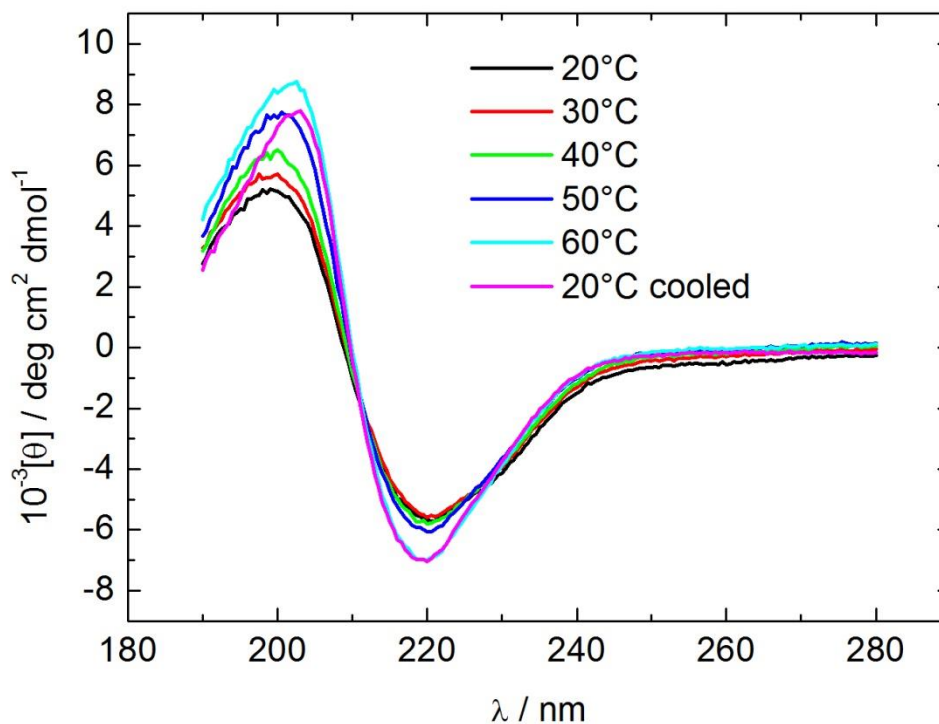


Figure 3 Temperature-dependent CD of 0.5 wt% MALP-2.

In the preparation of the MALP-2 samples, it was found that heating the sample up before experimentation gave more consistent results, potentially related to the poor solubility of MALP-2 without heating. For the FTIR measurements seen in figure 4 therefore, the solution was heated up to 60 °C initially, before cooling at 10 °C steps. This was in contrast to the usual protocol which raises the temperature at 10 °C intervals, at which measurements are then taken. In figure 4a, there is a gradual decrease in intensity of the broad 1454 cm^{-1} peak upon cooling. Due to issues seen around the time of experimentation, this can partly be attributed to evaporation from the FTIR cell. This peak can be attributed to methyl and methylene groups [23]. The peak at 1620 cm^{-1} , which doesn't change significantly in intensity above the

baseline in accordance with change in temperature, can be linked with the presence of β -sheets [24], and which agrees with β -sheet formation seen by CD. The small peak at 1672 cm^{-1} has also been seen before and is due to presence of TFA counterions [25], present in the MALP-2 sample and on a number of other manufactured lipopeptides, such as the Pam_nCSK₄ group [26].

Observing the spectra from $2800 - 3100\text{ cm}^{-1}$, which shows the area of CH₂ stretching in lipid chains [27], of which MALP-2 has many CH₂ groups, two small peaks can be seen at 2850 cm^{-1} and 2920 cm^{-1} (figure 4b). There is a lowering in intensity of peaks throughout the wavenumber range with decreasing temperature; however they are not restricted to the two peaks seen. It can therefore be suggested that the previously mentioned problem of evaporation in FTIR cell is responsible.

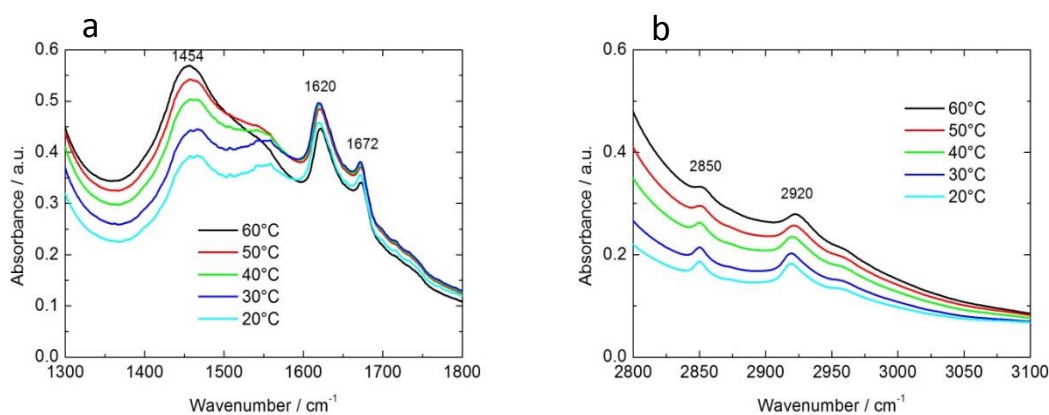


Figure 4 FTIR spectra of 0.5 wt% MALP-2 solution in D₂O. Temperature ramp from 60 – 20 °C. Wavenumber range a) $1300 - 1800\text{ cm}^{-1}$, and b) $2800 - 3100\text{ cm}^{-1}$.

Fibre XRD of MALP-2 was performed next to complement the spectroscopic data attained through CD and FTIR. The XRD pattern was found to be isotropic, and thus was reduced to a 1D intensity profile, shown in figure 5. The peaks seen in figure 5b were shown to be

associated with d-spacings of 12 Å, 4.72 Å, and 4.23 Å. The 12 Å peak can be attributed to the spacing between the β -sheet structures, and the 4.72 Å peak to spacing between the β -strands. These are expected values for “cross- β ” fibre diffraction patterns [28, 29].

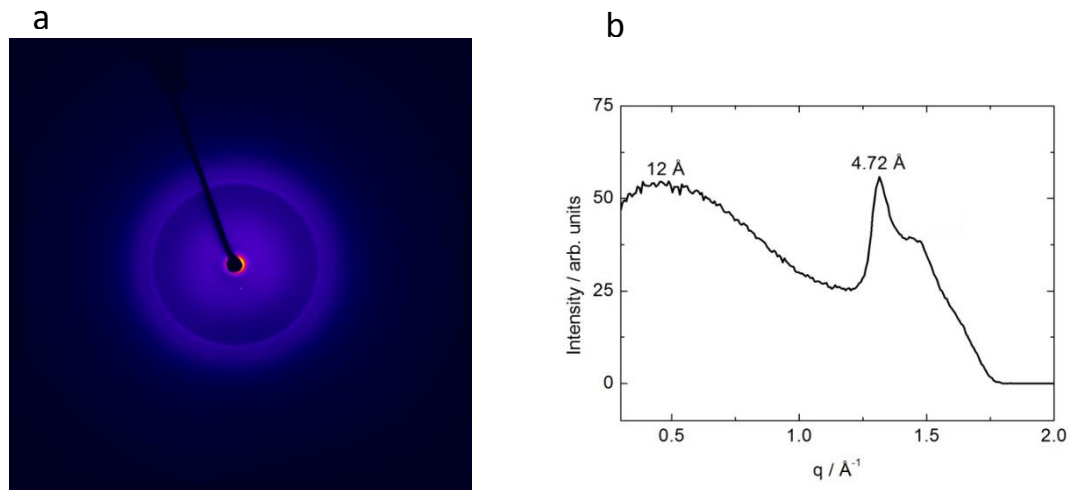


Figure 5 XRD data from 1 wt% stalk MALP-2 solution. a) 2D image, b) XRD intensity profile.

Cryo-TEM images of MALP-2 in solution were obtained by collaborators at the University of Aalto, Finland, shown in figure 6. There appears to be a mixture of individual tape-like fibers, alongside large masses of the fibers crossing and interlinked with others. The length of each fiber seems to have a large variation, from less than 100 nm to many hundreds of nanometres, but the width is fairly uniform.

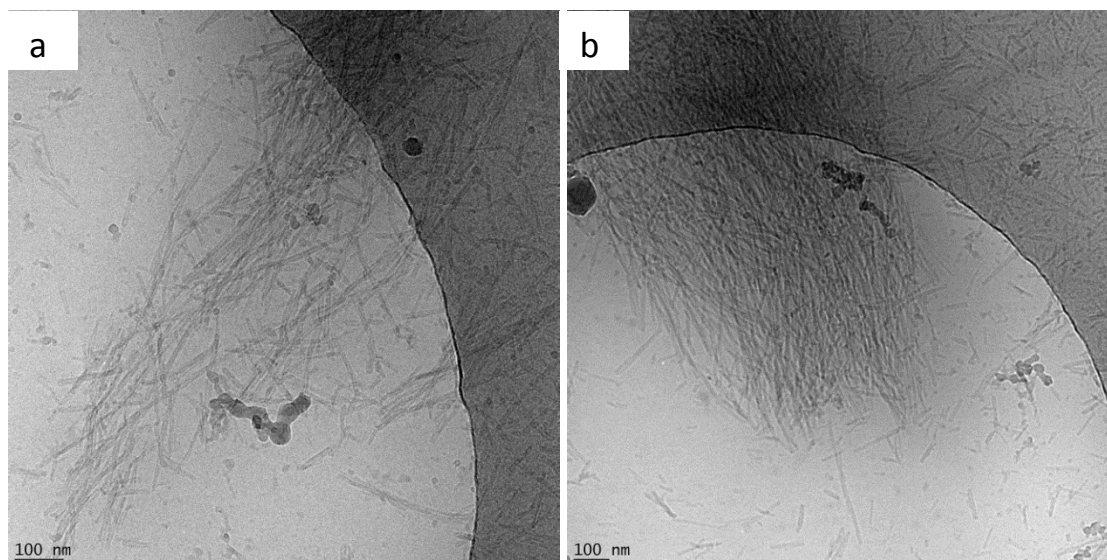


Figure 6 Representative cryo-TEM images of 0.5 wt% MALP-2.

At this point in the research, it was found that there were problems with preparation of the MALP-2 sample in achieving full dissolution. After a new compound from a different source was used, a colleague, Valeria Castelletto, repeated all experiments that had been undertaken so far. These repeated results can be seen in the full paper [30]. The cac measurements were repeated, with results shown in figure 7. The less toxic ANS [18, 31, 32], along with ThT [19, 32] were used, and it was found that the cac was less than ten times as high as the one determined using pyrene, with the wt% values from both methods being nearly the same.

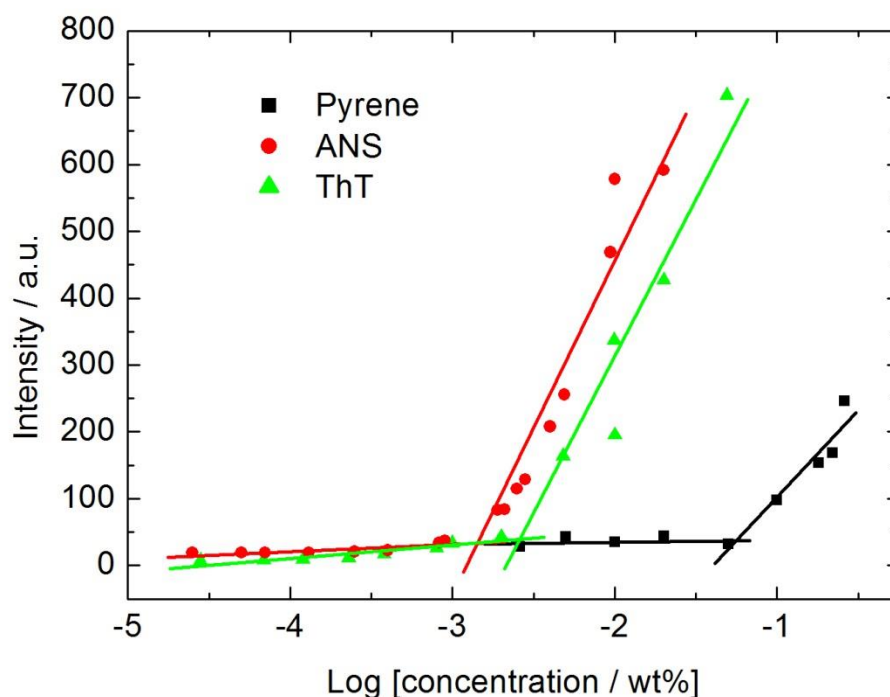


Figure 7 Comparison of fluorescence assays using pyrene, ANS and ThT.

CD results were the same, with both versions showing β -sheet formation, and FTIR was also fairly similar, albeit with more pronounced peaks in V. Castelletto's experiments. XRD showed additional lower q-range peaks which corresponded to the distance between peptides or chains within the structures. Cryo-TEM images also showed the long tape-like fibers, but also appeared to show much more organised raft-like structures formed from bound adjacent fibers (figure 9a).

Structures observed through cryo-TEM were then used as an input to constrain the form factor fitting of the raw SAXS data and to give specific structural parameters. SAXS data obtained over the temperature range also used in CD are shown in figure 8. The SAXS data were fitted to a bilayer structure, which show a slight increase in thickness from 30 Å to 35 Å across the temperature range. Parameters are shown in table 1.

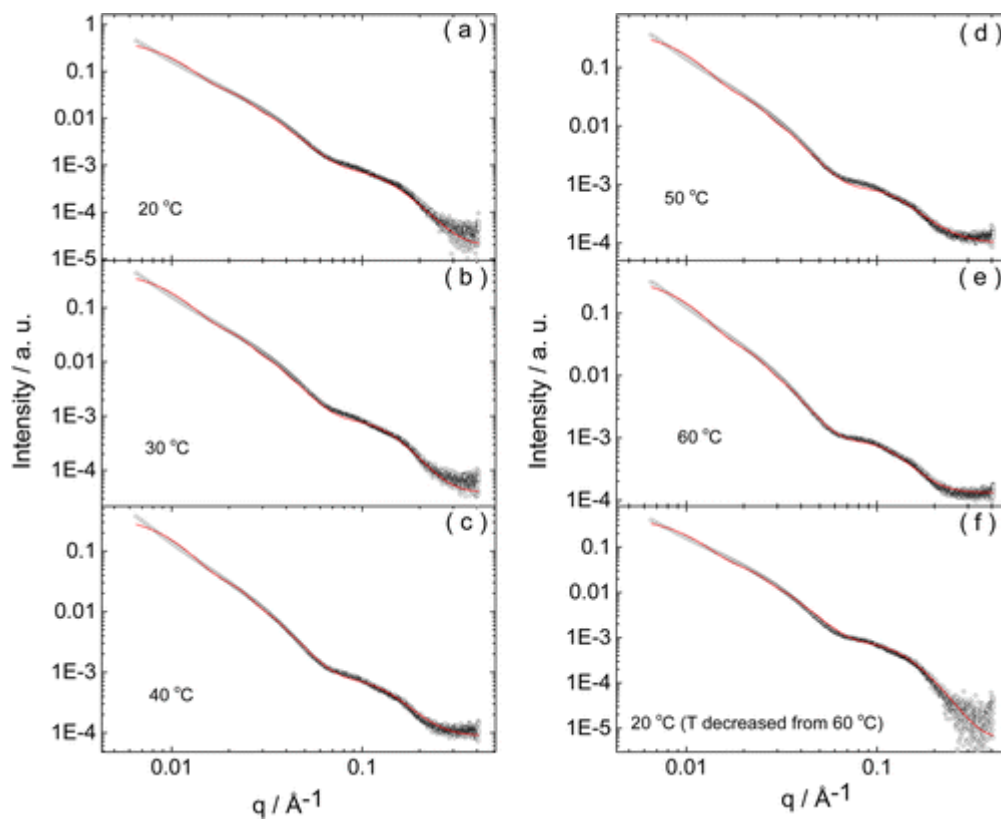


Figure 8 SAXS profiles of 0.5 wt% MALP-2 at a range of temperatures, from 20 – 60 °C, and then cooled back down to 20 °C. Black symbols represent data points, red line represents the fit. Figure courtesy of V. Castelletto.

| Parameter | 20 °C | 30 °C | 40 °C | 50 °C | 60 °C | 20 °C cooled |
|------------------------------|------------------------|------------------------|------------------------|-----------------------|------------------------|-----------------------|
| N ^a [arb. Units] | 1.08 | 1 | 1.27 | 1.16 | 1.01 | 1 |
| Δ^b [Å] | 18.4 | 17.6 | 18.18 | 17.95 | 18.76 | 17.88 |
| t ^c [Å] | 30.08 | 30 | 30.02 | 34.7 | 35.93 | 31.2 |
| σH^d [Å] | 4.74 | 5.08 | 4.67 | 5.1 | 5.76 | 5.3 |
| ρH^e [rel. units] | 1.69×10^{-7} | 1.72×10^{-7} | 1.47×10^{-7} | 1.02×10^{-7} | 1.31×10^{-7} | 1.59×10^{-7} |
| σc^f [Å] | 4.13 | 5.23 | 4.92 | 6.8 | 6.786 | 5.47 |
| ρc^g [rel. units] | -3.69×10^{-8} | -1.04×10^{-8} | -3.67×10^{-8} | -5.7×10^{-8} | -3.06×10^{-8} | -3.9×10^{-8} |
| Co ^h [arb. Units] | 2×10^{-5} | 4×10^{-5} | 9×10^{-5} | 1×10^{-5} | 1.3×10^{-4} | 3×10^{-6} |

Table 1 Parameters for SAXS fitting form factor models using SASfit software, with corresponding equations available online in the SASfit manual.

^a Scale factor

^b Gaussian half-width at half-maximum for polydispersity in layer thickness ^c

^d Gaussian half-width for outer layer surface (“headgroup”)

^e Relative electron density for headgroup

^f Gaussian half-width for inner layer

^g Relative electron density for inner layer

^h Constant background

Experiments on the peptide GNNDESNISFKEK were all performed by V. Castelletto. It was found that, in contrast to MALP-2, it dissolved very readily in water. It also had a measured isoelectric point at 4.44 in water, similar to the measured MALP-2 at 4.68 [33]. The cac was determined using ANS and ThT fluorescence assays, and was found to be 0.49 wt%, and 0.54 wt% respectively. As with MALP-2, these two values are very similar, and so it can be deduced that the fibril formation and that of the hydrophobic pockets occur concurrently.

A range of concentrations, from 0.5 to 10 wt% were used to determine the secondary structure through CD and FTIR. CD showed a transition from an unordered structure below the cac , to a β -sheet with β -turns, whilst FTIR also showed shifted peaks correlating to β -sheets. XRD, combined with SAXS data, were used to produce a model with an arranged β -sheet core, with a surrounding outer layer of hydrophilic residues. Cryo-TEM images showed fairly uniform twisted tapes with lengths up to micrometres, with antiparallel bilayer structure; hydrophobic core on the inside, with hydrophilic lysine residues on the outside (figure 9b).

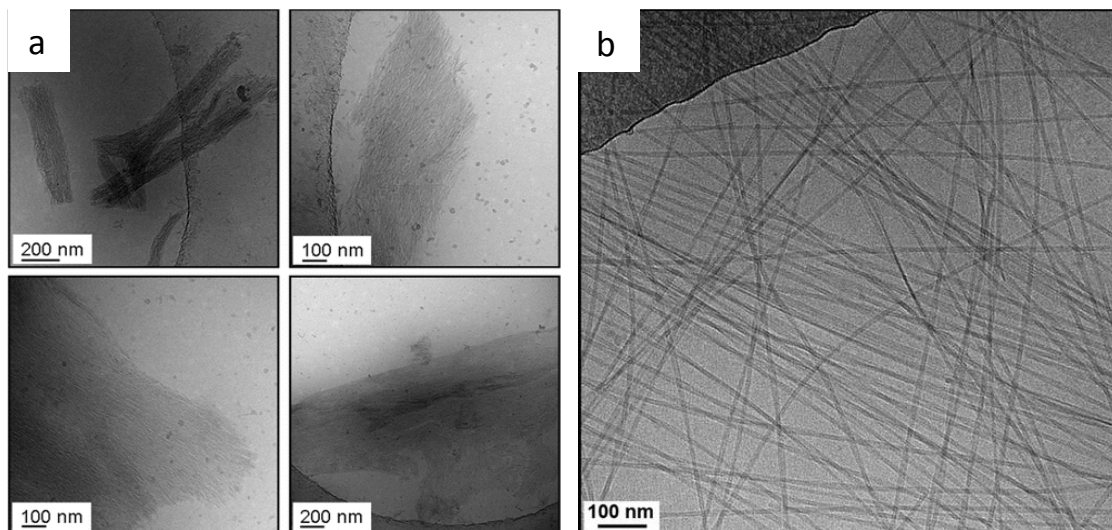


Figure 9 Representative cryo-TEM images from a) a 0.5 wt% solution of MALP-2, b) a 2 wt% solution of GNNDESNISFKEK. Figure courtesy of V. Castelletto [30].

The purpose of this research was to investigate the influence lipid chains have on the self-assembly of peptides. In this case, the presence of two lipid chains enabled interactions between otherwise individual fibers, and were able to form a raft-like structure composed of β -sheets above a cac . Self-assembly in compounds which have high hydrophobic lipid chain interaction usually lead to the formation of bilayered structures, whereas high β -sheet content generally leads to formation of fibrils [34]. These raft-like structures therefore pose an

interesting question of how they are formed, especially due to the lack of any other findings of raft-like structure formation from lipopeptides in literature. They may be intermediates between a bilayered planar nanosheet and a fibril structure, with a fine line between formation of one of these.

3.4 References

- [1] P. Muhlradt, M. Kiess, H. Meyer, R. Sussmuth and G. Jung, "Isolation, structure elucidation, and synthesis of a macrophage stimulatory lipopeptide from *Mycoplasma fermentans* acting at picomolar concentration.," *The Journal of Experimental Medicine*, vol. 185, no. 11, pp. 1951-1958, 1997.
- [2] Y. Wang, A. Lomakin, S. Kanai, R. Alex and G. Benedek, "Transformation of oligomers of lipidated peptide induced by change in pH," *Molecular Pharmaceutics*, vol. 12, no. 2, pp. 411-9, 2015.
- [3] M. Mueller, B. Lindner, S. Kusumoto, K. Fukase, A. Schromm and U. Seydel, "Aggregates Are the Biologically Active Units of Endotoxin," *Journal of Biological Chemistry*, vol. 279, no. 25, pp. 26307-26313, 2004.
- [4] "Role of the physical state of salmonella lipopolysaccharide in expression of biological and endotoxic properties," *Infection and Immunity*, vol. 61, no. 12, pp. 5351-5360, 1993.
- [5] "Physicochemical properties of the lipopolysaccharide unit that activates B lymphocytes," *Journal of Biological Chemistry*, vol. 265, no. 23, pp. 14023-14029, 1990.
- [6] A. Kaufmann, P. Muhlradt, D. Gemsa and H. Sprenger, "Induction of cytokines and chemokines in human monocytes by *Mycoplasma fermentans*-derived lipoprotein MALP-2," *Infection and Immunology*, vol. 67, no. 12, pp. 6303-6308, 1999.
- [7] K. Hoebe, P. Georgel, S. Rutschmann, X. Du, S. Mudd, K. Crozat, S. Sovath, L. Shamel, T. Hartung, U. Zahringer and B. Beutler, "CD36 is a sensor of diacylglycerides," *Nature*, vol. 433, no. 7025, pp. 523-527, 2005.
- [8] O. Takeuchi, T. Kawai, P. Muhlradt, M. Morr, J. Radolf, A. Zychlinsky, K. Takeda and S. Akira, "Discrimination of bacterial lipoproteins by Toll-like receptor 6," *International Immunology*, vol. 13, no. 7, pp. 933-940, 2001.
- [9] K. Reppe, T. Tschernig, A. Luhrmann, V. van Laak, K. Grote, M. Zemlin, B. Gutbier, H. Muller, M. Kursar, H. Schutte, S. Rosseau, R. Pabst, N. Suttorp and M. Witzernath, "Immunostimulation with macrophage-activating lipopeptide-2 increased survival in murine pneumonia," *American Journal of Respiratory cell and molecular biology*, vol. 40, no. 4, pp. 474-481, 2009.
- [10] R. Pabst, D. Durak, A. Roos, A. Luhrmann and T. Tschernig, "TLR2/6 stimulation of the rat lung: effects on lymphocyte subsets, natural killer cells and dendritic cells in different parts of the air-conducting compartments and at different ages," *Immunology*, vol. 126, no. 1, pp. 132-139, 2009.
- [11] O. Takeuchi, A. Kaufmann, K. Grote, T. Kawai, K. Hoshino, M. Morr, P. Muhlradt and S. Akira, "Cutting edge: preferentially the R-stereoisomer of the mycoplasmal lipopeptide macrophage-activating lipopeptide-2 activates immune cells through a toll-like receptor 2- and MyD88-dependent signaling pathway," *Journal of Immunology*, vol. 164, no. 2, pp. 554-557, 2000.

- [12] K. Shingu, C. Kruschinski, A. Luhrmann, K. Grote, T. Tschernig, S. Von Horsten and R. Pabst, "Intratracheal macrophage-activating lipopeptide-2 reduces metastasis in the rat lung," *American Journal of Respiratory Cell and Molecular Biology*, vol. 28, no. 3, pp. 316-321, 2003.
- [13] U. Deiters, J. Barsig, B. Tawil and P. Muhlradt, "The macrophage-activating lipopeptide-2 accelerates wound healing in diabetic mice," *Experimental Dermatology*, vol. 13, no. 12, pp. 731-739, 2004.
- [14] M. Lachke, V. Augustin, S. Kleer, T. Tschernig and M. Menger, "Locally applied macrophage-activating lipopeptide-2 (MALP-2) promotes early vascularization of implanted porous polyethylene (Medpor (R))," *Acta Biomaterialia*, vol. 10, no. 11, pp. 4661-4669, 2014.
- [15] F. Rharbaoui, B. Drabner, S. Borsutzky, U. Winckler, M. Morr, B. Ensoli, P. Muhlradt and C. Guzman, "The Mycoplasma-derived lipopeptide MALP-2 is a potent mucosal adjuvant," *European Journal of Immunology*, vol. 32, no. 10, pp. 2857-2865, 2002.
- [16] K. Reppe, P. Radunzel, K. Dietert, T. Tschernig, T. Wolff, S. Hammerschmidt, A. Gruber, N. Suttrop and M. Witzernath, "Pulmonary immunostimulation with MALP-2 in influenza virus-infected mice increases survival after pneumococcal superinfection," *Infection and Immunology*, vol. 83, no. 12, pp. 4617-4629, 2015.
- [17] K. Wiesmuller, W. Bessler and G. Jung, "Synthesis of the mitogenic S-[2,3-bis(palmitoyloxy)propyl]-N-palmitoylpentapeptide from Escherichia coli lipoprotein," *Hoppe-Seyler's Zeitschrift fur Physiologische-Chemie*, vol. 364, no. 5, pp. 593-606, 1983.
- [18] A. Hawe, M. Sutter and W. Jiskoot, "Extrinsic Fluorescent Dyes as Tools for Protein Characterization," *Pharmaceutical Research*, vol. 25, no. 7, pp. 1487-1499, 2008.
- [19] H. LeVine, "Thioflavine T interaction with synthetic Alzheimer's disease beta-amyloid peptides: detection of amyloid aggregation in solution," *Protein Science*, vol. 2, no. 3, pp. 404-410, 1993.
- [20] O. Sumner Makin, P. Sikorski and L. Serpell, "CLEARER: a new tool for the analysis of X-ray fibre diffraction patterns and diffraction simulation from atomic structural models," *Journal of Applied Crystallography*, vol. 40, no. 5, pp. 966-972, 2007.
- [21] I. Hamley, "Peptide fibrillization," *Angewandte Chemie*, vol. 46, no. 43, pp. 8128-8147, 2007.
- [22] S. Kelly, T. Jess and N. Price, "How to study proteins by circular dichroism," *Biochimica et Biophysica Acta*, vol. 1751, no. 2, pp. 119-139, 2005.
- [23] F. Miller and C. Wilkins, "Infrared spectra and characteristic frequencies of inorganic ions," *Analytical Chemistry*, vol. 24, no. 8, pp. 1253-1294, 1952.
- [24] M. Jackson and H. Mantsch, "The use and misuse of FTIR spectroscopy in the determination of protein structure," *Critical Reviews in Biochemistry and Molecular Biology*, vol. 30, no. 2, pp. 95-120, 1995.

- [25] J. Pelton and L. McLean, "Spectroscopic methods for analysis of protein secondary structure," *Analytical Biochemistry*, vol. 277, no. 2, pp. 167-176, 2000.
- [26] I. Hamley, S. Kirkham, A. Dehsorkhi, V. Castelletto, M. Reza and J. Ruokolainen, "Toll-like receptor agonist lipopeptides self-assemble into distinct nanostructures," *Chemical Communications*, vol. 50, no. 100, pp. 15948-15951, 2014.
- [27] H. Casal and H. Mantsch, "Polymorphic phase-behaviour of phospholipid-membranes studied by infrared spectroscopy," *Biochimica et Biophysica Acta*, vol. 779, no. 4, pp. 381-401, 1984.
- [28] L. Serpell, "Alzheimer's amyloid fibrils: structure and assembly," *Biochimica et Biophysica Acta*, vol. 1502, no. 1, pp. 16-30, 2000.
- [29] S. Gras, "Amyloid fibrils: from disease to design. New biomaterial applications for self-assembling cross- β fibrils," *Australian Journal of Chemistry*, vol. 60, no. 5, pp. 333-342, 2007.
- [30] V. Castelletto, S. Kirkham, I. Hamley, R. Kowalczyk, M. Rabe, M. Reza and J. Ruokolainen, "Self-assembly of the toll-like receptor agonist macrophage-activating lipopeptide MALP-2 and of its constituent peptide," *Biomacromolecules*, vol. 17, no. 2, pp. 631-640, 2016.
- [31] O. Gasymov and B. Glasgow, "ANS fluorescence: potential to augment the identification of the external binding sites of proteins," *Biochimica et Biophysica Acta*, vol. 1774, no. 3, pp. 403-411, 2007.
- [32] M. Lindgren, K. Sorgjerd and P. Hammarstrom, "Detection and characterization of aggregates, prefibrillar amyloidogenic oligomers, and protofibrils using fluorescence spectroscopy," *Biophysical Journal*, vol. 88, no. 6, pp. 4200-4212, 2005.
- [33] T. Akazawa, N. Inoue, H. Shime, K. Kodama, M. Matsumoto and T. Seya, "Adjuvant engineering for cancer immunotherapy: Development of a synthetic TLR2 ligand with increased cell adhesion," *Cancer Science*, vol. 101, no. 7, pp. 1596-15603, 2010.
- [34] D. Mandal, A. Shirazi and K. Parang, "Self-Assembly of Peptides to Nanostructures," *Organic and Biomolecular Chemistry*, vol. 12, no. 22, pp. 3544-3561, 2014.

Chapter 4 - Addition of dileucine motif to FITC fluorophore enables use in cell labelling

4.1 Introduction

The effect lipid chains attached to peptides can have on self-assembly has already been discussed, but as well as those, aromatic side chains also have the ability to modify self-assembly, through hydrophobic effects as well as stacking interactions between the aromatic moieties. There are a number of often used substituents, including Fmoc [9-fluorenylmethoxycarbonyl chloride] [1-3], Boc [tert-butyloxycarbonyl] [4, 5], naphthalene [6-8], pyrene [8, 9], and also fluorene [8]. These are usually used in order to make hydrogel/organogel formulations. Attached conjugates may be used in biomedical applications, in some cases through direct influence of the amino acids present. One study which used a peptide sequence attached to a number of different fluorophores found that they each self-assembled differently to each other, and one had the effect of maintaining cell adhesion due to inhibition of an actin toxin [10]. The attachment of functional units, including Nonsteroidal anti-inflammatory drugs (NSAIDs), can also be used. Upon addition of an NSAID, in this case Naproxen, to D-amino acids, it was found that proteolytic resistance increased, as did selectivity of Naproxen for COX-2, an enzyme involved in the inflammation and pain response [11]. The same group also investigated the effect conjugation of a small peptide to a range of NSAIDs would have on self-assembly and bioactivity [12]. They found further evidence of molecular nanofiber formation, and also increased target selectivity for NSAIDs, as well as preservation of activities in those NSAIDs bound to D-amino acids. Li et al. also used Taxol as a conjugating moiety, and upon attachment to phosphorylated D-peptides produced different precursors which were able to form biostable or biocompatible hydrogels [13]. There

are also a number of other therapeutic agents used as conjugates bound to peptides with uses in biomedical applications, listed in more detail by Zhao et al. [14].

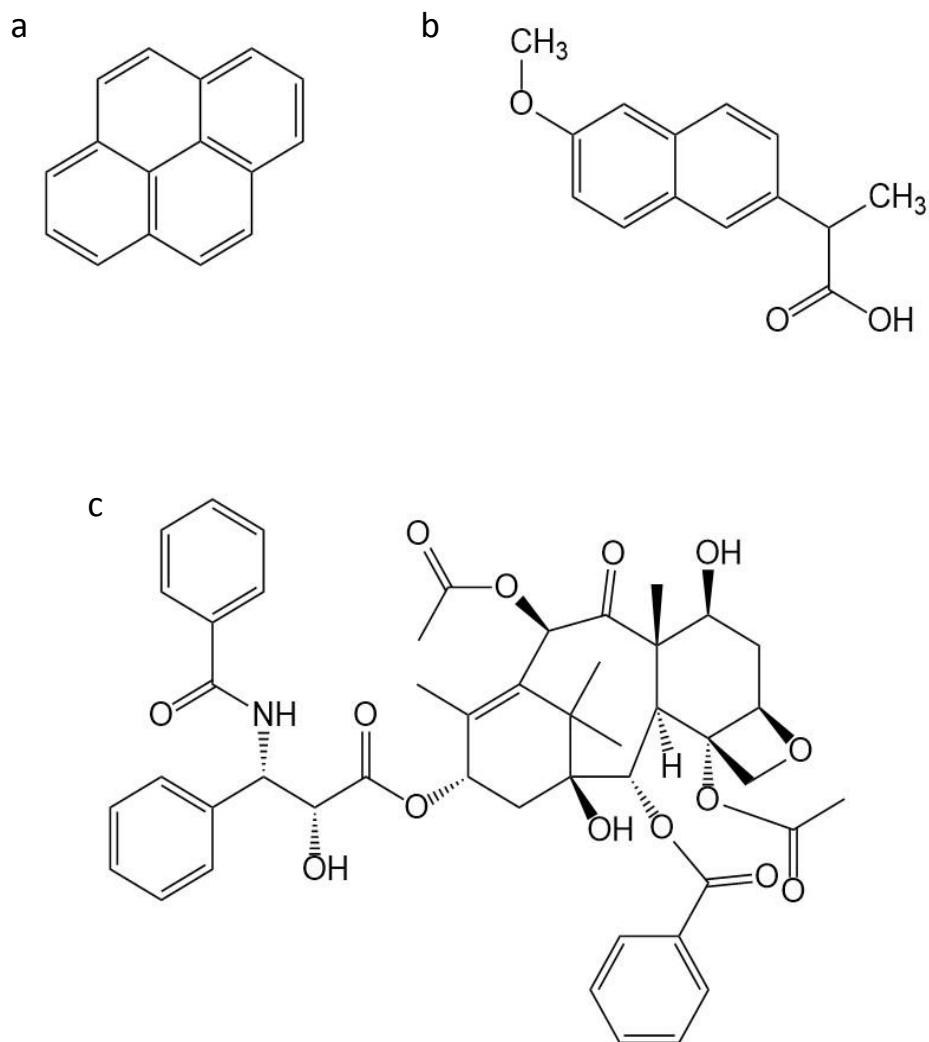


Figure 1 Molecular structure of a range of aromatic substituents, described in the text, including a) pyrene, b) Naproxen, and c) Taxol.

In this chapter, we investigated a peptide amphiphile consisting of a bulky hydrophobic fluorophore, fluorescein isothiocyanate (FITC), attached to a di-leucine peptide motif at the N-terminus (shown in figure 2). It was developed as a custom synthesised peptide for the potential to be used in cell labelling with its added biocompatibility. FITC has previously been

used in cellular fluorescence labelling when bound to a peptide chain [15]. Xentry, a short peptide sequence of LCLRPVG, is a cell penetrating peptide (CPP) derived from the hepatitis B virus, and was visually able to be seen within cells due to the fluorescence from FITC. A novel peptide chain, KRKRWHW, was developed as a CPP to have a lower cytotoxicity and to deliver non-permeable trehalose into cells [16]. The peptide chain was attached to FITC to determine the location in which it accumulated. FITC was also used bound to another peptide chain, YG(R)₉, to determine the localisation of its accumulation in cells [17].

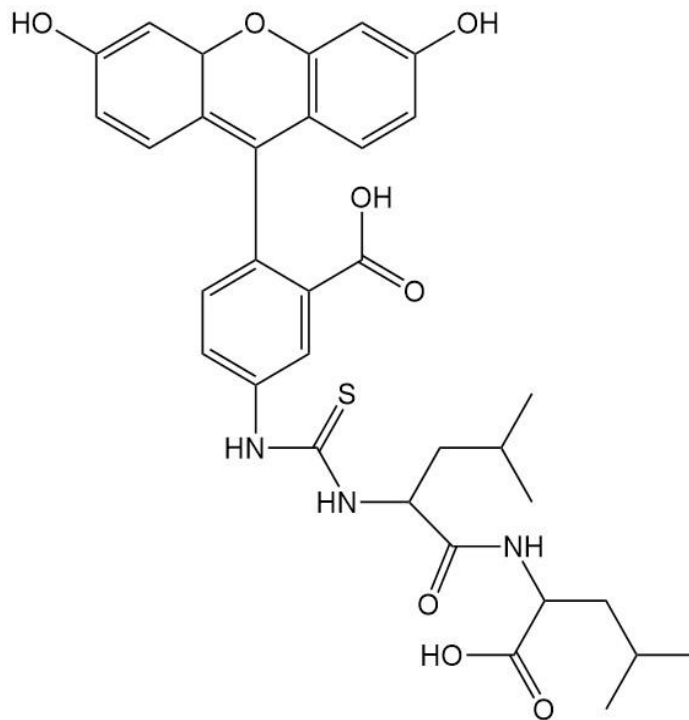


Figure 2 Molecular structure of FITC-LL.

4.2 Materials and methods

FITC-LL was synthesised by Dr A.M. Smith using FITC and LL initially as separate compounds. The mass was 634.5 g mol^{-1} (measured), $635.73 \text{ g mol}^{-1}$ (expected). The full synthesis protocol can be found in the supplementary data of the published paper [18].

For the self-assembly studies, in order for the FITC-LL to form a solution or gel (at higher concentration), pH had to be controlled. Distilled water was first added to the FITC-LL powder to total between a third and a half of the target final total volume in order to establish a concentration of around 5 mg/ml. 1 M NaOH was added at a quarter of the target final total volume of in order for the FITC-LL to dissolve in the solution, with gentle swirling, to raise the pH to 9-10. A solution of 1M HCl was then titrated to lower the pH to below 7 to form the solution or gel, with incubation in the fridge at 2-5 °C sometimes needed for gel formation. Due to their light-sensitive nature, the FITC-LL compound and solutions were shielded from light when possible.

4.2.1 Fluorescence Spectroscopy

The λ_{exc} was determined through a concentration-dependent fluorescence assay. Fluorescence spectra were recorded with a Varian Cary Eclipse Fluorescence Spectrometer with samples in 10 mm inner width quartz cuvettes. The fluorescence assays were performed using 0.05 – 0.4 wt% FITC-LL solutions in distilled water. The samples were excited at $\lambda_{\text{exc}} = 495 \text{ nm}$, and the fluorescence emission was measured for $\lambda = (480-650) \text{ nm}$.

4.2.2 Circular Dichroism (CD)

Spectra were recorded using a Chirascan spectropolarimeter (Applied Photophysics, UK). A solution of FITC-LL in water (0.4 wt%) was placed in a cover slip cuvette (0.01 mm thick).

Spectra are presented with absorbance $A < 2$ at any measured point with a 0.5 nm step, 1 nm bandwidth, and 1 second collection time per step at 20 °C. The post-acquisition smoothing tool in the Chirascan software was used to remove random noise elements from the averaged spectra. A residual plot was generated for each curve in order to verify whether or not the spectrum has been distorted during the smoothing process. The CD signal from water was subtracted from the CD data of the peptide solutions.

4.2.3 Fourier Transform Infra-red (FTIR) spectroscopy

Spectra were recorded using a Thermo Scientific Nicolet IS5 and a Nexus-FTIR spectrometer, both equipped with a DTGS detector. A solution of FITC-LL (0.73 wt% in water) was sandwiched between two CaF₂ plate windows (spacer 0.012 or 0.025 mm thick). Spectra were scanned 128 or 168 times over the range of 900-4000 cm⁻¹.

4.2.4 Cryo-Transmission electron microscopy (cryo-TEM)

Experiments were carried out by our collaborators at Aalto University in Finland using a field emission cryo-electron microscope (JEOL JEM-3200FSC) operating at 300 kV. Images were taken using bright-field mode and zero loss energy filtering (omega type) with a slit with 20 eV. Micrographs were recorded using a Gatan UltraScan 4000 CCD camera. The specimen temperature was maintained at -187 °C during the imaging. Vitrified specimens were prepared using an automated FEI Vitrobot device using Quantifoil 3.5/1 holey carbon copper grids with 3.5 µm hole sizes. Grids were cleaned using a Gatan Solarus 9500 plasma cleaner just prior to use and then transferred into an environmental chamber of FEI Vitrobot at room temperature and 100% humidity. Thereafter, 3 µl of sample solution at 2 wt% concentration was applied on the grid, blotted once for 1 second and then vitrified in a 1/1 mixture of liquid ethane and propane at -180 °C. Grids with vitrified sample solutions were maintained in a liquid nitrogen atmosphere and then cryo-transferred into the microscope.

4.2.5 Human fibroblast cell culturing and cell viability and uptake assays

4.2.5.1 Cell culture

Human corneal fibroblasts were isolated and cultured as previously described [19], by R. Gouveia. Upon confluence, cells were passaged by gentle wash with phosphate buffered saline (PBS) followed by 5 min incubation with TrypLE enzyme (Life Technologies), mechanical dislodgement, centrifugation at 500 ×g for 5 min, re-suspension in fresh culture medium, and seeding to new tissue culture flasks. Cells up to passage four were used in subsequent experiments.

4.2.5.2 FITC-LL uptake assays

Cells were seeded into 24-well plates at 1×10^5 cells/cm² and cultured with serum-free medium for 48 h at 37 °C. Cultures were washed thrice with PBS and incubated with serum-free culture medium containing 7.5×10^{-3} wt% FITC-LL or non-conjugated FITC control for 24 h at 37 °C. Cells were then washed thrice with PBS to remove all non-internalised fluorophore, and imaged by bright-field and fluorescence microscopy using the LumaScope 500 inverted fluorescence microscope (Etaluma). To examine FITC-LL intracellular localization, cells were treated as described above, but with the additional step of adding the 4',6-diamidino-2-phenylindole (DAPI) nuclear stain (Life Technologies) just prior to imaging using the AxioVert 200 inverted fluorescence microscope (Zeiss). Bright-field and fluorescence signals were obtained using independent channels, which were then composed post-imaging using the ImageJ software (version 1.49). Uptake assays were performed in duplicate, in three independent experiments using different cell donors.

4.2.5.3 Cell viability assays

Cells were seeded into glass coverslips in 24-well plates at 1×10^5 cells/cm² and cultured with serum-free medium for 48 h at 37 °C. Cultures were washed thrice with PBS and incubated with serum-free culture medium containing 7.5×10^{-3} wt% FITC-LL or non-conjugated FITC control for 24 h at 37 °C. Cells were then washed thrice with PBS to remove all non-internalised fluorophore, and incubated with Live/Dead cell Double Staining kit (Calbiochem) according to the manufacturer's instructions. Briefly, the green-fluorescent, membrane-permeable Cyto-Dye and the red-fluorescent, membrane-impermeable propidium iodide were added to staining buffer at the 1:1:1000 ratio. Cell were incubated with these dyes for 15 min at 37 °C, washed thrice with PBS to remove all unbound dye, and imaged by fluorescence microscopy using the AxioVert 200 inverted fluorescence microscope (Zeiss). Green and red fluorescence signals were obtained using independent channels, and then composed post-imaging using the ImageJ software (version 1.49). Cell viability assays were performed in duplicate, in two independent experiments using different cell donors.

4.3 Results and discussion

4.3.1 Self-assembly studies

The self-assembly of FITC-LL in aqueous solution was investigated. As with the other chapters, this began with fluorescence measurements to determine the critical aggregation concentration (cac) of FITC-LL. Due to the compound having its own documented self-fluorescence properties, we performed a concentration-dependent assay over a range of concentrations, but without the addition of pyrene, ANS or ThT. Using FITC's documented excitation peak of 495 nm [20], the broad emission peak was found at 525 nm. It was found that at the higher concentrations, fluorescence diminished, leading to the belief that there is a

self-quenching effect when self-assembled structures are formed. The cac was determined to be 0.25 wt% (figure 3).

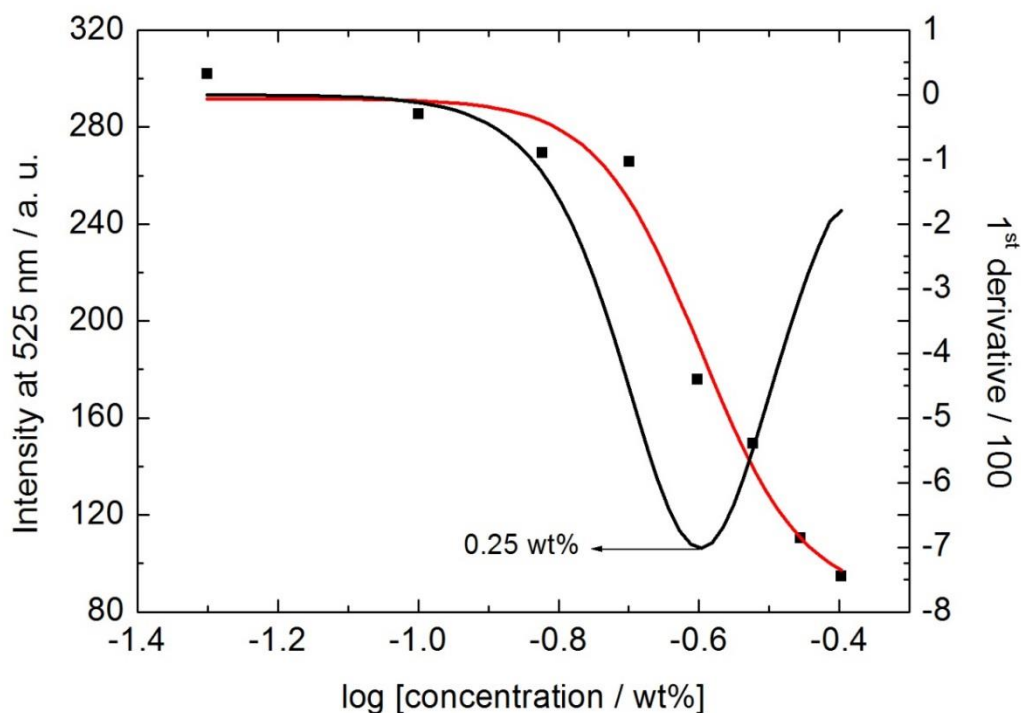


Figure 3 Critical aggregation concentration of FITC-LL, fitted through a sigmoidal curve (red line), and cac obtained from the minimum of the first derivative (black line).

Next the secondary structure of the compound was investigated through the use of CD and FTIR. In the latter spectrum, shown in figure 4, there is a peak in the amide I region at 1633 cm^{-1} . This peak can be attributed to β -sheet formation [21]. There is also a larger peak at 1578 cm^{-1} , the amide II region, which is attributed to stretching of C—N/ bending of N—H [22].

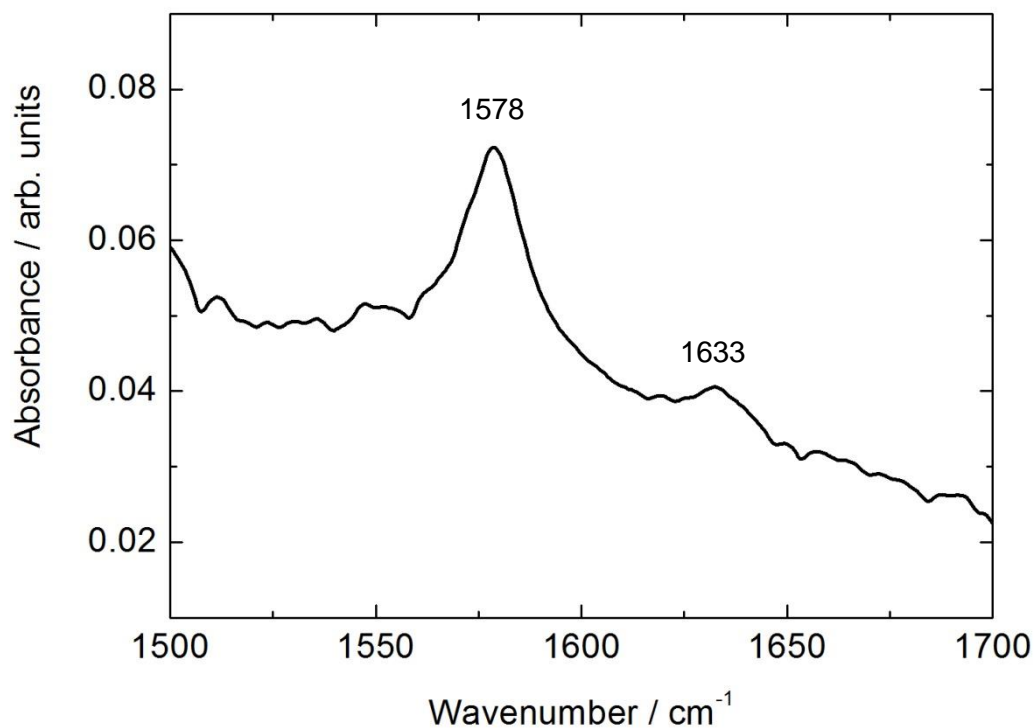


Figure 4 FTIR spectrum of 0.73 wt% FITC-LL solution in D₂O.

In contrast to the corresponding β -sheet peak seen in the FTIR data, the CD spectrum in figure 5 does not show a curve which typically resembles that of a β -sheet structure. This is usually characterised by a maximum at around 200 nm combined with a negative at around 216 nm [21, 23]. This however may in part be due to the UV absorbance seen with FITC (in figure 6) [24, 25], as well as the presence of the highly extended nanostructures. The wavelength range studies for the compound was extended up to 550 nm in order to examine any chiral ordering of FITC due to its attachment to the dipeptide. Indeed, a broad peak was observed at around 520 nm.

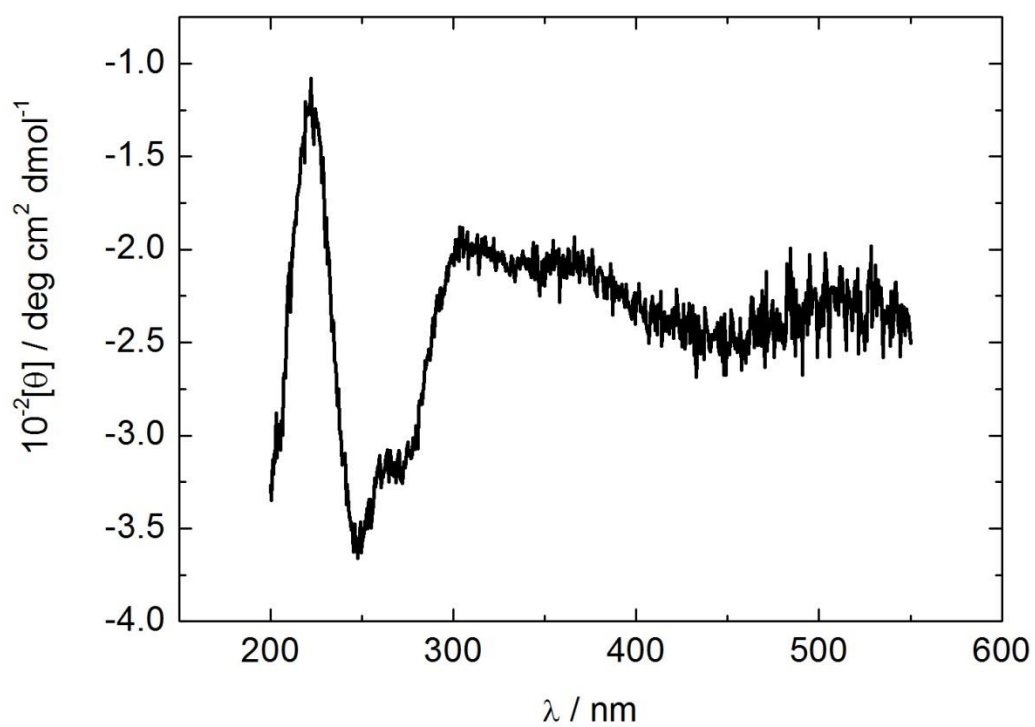


Figure 5 CD spectrum from 0.4 wt% FITC-LL solution.

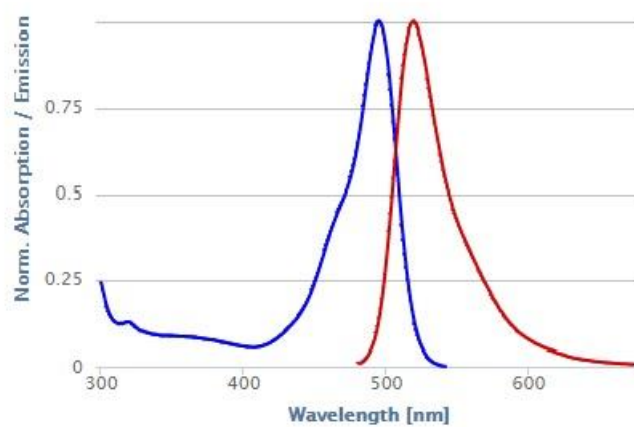


Figure 6 Spectra of FITC absorbance/emission. Blue line denotes excitation, red line denotes emission. Figure from reference [25].

The next step was sending samples off to our collaborators at the University of Aalto in Finland for cryo-TEM. The images (figure 7) showed the formation of large sheets of varying size and width. It can also be seen that the sheets have thin edges, seen particularly in figure 6a within the black circle. These sheets are particularly interesting as, to our knowledge; these structures have not previously been seen with dipeptide motif attached to bulky aromatic substituents. Instead, short peptide sequences attached to aromatic conjugates typically form fibrils [2, 26, 27].

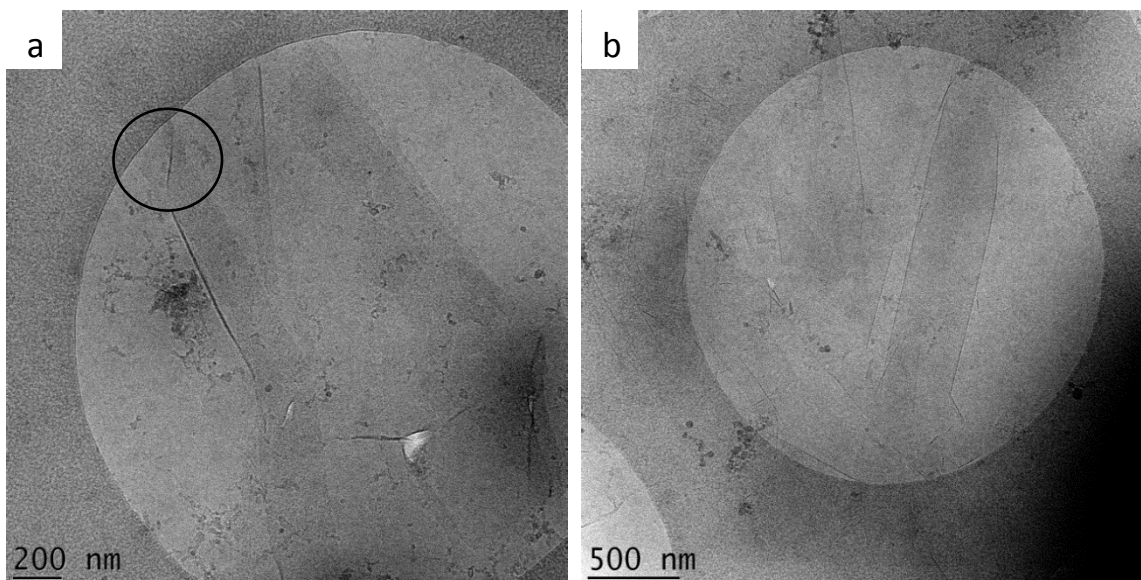


Figure 7 Representative cryo-TEM images from a 0.73 wt% solution.

As with the other chapters, we used the cryo-TEM images as a constraint to the form factor modelling of SAXS data. In figure 8, it is shown that the data was fitted accurately to a Gaussian bilayer model, which has also been used by other colleagues in the research group previously to fit other layered peptide assemblies [28-30]. Although FITC-LL did not form a bilayer as such, the parameters within the form factor mean that the dileucine motif is seen as

the outer layer of the bilayer, and FITC as the inner layer. The specific properties and dimensions of the structures it was fitted to can be found in table 1.

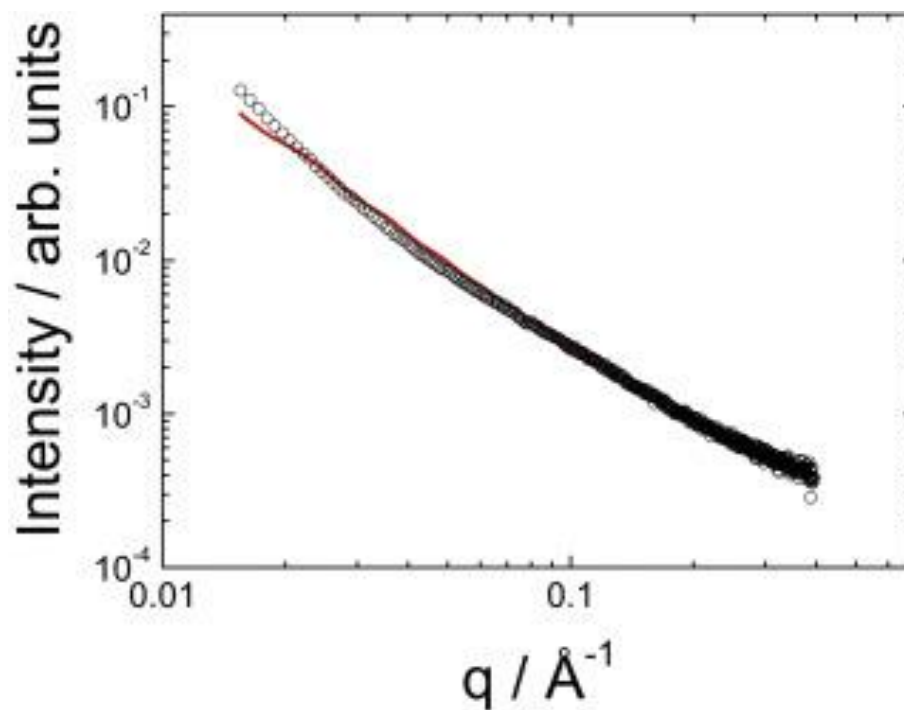


Figure 8 SAXS data (open black symbols) with model form factor fit (red line).

| Gaussian bilayer form factor | | | | | | |
|------------------------------|-------------------------|------------------------|--------------------|---------------------------------|------------------------|------------------------|
| Layer thickness (t) | Lipid core (ρ_c) | Headgroup (ρ_h) | Background (B) | Gaussian function width (fixed) | Bilayer radius (fixed) | Scaling factor (F) |
| 8.9 | -2.36×10^{-5} | 6.4×10^{-6} | 0.0004 | 5 Å | 500 Å | 0.001 |

Table 1 Parameters for SAXS fitting form factor models using SASfit software, with corresponding equations available online in the SASfit manual.

4.3.2 Cell viability and compatibility studies

After investigating the self-assembly and the nature of the formed structures, FITC-LL's effect on cells was determined. Initially it was tested whether FITC-LL, and the fluorophore FITC on

its own, was toxic to cells through a live/dead cell assay. This showed live cells in green and dead cells in red. As can be seen in figure 9, incubation with either FITC or FITC-LL showed no toxicity to cells, demonstrated by a lack of red-stained cells in both images.

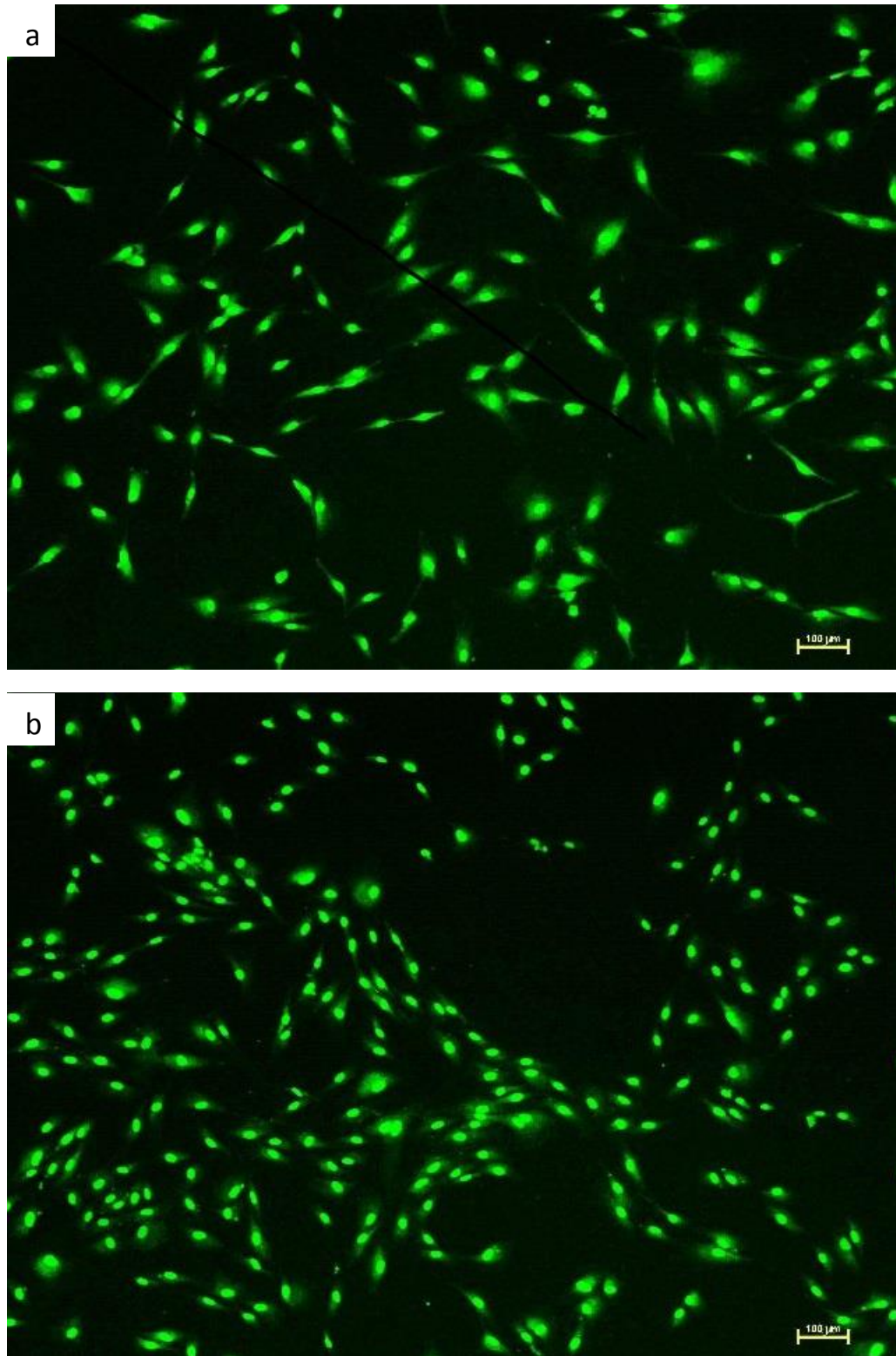


Figure 9 Representative images showing live/dead cell assay of a) FITC-LL, and b) FITC, both at 7.5×10^{-3} wt% incubated with human fibroblasts. Green fluorescence indicates live cells, red indicates dead cells.

As the lack of toxicity was established, the next objective was to determine whether the compounds were able to be uptaken by cells. Figure 10 shows the comparison between the uptake of FITC when compared with FITC-LL. There is a clear difference between the two, with FITC-LL very readily being uptaken into cells, compared with FITC which has specks of green fluorescence. These specks may be explained through the washing of the cells, rather than any cellular uptake, due to the aggregated nature of the fluorescence and the presence of it outside of cells. FITC-LL on the other hand was shown to be uptaken by the majority of cells, with very little fluorescence outside of them.

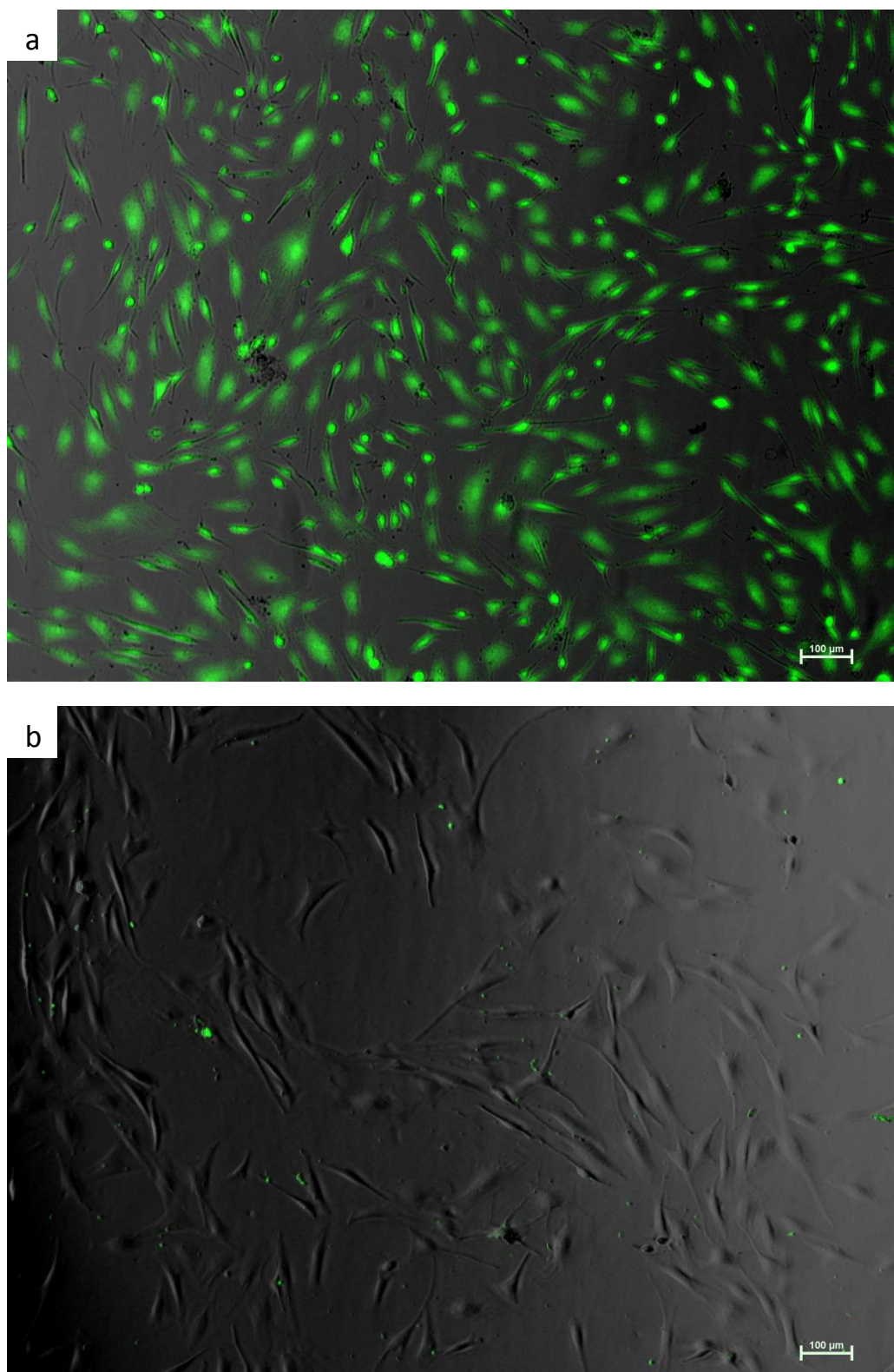


Figure 10 Representative images showing uptake cell assay of a) FITC-LL, and b) FITC, both at 7.5×10^{-3} wt% incubated with human fibroblasts. Green fluorescence is from intrinsic fluorescence of the fluorophore, which shows cells have uptake the compound.

In order to discover more on the regions of the cell FITC-LL is uptaken into, a nuclear staining dye, DAPI (4',6-diamidino-2-phenylindole), was also incubated alongside the compound, and higher resolution images were taken by one of our collaborators at Newcastle University. In figure 11, it appears that FITC-LL is present throughout most of the cell, potentially with a small amount also present in the nucleus, shown by the slight overlap of FITC green and DAPI blue fluorescence. However, it can't be confirmed due to the two dimensional nature of the images. The images do show a large localisation of FITC-LL in the peri-nuclear region, shown through light blue staining, and inside vesicle-shaped intracellular compartments, indicated by the arrows in figure 11b. Further experiments were due to be undertaken to create a 3 dimensional view of how the compound is uptaken, to further characterise the localisation of FITC-LL in the cell. However, the collaboration with the group involved with the cellular section ended before the experiments were able to be done.

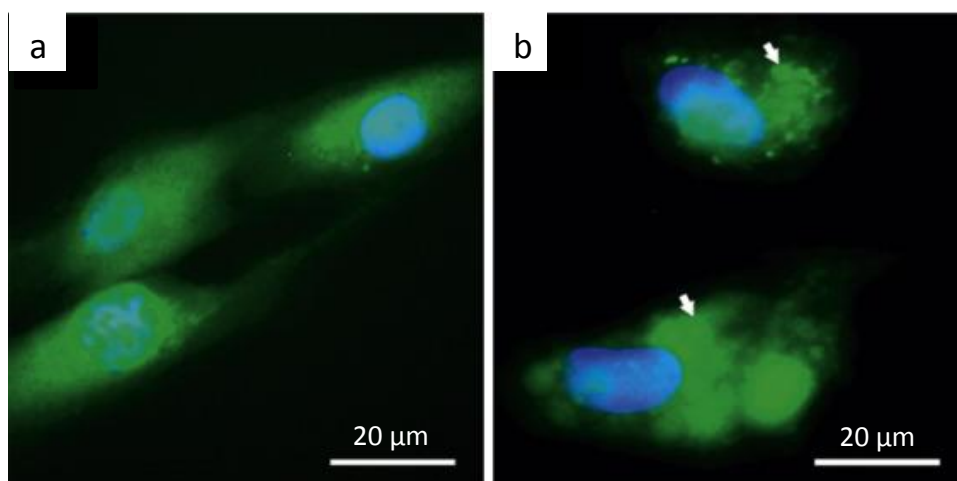


Figure 11 Representative images of fibroblasts incubated with 7.5×10^{-3} wt% FITC-LL and stained with nuclear stain DAPI. The scale bars correspond to 20 μm . Experiments performed by R.M. Gouveia at Newcastle University.

The aims in this chapter were to characterise the self-assembly properties of a bulky aromatic fluorophore bonded to a dileucine motif. It was shown that FITC-LL is able to self-assemble above a cac , at which self-quenching, potentially due to the formation of the structures, occurs. FTIR and CD data appeared to show conflicting data, with the former showing peaks which could be attributed to β -sheet formation, not seen in the CD spectra. This however could potentially have been due to other factors such as the UV absorbance and presence of extended nanostructures, seen in cryo-TEM and its dimensions revealed through SAXS. Another aim in the chapter was to determine the cytocompatibility and uptake in cells. Here, it was proven that the bonding of the dileucine motif to FITC enabled it to be uptaken into cells, when compared with the fluorophore on its own, and that neither was cytotoxic.

Future work concerning FITC-LL could focus on the mechanism of how such a short peptide sequence enables a compound to be uptaken, and whether this is specific to dileucine. As the peptide sequence is too short to be a transporter sequence, there must be another mechanism involved. There is potentially a correlation between self-assembly and FITC-LL uptake through a local concentration enhancement in close proximity to the cell membrane. The FITC-LL concentration used in the cell studies was below the cac , so localised increase of the compound near to the membrane would need to occur in order for the theory to be correct. The large lack of FITC-LL in the nucleus may be explained through the fact that Nuclear Export Signals (NES), short amino acid sequences found on molecules which allow for export from the nucleus, are leucine-rich [31, 32]. It is therefore possible that the movement of FITC-LL is facilitated through these NES systems through the dileucine sequence.

4.4 References

- [1] Y. Zhang, H. Gu, Z. Yang and B. Xu, "Supramolecular hydrogels respond to ligand–receptor interaction," *Journal of the American Chemical Society*, vol. 125, no. 45, pp. 13680-13681, 2003.
- [2] A. Smith, R. Williams, C. Tang, P. Coppo, R. Collins, M. Turner, A. Saiani and R. Ulijn, "Fmoc-Diphenylalanine self assembles to a hydrogel via a novel architecture based on π – π interlocked β -sheets," *Advanced Materials*, vol. 20, no. 1, pp. 37-41, 2008.
- [3] D. Ryan, S. Anderson and B. Nilsson, "The influence of side-chain halogenation on the self-assembly and hydrogelation of Fmoc-phenylalanine derivatives," *Soft Matter*, vol. 6, no. 14, pp. 3220-3231, 2010.
- [4] B. Adhikari, G. Palui and A. Banerjee, "Self-assembling tripeptide based hydrogels and their use in removal of dyes from waste-water," *Soft Matter*, vol. 5, no. 18, pp. 3452-3460, 2009.
- [5] S. Yuran, Y. Razvag and M. Reches, "Coassembly of aromatic dipeptides into biomolecular necklaces," *ACS Nano*, vol. 6, no. 11, pp. 9559-9566, 2012.
- [6] L. Chen, K. Morris, A. Laybourn, D. Elias, M. Hicks, A. Rodgers, L. Serpell and D. Adams, "Self-assembly mechanism for a naphthalene–dipeptide leading to hydrogelation," *Langmuir*, vol. 26, no. 7, pp. 5232-5242, 2010.
- [7] J. Zhou, X. Du, Y. Gao, J. Shi and B. Xu, "Aromatic–aromatic interactions enhance interfiber contacts for enzymatic formation of a spontaneously aligned supramolecular hydrogel," *Journal of the American Chemical Society*, vol. 136, no. 8, pp. 2970-2973, 2014.
- [8] M. Ma, Y. Kuang, Y. Gao, Y. Zhang, P. Gao and B. Xu, "Aromatic-aromatic interactions induce the self-assembly of pentapeptidic derivatives in water to form nanofibers and supramolecular hydrogels," *Journal of the American Chemical Society*, vol. 132, no. 8, pp. 2719-2728, 2010.
- [9] B. Adhikari, J. Nanda and A. Banerjee, "Pyrene-containing peptide-based fluorescent organogels: inclusion of graphene into the organogel," *Chemistry*, vol. 17, no. 41, pp. 11488-11496, 2011.
- [10] Y. Gao, Y. Kuang, X. Du, J. Zhou, P. Chandran, F. Horkay and B. Xu, "Imaging self-assembly dependent spatial distribution of small molecules in a cellular environment," *Langmuir*, vol. 29, no. 49, pp. 16191-15200, 2013.
- [11] J. Li, Y. Kuang, Y. Gao, X. Du, J. Shi and B. Xu, "D-amino acids boost the selectivity and confer supramolecular hydrogels of a nonsteroidal anti-inflammatory drug (NSAID)," *Journal of the American Chemical Society*, vol. 135, no. 2, pp. 542-545, 2013.
- [12] J. Li, Y. Kuang, J. Shi, Y. Gao, J. Zhou and B. Xu, "The conjugation of nonsteroidal anti-inflammatory drugs (NSAID) to small peptides for generating multifunctional supramolecular nanofibers/hydrogels," *Beilstein Journal of Organic Chemistry*, vol. 9, pp.

908-917, 2013.

- [13] J. Li, Y. Gao, Y. Kuang, J. Shi, X. Du, J. Zhou, H. Wang, Z. Yang and B. Xu, "Dephosphorylation of D-peptide derivatives to form biofunctional, supramolecular nanofibers/hydrogels and their potential applications for intracellular imaging and intratumoral chemotherapy," *Journal of the American Chemical Society*, vol. 135, no. 26, pp. 9907-9914, 2013.
- [14] F. Zhao, M. Ma and B. Xu, "Molecular hydrogels of therapeutic agents," *Chemical Society Reviews*, vol. 38, no. 4, pp. 883-891, 2009.
- [15] K. Montrose, Y. Yang, X. Sun, S. Wiles and G. Krissansen, "Xentry, a new class of cell-penetrating peptide uniquely equipped for delivery of drugs.," *Scientific Reports*, vol. 3, p. 1661, 2013.
- [16] Y. Wei, C. Li, L. Zhang and X. Xu, "Design of novel cell penetrating peptides for the delivery of trehalose into mammalian cells," *Biochimica et Biophysica Acta*, vol. 1838, no. 7, pp. 1911-1920, 2014.
- [17] J. Zaro, J. Vekich, T. Tran and W. Shen, "Nuclear localization of cell-penetrating peptides is dependent on endocytosis rather than cytosolic delivery in CHO cells," *Molecular Pharmaceutics*, vol. 6, no. 2, pp. 337-344, 2009.
- [18] S. Kirkham, I. Hamley, A. Smith, R. Gouveia, C. Connon, M. Reza and J. Ruokolainen, "A self-assembling fluorescent dipeptide conjugate for cell labelling," *Colloids and Surfaces B, Biointerfaces*, vol. 137, pp. 104-108, 2016.
- [19] R. Gouveia, V. Castelletto, S. Alcock, I. Hamley and C. Connon, "Bioactive films produced from self-assembling peptide amphiphiles as versatile substrates for tuning cell adhesion and tissue architecture in serum-free conditions," *Journal of Materials Chemistry B*, vol. 1, no. 44, pp. 6157-6169, 2013.
- [20] J. Suh, J. Lee, G. Lee, C. Chung and Y. Park, "Simultaneous imaging and restoration of cell function using cell permeable peptide probe," *Biomaterials*, vol. 35, no. 24, pp. 6287-6298, 2014.
- [21] I. Hamley, "Peptide fibrillisation," *Angewandte Chemie*, vol. 46, no. 43, pp. 8128-8147, 2007.
- [22] B. Stuart, *Biological Applications of Infrared Spectroscopy*, Chichester: Wiley, 1997.
- [23] S. Kelly, T. Jess and N. Price, "How to study proteins by circular dichroism," *Biochimica et Biophysica Acta*, vol. 1751, no. 2, pp. 119-139, 2005.
- [24] J. Lakowicz, *Principles of Fluorescence Spectroscopy*, New York: Kluwer, 1999.
- [25] 21 09 2016. [Online]. Available: <http://www.fluorophores.tugraz.at/substance/252>.
- [26] M. Zhou, A. Smith, A. Das, N. Hodson, R. Collins, R. Ulijn and J. Gough, "Self-assembled peptide-based hydrogels as scaffolds for anchorage-dependent cells," *Biomaterials*, vol. 30, no. 13, pp. 2523-2530, 2009.

- [27] Z. Yang, G. Liang and B. Xu, "Enzymatic hydrogelation of small molecules," *Accounts of Chemical Research*, vol. 41, no. 2, pp. 315-326, 2008.
- [28] V. Castelletto, G. Cheng, C. Stain, C. Connon and I. Hamley, "Self-assembly of a peptide amphiphile containing l-carnosine and its mixtures with a multilamellar vesicle forming lipid," *Langmuir*, vol. 28, no. 31, pp. 11599-11608, 2012.
- [29] I. Hamley, A. Dehsorkhi and V. Castelletto, "Self-assembled arginine-coated peptide nanosheets in water," *Chemical Communications*, vol. 49, no. 18, pp. 1850-1852, 2013.
- [30] V. Castelletto, R. Gouveia, C. Connon and I. Hamley, "New RGD-peptide amphiphile mixtures containing a negatively charged diluent," *Faraday Discussions*, vol. 166, pp. 381-397, 2013.
- [31] U. Fischer, J. Huber, W. Boelens, I. Mattaj and R. Luhrmann, "The HIV-1 Rev activation domain is a nuclear export signal that accesses an export pathway used by specific cellular RNAs," *Cell*, vol. 82, no. 3, pp. 475-483, 1995.
- [32] W. Wen, J. Meinkoth, R. Tsien and S. Taylor, "Identification of a signal for rapid export of proteins from the nucleus," *Cell*, vol. 82, no. 3, pp. 463-473, 1995.

Chapter 5- The self-assembly of commercially available anti-fungal drug

Amphotericin B

5.1 Introduction

In this chapter, the self-assembly of a macrolide polyene antifungal drug, Amphotericin B (AmB), is considered. It is produced by a soil actinomycete called *Streptomyces nodosus* and has been used in medicine since approval by the FDA in 1959 [1]. When used therapeutically, it is usually combined with a detergent, often sodium deoxycholate, and then administered intravenously [2]. Examples of these formulations include Fungizone and AmBisome [3, 4]. These formulations are also required as AmB is not water soluble at neutral pH [5]. Despite its long use, it has retained good antifungal properties against a large spectrum of targets, including many *Candida* and *Aspergillus* species, and other filamentous fungi, including *Mucorales* [6]. Its structure is shown in figure 1, and consists of a hydrophobic polyene backbone on one side, and a hydrophilic side consisting of hydroxyl groups, and a carboxyl and mycosamine group.

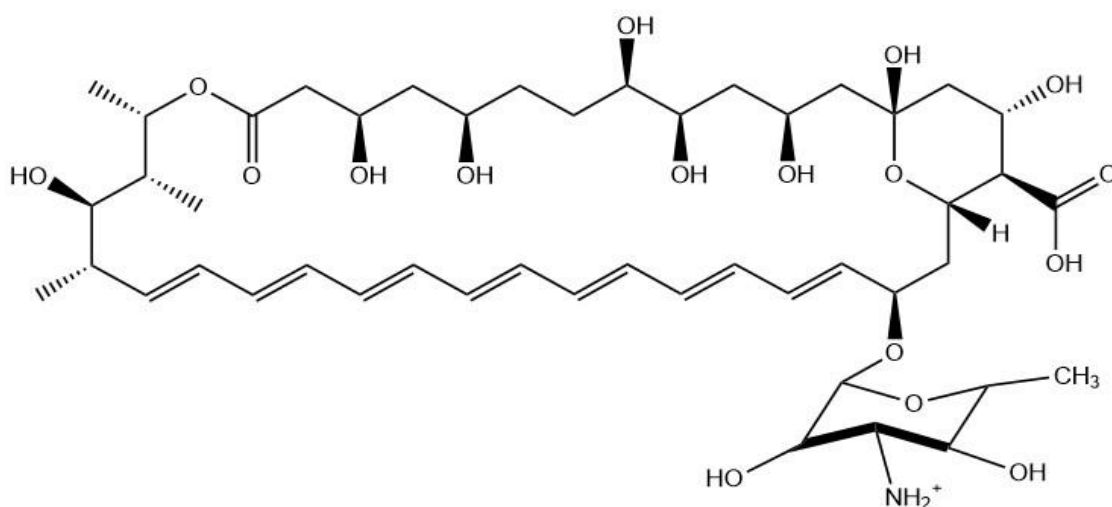


Figure 1 The molecular structure of amphotericin B.

Its mechanism of activity involves binding selectively to ergosterol, found in fungal cell membranes but not in humans, where cholesterol is instead present [7], and formation of a pore. There is thought to be some binding to cholesterol, but at much lower affinity [8]. Ergosterol is a critical part of the physiology of yeasts which performs many of the same functions in fungi as cholesterol does in animal cells, namely to influence membrane rigidity, fluidity and permeability [9]. It has been shown that mutations which alter the biosynthesis of ergosterol, and thus would offer resistance, have led to a decrease in virulence [10]. This therefore contributes to amphotericin B's evasion of fungal resistance thus far.

The two domains previously mentioned, hydrophobic and hydrophilic, play a key role in its activity. The hydrophobic regions of AmB, through the polyene backbone, interact to form dimers, and then further interact to stack together and form a helical array [11]. These interactions are required as the monomeric form of AmB is not believed to be able to permeate the membrane on its own [12]. Pore formation in the membrane causes the rapid outflow of K^+ and Mg^{2+} ions, as well as fungal glycolysis inhibition and subsequent influx of protons into the cell [13]. This causes acidification of the fungal cell, leading to cytoplasm precipitation, and finally death of the cell.

A large proportion of the research around AmB has involved how the drug reacts in formulations. One such study investigated self-assembly of AmB and heavily influenced the research undertaken in this chapter [14]. The structures formed by AmB in a range of different solvents that simulate physiological environments were investigated, and it was found that AmB was present in two different dimer forms, parallel and anti-parallel. These can then further self-assemble, shown by time evolution CD spectra, to form tetramers. These structures were previously investigated through fluorescence spectroscopy by members of the same group [15]. The authors suggest that the dimer form of AmB is the one responsible for the toxicity seen in with the drug, which can then associate into tetramers responsible for the

transmembrane pore. Grudzinski et al. also used fluorescence lifetime imaging microscopy to investigate AmB in a singular bilayer system, finding the most favourable conditions for entering the lipid phase, including the structure and orientation [16]. Block copolymers have also been used in order to increase the water-solubility of AmB, although release from these vectors was shown to either be slow or they did not release at all [17].

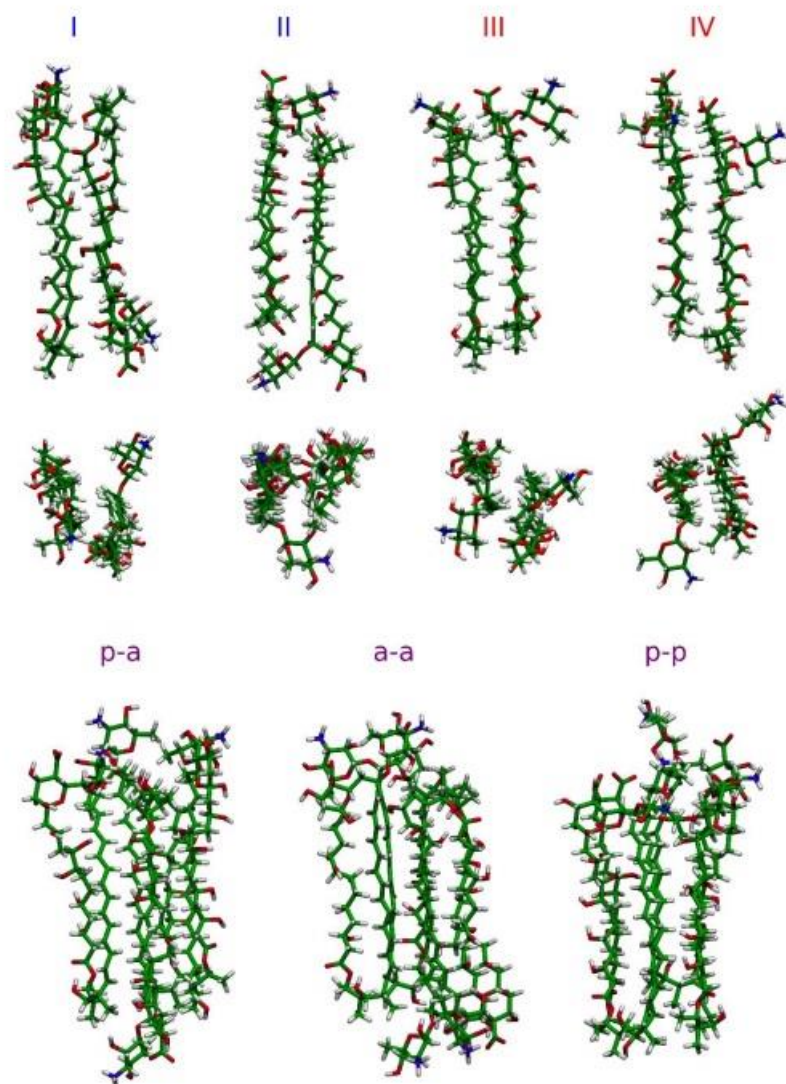


Figure 2 Visualisation of simulations showing the range of geometries and structures amphotericin B is proposed to be present in or able to form. I-IV show dimer structures, and tetramer structures are shown by p-a (parallel-antiparallel), a-a (antiparallel- antiparallel), and p-p (parallel-parallel). [32]

This research aims to build upon existing knowledge of the self-assembly of AmB in water. To our knowledge, the assembly of AmB has not been investigated at concentrations as high as we have used here. The samples used in these experiments however will also have the pH adjusted to 12 in order to keep increase the solubility, such as in other papers [14]. AmB at pH above 10 has also been shown to be present in the monomeric form, owing to the negative electric charge on the molecule [18]. DMSO is also used in the fluorescence lifetime imagine microscopy (FLIM) experiments in order to test the results from a previous paper [14]. A number of solvents known to present AmB in the forms of monomer, dimer and tetramers were used in this study. With the dimer form, it was found that there were two different photon lifetimes, caused by a parallel and antiparallel dimer. The percentage of each lifetime fraction also varied between solvent types, polar protic, polar aprotic and nonpolar. Water alkalisied to pH 12 and DMSO were chosen in our research in order to compare the results of solvents with differing polarities.

5.2 Materials and methods

Amphotericin B (AmB) was obtained in the form of powder from Merck Millipore (Nottingham, U.K.). The purity of the compound was determined by analytical HPLC to be 92.5%, and the molecular weight was obtained by electrospray-mass spectrometry (performed by Radoslaw Kowalczyk at the University of Reading) to be 924.1. In this work, weighed amounts of AmB were dissolved in ultrapure water from a Barnstead Nanopure system to the desired concentration. pH was then adjusted to 12 through addition of NaOH from Fisher Scientific (USA), dissolved pellets in water to give a 5M solution.

5.2.1 Pyrene fluorescence

Fluorescence spectra were recorded with a Varian Cary Eclipse Fluorescence Spectrometer with samples in 4 mm inner Quartz cuvettes. The assays were performed using 1.3×10^{-3} – 0.13 wt% AmB, in 2.3×10^{-5} wt% pyrene solution. The samples were excited at $\lambda_{\text{ex}}=380$ nm, and the fluorescence emission was measured for $\lambda=$ (400-550nm).

5.2.2 Cryo-TEM

Experiments were carried out by our collaborators at Aalto University in Finland using a field emission cryo-electron microscope (JEOL JEM-3200FSC) operating at 200 kV. Images were taken using bright-field mode and zero loss energy filtering (omega type) with a slit with 20 eV. Micrographs were recorded using a Gatan UltraScan 4000 CCD camera. The specimen temperature was maintained at -187 °C during the imaging. Vitrified specimens were prepared using an automated FEI Vitrobot device using Quantifoil 3.5/1 holey carbon copper grids with 3.5 μm hole sizes. Grids were cleaned using a Gatan Solarus 9500 plasma cleaner just prior to use and then transferred into an environmental chamber of FEI Vitrobot at room temperature and 100% humidity. Thereafter, 3 μl of sample solution at 1 wt% concentration was applied on the grid, blotted once for 1 second and then vitrified in a 1/1 mixture of liquid ethane and propane at -180 °C. Grids with vitrified sample solutions were maintained in a liquid nitrogen atmosphere and then cryo-transferred into the microscope.

5.2.3 Small-angle X-ray scattering (SAXS)

Experiments were performed on beamline ID02 at the ESRF (Grenoble, France). Samples were placed in a glass capillary mounted in a brass block for temperature control. Micropumping was used to minimise beam damage by displacing a drop of the sample by 0.01 - 0.1 mm for

each exposure. The sample-to-detector distance was 2 m, and the X-ray energy was 12.46 keV. The $q = 4\pi \sin \vartheta/\lambda$ range was calibrated using silver behenate. Data processing (background subtraction, radial averaging) was performed using the software SAXSutilities.

5.2.4 Circular Dichroism (CD)

CD spectra were recorded using a Chirascan spectropolarimeter (Applied Photophysics, UK). The sample (0.01 - 1 wt% in water, pH raised to 12 with NaOH) was placed in a cover slip cuvette (0.1 mm thick). Spectra are presented with absorbance $A < 2$ at any measured point with a 0.5 nm step, 1 nm bandwidth, and 1 second collection time per step at 20 °C. In temperature-dependent experiments, the AmB solution was acclimatised at each temperature point for 5 minutes before measurements were taken. The CD signal from the pH 12 alkalised water was subtracted from the CD data of the AmB solution.

5.2.5 Fourier transform infrared spectroscopy (FTIR)

For the secondary structure studies, spectra were recorded using a Thermo Scientific Nicolet IS5 and a Nexus-FTIR spectrometer, both equipped with a DTGS detector. A 40 μ L drop of the sample (in D₂O with pH raised to 12) was sandwiched between two CaF₂ plate windows, with a 0.006 mm thick Mylar spacer) in a Specac GS20500 sample cell holder. Spectra were scanned 128 times over the range of 900–4000 cm^{-1} .

5.2.6 Two-photon fluorescence lifetime imaging

Two-photon-induced fluorescence lifetime images were obtained with multiphoton microscopy apparatus constructed on an Eclipse TE2000 (Nikon) with Becker and Hickl

confocal scanning (DCS120) capability FLIM. Briefly, a high-powered titanium sapphire laser (MIRA 900; Coherent Lasers) was pumped by a frequency-doubled neodymium:vanadate laser (Verdi V10; Coherent Lasers, UK) to produce a 700-930 nm laser light of 180-fs pulses at 76 MHz. Specimens on a Nikon TE2000U microscope stage were excited by focusing the near-infrared laser beam to a diffraction-limited spot through a 60× water immersion objective (numerical aperture [NA], 1.2). Fluorescence emissions from specimens were collected, bypassing the scanning system, through a band-pass filter (BG39, Comar) using a non-descanned port of the confocal microscope. Single-photon pulses were detected by an external fast microchannel plate photomultiplier tube (Hamamatsu R3809U). The scan, which was operated in a normal mode and line, frame, and pixel clock signals were synchronized and collected with a time-correlated single-photon-counting (TCSPC) PC module (SPC-830; Becker and Hickl, Germany).

5.3 Results and discussion

The critical aggregation concentration (cac) of AmB was determined using pyrene, as with the other compounds mentioned in some previous chapters. Interestingly, it was found that with increasing concentration of AmB, the already low pyrene fluorescence peak at 373 nm compared with previous pyrene fluorescence experiments, decreased. This is shown in figure 3a. Conversely, increasing concentration eventually lead to an increase of peak at 475 nm, which is usually seen in pyrene fluorescence assays at 373 nm. The reason for this is so far unknown, although similar emission spectra have been noted previously with AmB [19]. The intersection of the two lines showing this point, shown in figure 3b, was used as the critical aggregation point, found to be 0.06 wt% (± 0.01 wt%).

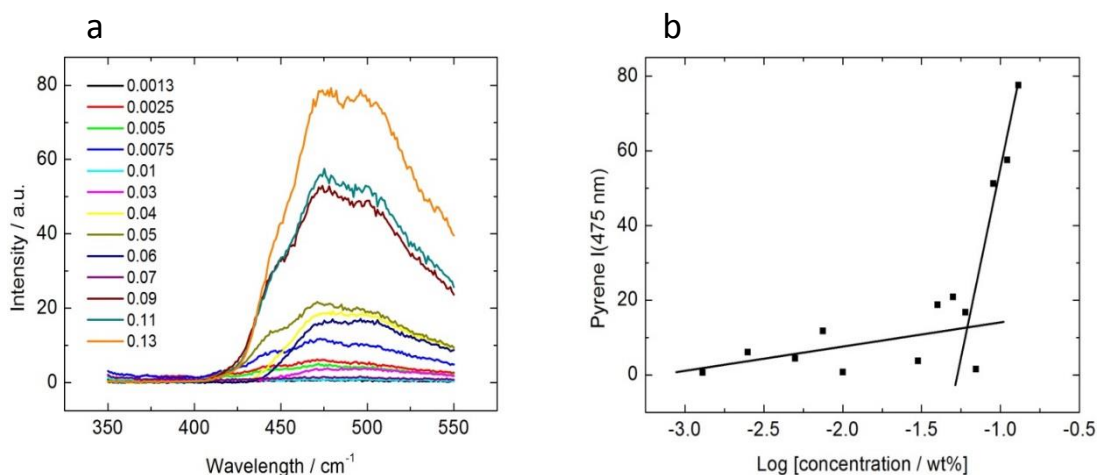


Figure 3 Fluorescence assay of amphotericin B using pyrene. a) Shows the spectra of each concentration across the range used, b) shows the intensity of each concentration at the peak value at 475 nm, with cac indicated at the intersection of the lines.

The self-assembly of AmB was investigated through the use of cryo-TEM and SAXS. Cryo-TEM has previously only been used to observe AmB when in lipid or surfactant-based particle systems [20, 21]. The cryo-TEM images in figure 4 reveal a mixture of mostly cylindrical micelles of varying lengths, but also very long twisting tape-like structures in a) and b). The diameters of the cylindrical micelles were measured at around 5 nm, which was also confirmed in the SAXS fitting profile (figure 5). The fit used a long cylindrical shell form factor, a scaling factor of 0.03, diameter 6.7 nm, shell thickness 2.2 nm, solvent side bilayer thickness of 0.28 nm, inner bilayer thickness of 1.2 nm, and scattering length densities of solvent, solvent side bilayer, and inner bilayer of 0.00033-0.00068 nm, and background parameter of 0.00034.

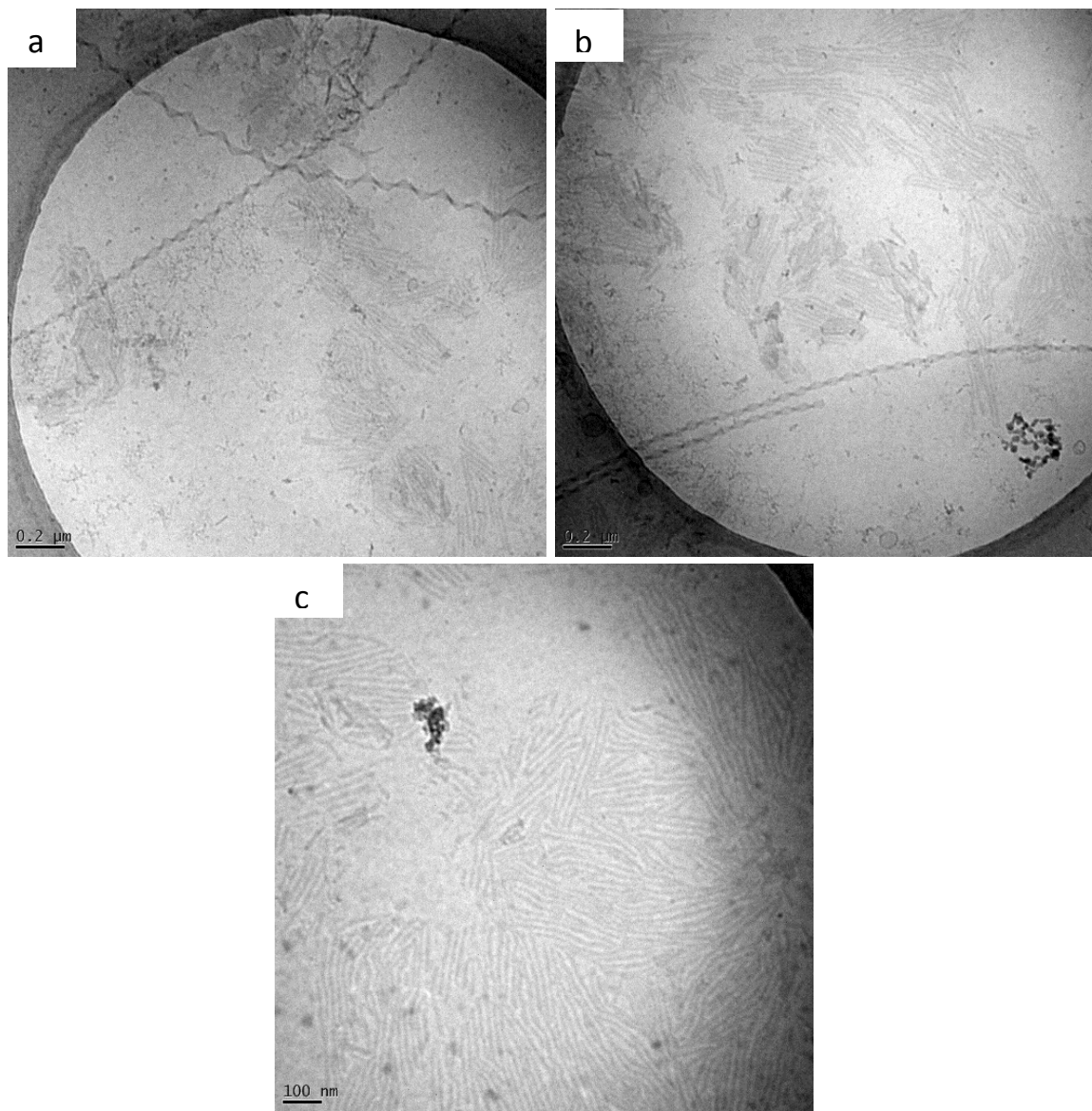


Figure 4 Representative cryo-TEM images of 1 wt% amphotericin B.

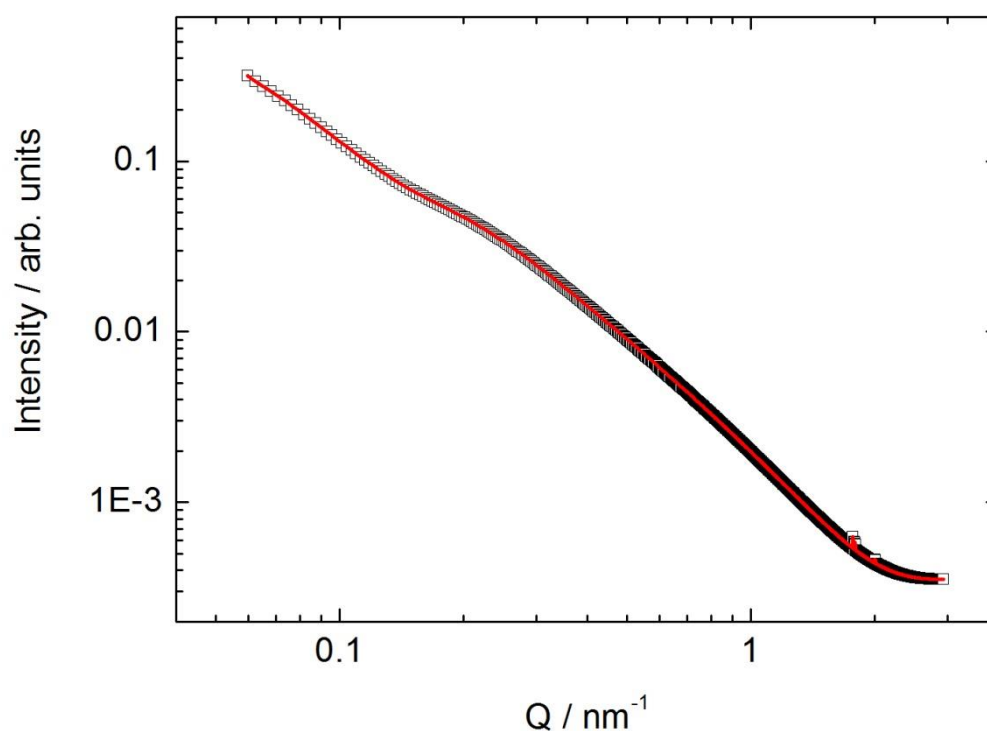


Figure 5 SAXS data (black symbols) with model form factor (red line) of a 0.1 wt% solution of amphotericin B. Specific dimensions for the fit are described in the text.

The secondary structure was investigated firstly through CD spectroscopy in water alkalisied to pH 12, which it has been suggested favours AmB dimerization at lower concentrations [22]. At 20°C, results, shown in figure 6, showed a similar shaped spectrum to that previously attributed to the aggregated form whilst in PBS, shown in figure 8 [14]. This consisted of a series of small descending negative peaks at 422, 392 and 372 nm, followed by a large positive peak at 336 nm. This spectrum has also been observed a number of other times with AmB [22-24]. However, this developed into a different spectrum, with a transition around 30°C, shown by the inclusion of two successive scans at 30°C. Upon heating, the spectrum shape changes to one with a pronounced negative peak at 326 nm, which to our knowledge has not seen with AmB before. This therefore was ascribed to the novel AmB structures seen in the cryo-TEM images in figure 4. The next set of experiments further explored this, leaving the 0.1 wt% AmB

sample at the same temperature, with CD signal measured at various time points (figure 7a), which showed a similar starting spectrum shape and progression to the spectrum with minimum at 326 nm shown in figure 6. The absorbance spectrum (figure 7b) is comparable with that seen in figure 8, but with AmB in DMSO and alkalis water, attributed to a monomeric form. This consists of three peaks, which are retained over the 24 hours, along with the development of another small peak at 326 nm. This correlates with the large minimum seen in the CD spectrum in figure 7a. A time-dependent change had also been observed by the Starzyk group [14]. A hypothesis was proposed that the UV light emitted from the CD machine during experimentation was causing cross-linking within the polyene backbone.

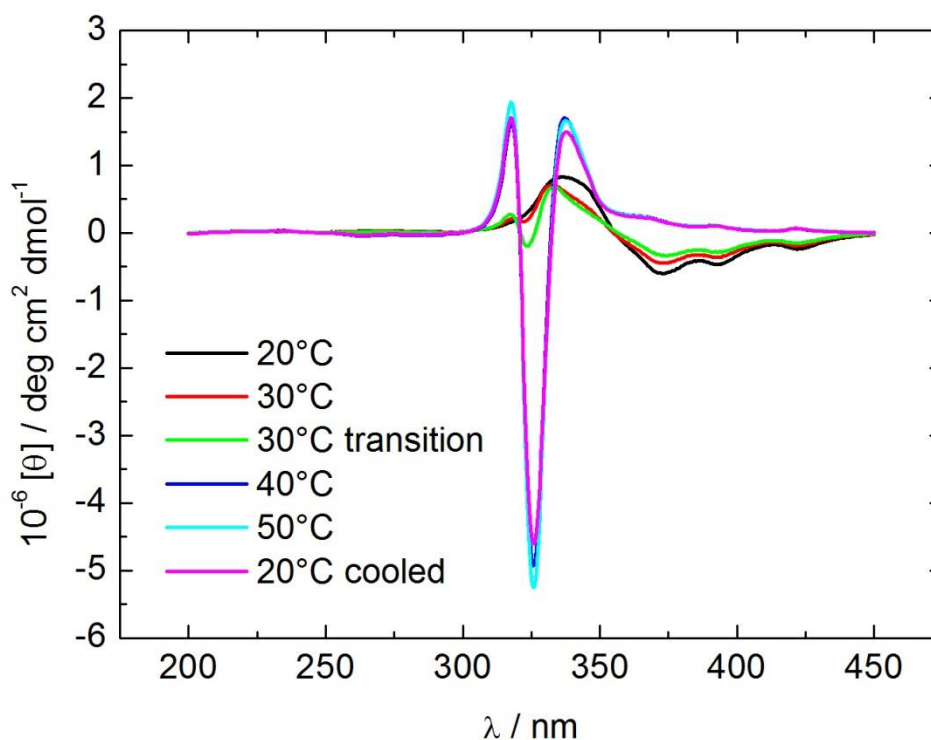


Figure 6 Temperature-dependent CD spectrum of 0.1 wt% solution of amphotericin B, with observed transition when measured twice at 30°C.

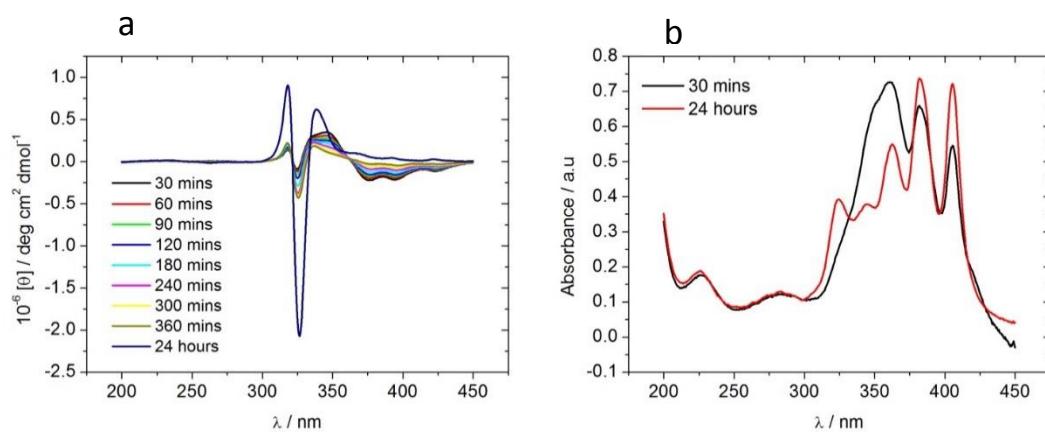


Figure 7 a) Time-dependent CD spectrum of 0.1 wt% solution of amphotericin B at 20°C, b) corresponding absorbance spectrum.

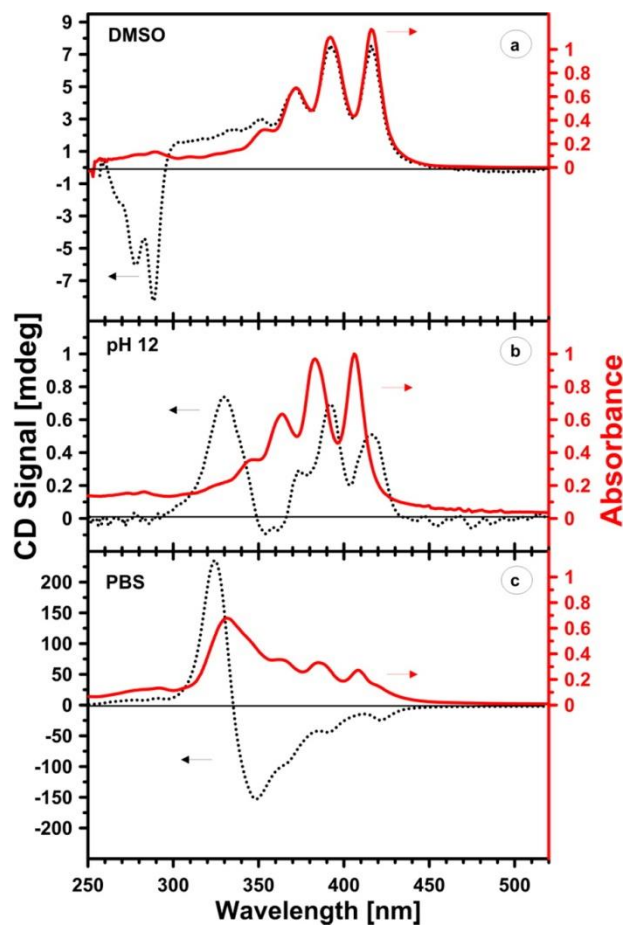


Figure 8 Absorption (red) and CD (black) spectra of AmB in various solutions by the Starzyk group [14].

This was tested through FTIR experimentation, which does not emit UV light, but still reveals information about secondary structure. Shown in figure 9, there is also a change observed over time. There is a very large broad peak seen which stretches from $\sim 3100\text{-}3600\text{ cm}^{-1}$. This can be attributed to O-H stretch bonds, which have been shown to give large broad peaks in this area, along with amine stretch [25]. The peak is clearly shown to increase in absorbance relative to time, and shows no sign of plateauing, even at the latest time point at 72 hours. Due to time constraints on the CD experiments, it could not be seen whether the negative peak continued to increase (figure 7a) as the FTIR one had. The fact these changes occur during FTIR experimentation implies that these changes seen using CD in figure 6 and 7a are not due to UV exposure.

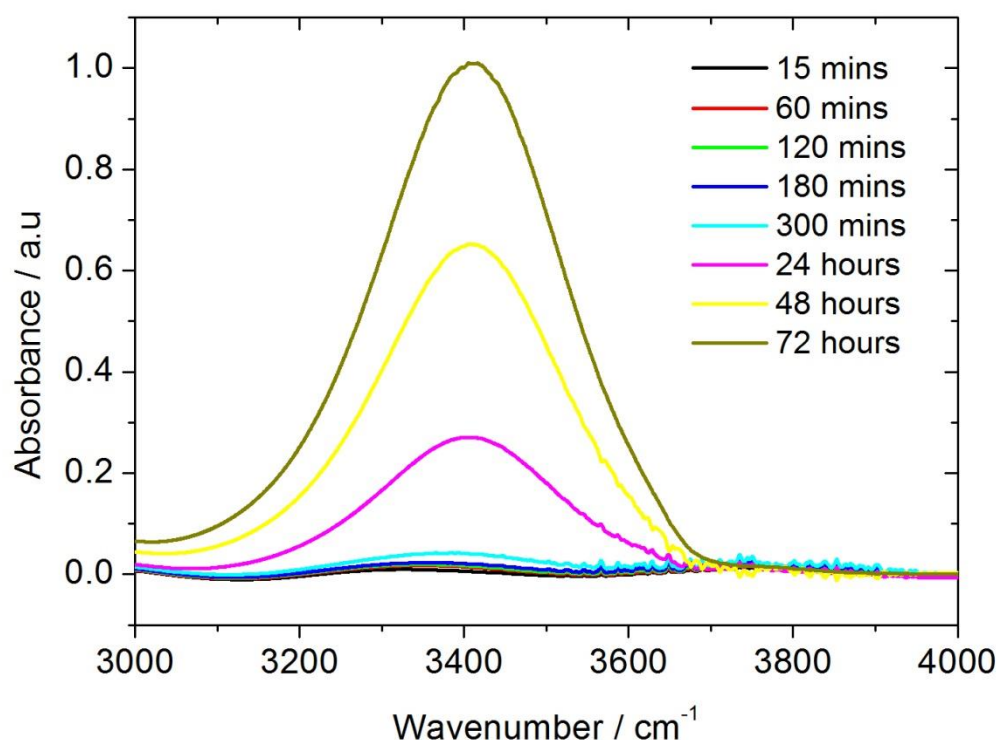


Figure 9 Time-dependent FTIR spectrum of 0.1 wt% solution of amphotericin B at 20°C.

With evidence that the changes in structure were not temperature-dependent, and that UV exposure was not the cause, a hypothesis was proposed that the time taken between the preparation of the sample and the measurements was responsible. Work to test this was not carried out due to the lack of time, but is a new area of interest and can be explored in future work. It has previously been seen with AmB that auto-oxidation can occur in some cases [26, 27]. Mass spec and ^1H and ^{13}C NMR, performed by collaborator Radoslaw M. Kowalczyk at the University of Reading, were therefore undertaken on aged samples of the compound. These results are shown in the supplementary information of the published paper [187] and revealed no evidence of any molecular degradation or auto-oxidation.

As part of some preliminary measurements, AmB was investigated through fluorescence lifetime imaging microscopy (FLIM). It has previously been proposed that AmB can be present in different forms, both a parallel and antiparallel dimer, based on the observed differing lifetimes [14]. In these experiments, the same concentration was used, but in different solvents, DMSO and alkalised water, and with different excitation wavelengths. Two-photon excitation was used in this case in order to access UV wavelengths more easily than with single-photon excitation through a microscope set up (future studies aimed to include imaging AmB in live cells, but weren't able to be completed due to time constraints). The excited state decay curves obtained were best fitted using two exponential components. Figure 10 shows that the lifetime in the first component is unchanged by the differing excitation wavelengths in both water and DMSO. The second component however shows a large change in lifetime in the two solvents when excited at different wavelengths. These two components are likely due to different energy states in the molecule. This raises questions about the claim from the authors of ref [14] of AmB being present in different forms shown by the fluorescence lifetime-associated spectra, as merely changing the excitation wavelength here has been shown to give different lifetime values that are not too dissimilar to those reported in ref [14], but with concentration change. The motivation for using different excitation wavelength stems

from the features in the absorption spectra. Originally, the wavelength started with was the same as the authors in reference [14], but it was soon realised that 810 nm wasn't the maximum excitation, particularly when using multiphoton excitation.

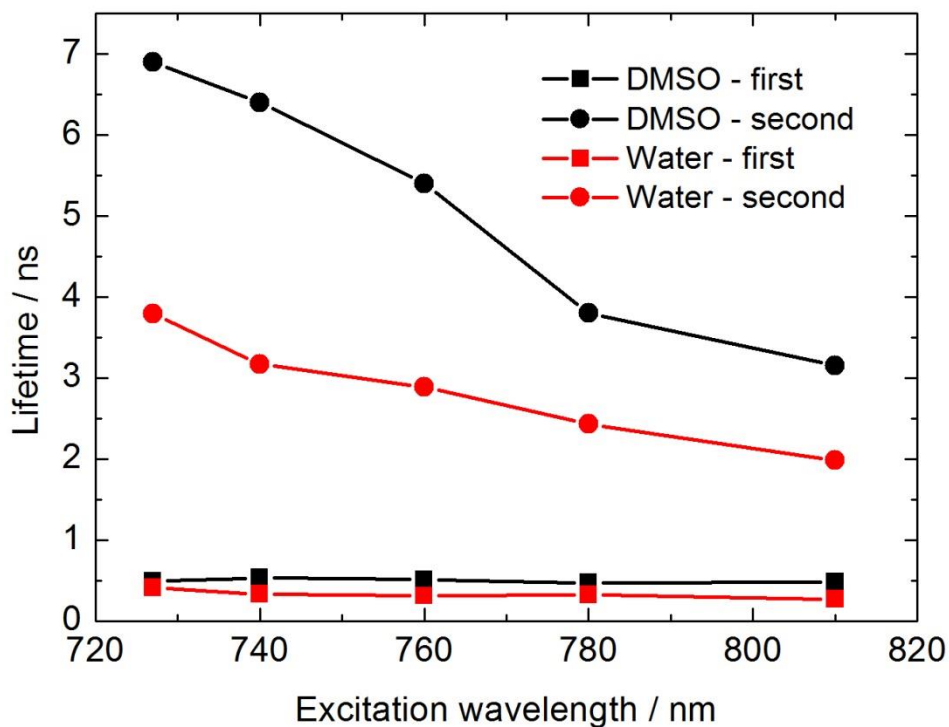


Figure 10 Two-photon excitation FLIM data of amphotericin B at various excitation wavelengths showing first and second components.

In this chapter, a number of techniques were used to determine the self-assembling of properties of AmB in water alkalisied to pH12. As the structures which the drug is able to form have been linked with toxicity in patients [14, 29, 30], this research can have important information in helping reduce the toxicity. At the concentrations we have used, it seems AmB forms aggregated structures, with the suggestion that they can change over time to give even larger aggregations in different forms. In contrast to previous studies [14], these changes seem to not merely lead to shifted spectra which retain their structure, but completely different assemblies with very large intensities. We have also proven that, unlike some earlier

hypotheses, these changes are not specifically due to temperature, nor are they UV light-induced. It was only proposed later on in the research that the length of time between the preparation of the samples, and then the use of them in experiments, could have an effect on what structure it is present in.

Further cryo-TEM images to compare a freshly prepared sample with an older one/one which has been heated and cooled again may provide interesting results, to observe whether these changes in CD signal are reflected in a changing structure. The long tape-like structures were seen in the cryo-TEM images, but the SAXS profile was fitted to a form factor for the cylindrical micelles. These structures were much more abundant, and it may be that the tape-like structures were too few to contribute to the SAXS profile. Cryo-TEM was at 1 wt%, and SAXS at 0.1 wt%, therefore there is also the possibility that the structures may only be a product of the higher concentration. Uniformity across different experiment types, so that direct conclusions may be made, would therefore be beneficial.

Previously it has been proposed, through the use of FLIM, that AmB at concentrations below our determined cac (0.00085 wt%, versus 0.1-1 wt% in this chapter) is present in two different dimer forms, parallel and antiparallel [22]. Our FLIM data, at concentrations above our experimentally determined cac, suggest that further research is needed to understand the wavelength-dependent intensities. Due to time constraints, these extra FLIM experiments weren't able to be done. However, if indeed the previous model [14] is correct and AmB is present in the two forms, it may also give information on why two different CD spectra have been seen.

The presence of two aggregated forms of AmB could have interesting implications in the pursuit of reducing toxicity. As previously referred to, it has been suggested that an AmB aggregate is responsible for the more recently found mechanism of action upon binding ergosterol, which then forms the transmembrane channel [31]. Further work into comparisons

of the types of aggregates formed under different conditions would be interesting. Use of liposomes to mimic lipid bilayers, and other solvents which better resemble the physiological environment of the body, would shed more light on whether these new aggregated structures are responsible for the toxic effects of the drug.

5.4 References

- [1] R. Hamill, "Amphotericin B formulations: a comparative review of efficacy and toxicity," *Drugs*, vol. 73, no. 9, pp. 919-934, 2013.
- [2] H. Gallis, R. Drew and W. Pickard, "Amphotericin B: 30 years of clinical experience," *Reviews of Infectious Diseases*, vol. 12, no. 2, pp. 308-329, 1990.
- [3] J. Torrado, R. Espada, M. Ballesteros and S. Torrado-Santiago, "Amphotericin B formulations and drug targeting," *Journal of Pharmaceutical Sciences*, vol. 97, no. 7, pp. 2405-2425, 2008.
- [4] J. Sanchez-Brunete, M. Dea, S. Rama, F. Bolas, J. Alunda, R. Raposo, M. Mendez, S. Torrado-Santiago and J. Torrado, "Treatment of experimental visceral leishmaniasis with amphotericin B in stable albumin microspheres," *Antimicrobial Agents and Chemotherapy*, vol. 48, no. 9, pp. 3246-3252, 2004.
- [5] T. Ehrenfreund-Kleinman, T. Azzam, R. Falk, I. Polacheck, J. Golenser and A. Domb, "Synthesis and characterization of novel water soluble amphotericin B-arabinogalactan conjugates," *Biomaterials*, vol. 23, no. 5, pp. 1327-1335, 2002.
- [6] N. Engleberg, T. Dermody and V. DiRita, *Schaechter's Mechanisms of Microbial Disease*, Lippincott Williams & Wilkins, 2012.
- [7] J. Kotler-Brajtburg, G. Medoff, G. Kobayashi, S. Boggs, D. Schlessinger, R. Pandey and K. Rinehart, "Classification of polyene antibiotics according to chemical structure and biological effects," *Antimicrobial Agents and Chemotherapy*, vol. 15, no. 5, pp. 716-722, 1979.
- [8] C. Hsueh and D. Feingold, "Selective membrane toxicity of the polyene antibiotics: studies on natural membranes," *Antimicrobial Agents and Chemotherapy*, vol. 4, no. 3, pp. 316-319, 1973.
- [9] L. Parks and W. Casey, "Physiological implications of sterol biosynthesis in yeast," *Annual Review of Microbiology*, vol. 49, pp. 95-116, 1995.
- [10] B. Vincent, A. Lancaster, R. Scherz-Shouval, L. Whitesell and S. Lindquist, "Fitness trade-offs restrict the evolution of resistance to amphotericin B," *PLoS Biology*, vol. 11, no. 10, p. e1001692, 2013.
- [11] J. Milhaud, V. Ponsinet, M. Takashi and B. Michels, "Interactions of the drug amphotericin B with phospholipid membranes containing or not ergosterol: new insight into the role of ergosterol," *Biochimica et Biophysica Acta*, vol. 1558, no. 2, pp. 95-108, 2002.

- [12] M. Gagos and M. Arczewska, "Spectroscopic studies of molecular organization of antibiotic amphotericin B in monolayers and dipalmitoylphosphatidylcholine lipid multibilayers," *Biochimica et Biophysica Acta*, vol. 1798, no. 11, pp. 2124-2130, 2010.
- [13] S. Kinsky, "Antibiotic interaction with model membranes," *Annual Review of Pharmacology*, vol. 10, pp. 119-142, 1970.
- [14] J. Starzyk, M. Gruszecki, K. Tutaj, R. Luchowski, R. Szlajak, P. Wasko, W. Grudzinski, J. Czub and W. Gruszecki, "Self-association of amphotericin b: spontaneous formation of molecular structures responsible for the toxic side effects of the antibiotic," *The Journal of Physical Chemistry B*, vol. 118, no. 48, pp. 13821-13832, 2014.
- [15] P. Wasko, R. Luchowski, K. Tutaj, W. Grudzinski, P. Adamkiewicz and W. Gruszecki, "Toward understanding of toxic side effects of a polyene antibiotic amphotericin B: fluorescence spectroscopy reveals widespread formation of the specific supramolecular structures of the drug," *Molecular Pharmaceutics*, vol. 9, no. 5, pp. 1511-1520, 2012.
- [16] W. Grudzinski, J. Sagan, R. Welc, R. Luchowski and W. Gruszecki, "Molecular organization, localization and orientation of antifungal antibiotic amphotericin B in a single lipid bilayer," *Scientific Reports*, vol. 6, p. 32780, 2016.
- [17] N. Pippa, M. Mariaki, S. Pispas and C. Demetzos, "Preparation, development and in vitro release evaluation of amphotericin B-loaded amphiphilic block copolymer vectors," *International Journal of Pharmaceutics*, vol. 473, no. 1-2, pp. 80-86, 2014.
- [18] M. Gagos, M. Herec, M. Arczewska, G. Czernel, S. M. Dalla and W. Gruszecki, "Anomalously high aggregation level of the polyene antibiotic amphotericin B in acidic medium: implications for the biological action," *Biophysical Chemistry*, vol. 136, no. 1, pp. 44-49, 2008.
- [19] I. Asher and G. Schwartzman, "Amphotericin B," in *Profiles of Drug Substances, Excipients and Related Methodology*, London, Academic Press, 1977, p. 24.
- [20] W. Perkins, I. Ahmad, X. Li, D. Hirsh, G. Masters, C. Fecko, J. Lee, S. Ali, J. Nguyen, J. Schupsky, C. Herbert, A. Janoff and E. Mayhew, "Novel therapeutic nano-particles (lipocores): trapping poorly water soluble compounds," *International Journal of Pharmaceutics*, vol. 200, no. 1, pp. 27-39, 2000.
- [21] Z. Yang, X. Peng, Y. Tan, M. Chen, X. Zhu, M. Feng, Y. Xu and C. Wu, "Optimization of the preparation process for an oral phytantriol-based amphotericin B cubosomes," *Journal of Nanomaterials*, vol. 2011, pp. 1-10, 2011.
- [22] L. Jameson and S. Dzyuba, "Circular dichroism studies on intermolecular interactions of amphotericin B in ionic liquid-rich environments," *Chirality*, vol. 25, no. 7, pp. 427-432, 2013.

- [23] M. Larabi, A. Gulik, J. Dedieu, P. Legrand, G. Barratt and M. Cheron, "New lipid formulation of amphotericin B: spectral and microscopic analysis," *Biochimica et Biophysica Acta*, vol. 1664, no. 2, pp. 172-181, 2004.
- [24] A. Balakrishnan and K. Easwaran, "Lipid-amphotericin B complex structure in solution: a possible first step in the aggregation process in cell membranes," *Biochemistry*, vol. 32, no. 15, pp. 4139-4144, 1993.
- [25] L. Bellamy, *The Infrared Spectra of Complex Molecules*, London: Springer Netherlands, 1980.
- [26] M. Lamy-Freund, V. Ferreira, A. Faljoni-Alario and S. Schreier, "Effect of aggregation on the kinetics of autoxidation of the polyene antibiotic amphotericin B," *Journal of Pharmaceutical Sciences*, vol. 82, no. 2, pp. 162-166, 1993.
- [27] P. Kovacic and A. Cooksy, "Novel, unifying mechanism for amphotericin B and other polyene drugs: electron affinity, radicals, electron transfer, autoxidation, toxicity, and antifungal action," *MedChemComm*, vol. 3, pp. 274-280, 2012.
- [28] I. Hamley, S. Kirkham, R. Kowalczyk, V. Castelletto, M. Reza and J. Ruokolainen, "Self-assembly of the anti-fungal polyene amphotericin B into giant helically-twisted nanotapes," *Chemical Communications*, vol. 51, no. 100, pp. 17680-17683, 2015.
- [29] J. Barwicz, S. Christian and I. Gruda, "Effects of the aggregation state of amphotericin B on its toxicity to mice," *Antimicrobial Agents and Chemotherapy*, vol. 36, no. 10, pp. 2310-2315, 1992.
- [30] R. Espada, S. Valdespina, C. Alfonso, G. Rivas, M. Ballesteros and J. Torrado, "Effect of aggregation state on the toxicity of different amphotericin B preparations," *International Journal of Pharmaceutics*, vol. 361, no. 1-2, pp. 64-69, 2008.
- [31] J. Brajtburg and J. Bolard, "Carrier effects on biological activity of Amphotericin B," *Clinical Microbiology Reviews*, vol. 9, no. 4, pp. 512-531, 1996.
- [32] J. Zielinska, M. Wieczor, T. Baczek, M. Gruszecki and J. Czub, "Thermodynamics and kinetics of amphotericin B self-association in aqueous solution characterized in molecular detail," *Scientific Reports*, vol. 6, p. 19109, 2016.

Chapter 6 - Self-assembly of daptomycin, and comparison with and without calcium chloride

6.1 Introduction

Daptomycin is a cyclic lipopeptide drug active against gram-positive bacteria, produced by the gram-positive bacterium *Streptomyces roseosporus* [1]. The drug is also effective against bacteria resistant to other drugs, such as methicillin-resistant *Staphylococcus aureus* (MRSA) and vancomycin-resistant *Enterococcus* (VRE) [2]. It is also known under its trade name Cubicin [3]. As shown in figure 1, it is composed of 13 amino acids, 10 making up the cyclic structure and the other 3 forming a chain. The cyclic section of the molecule is linked through an ester bond to the tail through the terminal kynurenine, an amino acid product of tryptophan metabolism only observed in daptomycin, and the threonine hydroxyl group [3]. The kynurenine residue, specifically the aniline component contained within, is also responsible for a fluorescence emission peak at 460 nm [4]. Another emission peak at 355 nm is due to Trp-1 [4].

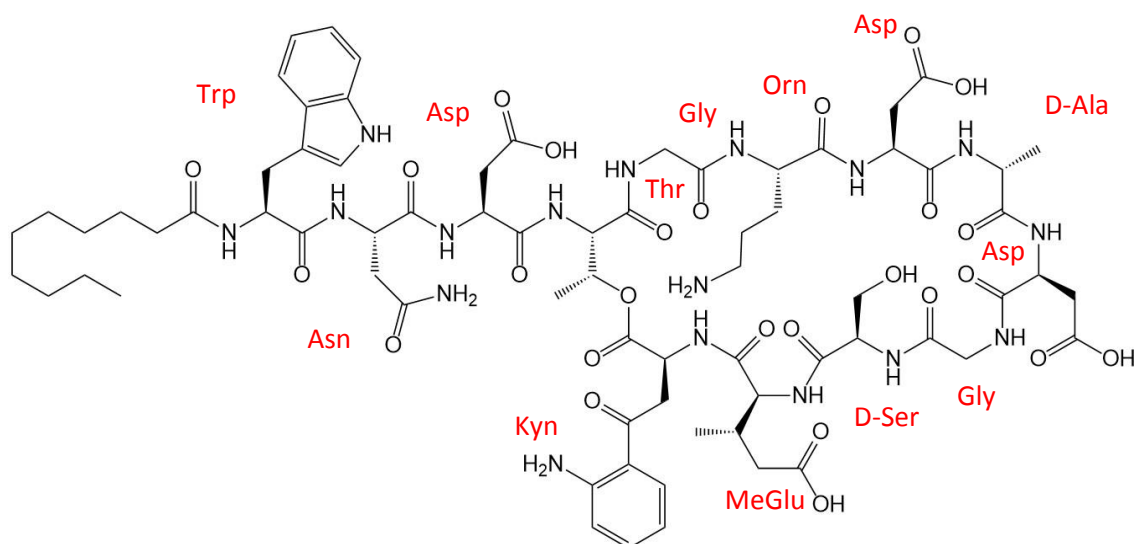


Figure 1 Molecular structure of daptomycin. Trp = tryptophan, Asn = asparagine, Asp = aspartic acid, Thr = threonine, Gly = glycine, Orn = ornithine, D-Ala = D-Alanine, D-Ser = D-Serine, MeGlu = methylglutamic acid, Kyn = kynurenine.

Daptomycin's concentration-dependent [5] mechanism of action has not been fully elucidated. One hypothesis was that inhibition of lipoteichoic acid (LTA) biosynthesis was responsible for daptomycin's antibiotic activity [6, 7]. However, more recent studies have shown a continued bactericidal activity in the absence of LTA synthesis [8]. The more favoured hypothesised mechanism is believed to involve disruption of the bacterial cell membrane by insertion of the daptomycin lipophilic N-terminal decanoyl chain into the membrane [9]. This then allows the flow of potassium ions out of the cell, and sodium influx [10], which causes depolarisation of the membrane, and is proposed to be the cause of cell death [11]. Daptomycin itself is able to cause this effect despite both it and the bacterial membrane being negatively charged. This is believed to be due to the presence of cations, in particular calcium ions, said to be vital for its antibiotic activity [12, 13]. These ions are believed to cause deeper penetration into the membrane due to the bridging of residual negative amino acids and negative phospholipids in the bacterial cell membrane [14]. There is also the possibility of further contribution towards cell death from oligomerization in the membrane in the presence of calcium ions, causing

disruption of cell membrane development when the oligomer dissociates at the bacterial membrane [15]. This antibacterial process is calcium-dependent, although the reasons are poorly understood. Daptomycin has also been shown to cause the inhibition of various cellular processes, including synthesis of proteins, DNA and RNA [16].

It has been reported that a 1:1 ratio of Ca^{2+} to daptomycin leads to micelle formation, although this does not lead to a change in the daptomycin conformation [17]. In the absence of calcium ions, one of three forms of daptomycin have been proposed, none of which are highly amphiphilic [15]. At a molar equivalent of added Ca^{2+} ions, it is proposed, based on NMR experiments, that 14-16 daptomycin monomers oligomerize, likely into a micelle [18]. Calcium ions are thought to bind between two of the aspartic acid residues on the daptomycin molecule, decreasing its net charge and increasing its hydrophobic area, allowing it to better interact with membranes [14]. When the oligomer is in close proximity to the bacterial membrane, it dissociates and the insertion process described above occurs.

Despite this prior work, there is no direct evidence for the nature of the self-assembled structures of daptomycin. This was therefore the aim set out for this chapter, with experiments performed both in the presence and absence of calcium ions. The ratios of daptomycin to CaCl_2 chosen and the use of 100 mM KCl solutions were selected based on previous reports [15, 17, 18].

6.2 Materials & Methods

Daptomycin was obtained from Merck Millipore (USA) with a molecular weight of 1620.7 g/mol and a purity of 100% determined by HPLC. Potassium chloride was from Fisher Scientific (UK) and calcium chloride from Sigma-Aldrich (USA). All samples were prepared in 100 mM KCl, based on previous literature [15, 17-19], unless otherwise mentioned.

6.2.1 Fluorescence Assays

Fluorescence spectra were recorded with a Varian Cary Eclipse Fluorescence Spectrometer with samples in 4 mm inner Quartz cuvettes. The assays were performed using 1.3×10^{-3} – 0.13 wt% daptomycin solutions in 100 mM KCl. The samples were excited at $\lambda_{\text{ex}}=380$ nm, and the fluorescence emission was measured for $\lambda=$ (400-550nm).

6.2.2 Cryo-Transmission electron microscopy (cryo-TEM)

Experiments were carried out by our collaborators at the University of Aalto, Finland using a field emission cryo-electron microscope (JEOL JEM-3200FSC) operating at 200 kV. Images were taken using bright-field mode and zero loss energy filtering (omega type) with a slit with 20 eV. Micrographs were recorded using a Gatan UltraScan 4000 CCD camera. The specimen temperature was maintained at -187 °C during the imaging. Vitrified specimens were prepared using an automated FEI Vitrobot device using Quantifoil 3.5/1 holey carbon copper grids with 3.5 μm hole sizes. Grids were cleaned using a Gatan Solarus 9500 plasma cleaner just prior to use and then transferred into an environmental chamber of FEI Vitrobot at room temperature and 100% humidity. Thereafter, 3 μl of sample solution at 0.5 wt% in 100 mM KCl was applied on the grid, blotted once for 1 second and then vitrified in a 1/1 mixture of liquid ethane and propane at -180 °C. Grids with vitrified sample solutions were maintained in a liquid nitrogen atmosphere and then cryo-transferred into the microscope.

6.2.3 Circular Dichroism (CD)

CD spectra were recorded using a Chirascan spectropolarimeter (Applied Photophysics, UK). Each sample (0.1 wt% daptomycin in 100 mM KCl and with 0 mM, 0.154 mM or 0.625 mM CaCl_2) was placed in a cover slip cuvette (0.1 mm thick). Spectra are presented with

absorbance $A < 2$ at any measured point with a 0.5 nm step, 1 nm bandwidth, and 1 second collection time per step at 20 °C. Each daptomycin solution was acclimatised at each temperature point for 10 minutes before measurements were taken. The CD signal from the background was subtracted from the CD data of the daptomycin solution.

6.2.4 Small-Angle X-ray Scattering (SAXS)

Experiments were performed on beamline B21 at the Diamond Light Source, Harwell, UK. Solutions of daptomycin (0.5, 1 and 2 wt% with 100 mM KCl and with or without CaCl₂) were loaded into the 96 well plate of an EMBL BioSAXS robot. Aliquots of solutions (25 µL) were then injected via an automated sample exchanger at a slow and very reproducible flux into a quartz capillary (1.8 mm internal diameter) in the X-ray beam. The quartz capillary was enclosed in a vacuum chamber to avoid parasitic scattering. After the sample was injected in the capillary and reached the X-ray beam, the flow was stopped during the SAXS data acquisition. SAXS frames were collected with a duration of 20 or 100 s. B21 operated with a fixed camera length (4.01 m) and fixed energy (12.4 keV). The images were captured using a Pilatus 2m detector. Data processing (background subtraction, radial averaging) was performed using the dedicated beamline software Scatter.

6.2.5 Fourier transform infrared spectroscopy (FTIR)

Spectra were recorded using a Thermo Scientific Nicolet IS5 and a Nexus-FTIR spectrometer, both equipped with a DTGS detector. A 40 µl drop of the sample (6.17 mM daptomycin in 100 mM KCl with or without 1.54 mM or 6.17 mM CaCl₂ in D₂O) was sandwiched between two CaF₂ plate windows, with a 0.006 mm thick Mylar spacer) in a Specac GS20500 sample cell holder. Cells were heated using a Specac 4000 series high stability heating controller, and a Specac electrical heating jacket. The sample was acclimatised at each temperature point for 10

minutes before measurements were taken. Spectra were scanned 128 times over the range of 900-4000 cm^{-1} .

6.3 Results and discussion

Firstly, the concentration at which daptomycin aggregates (the critical aggregation concentration, cac) was found through fluorescence assay. This was based on the self-fluorescence peak at 466 nm, similar to the 460 nm peak described in the introduction, rather than the usual method of using pyrene. The spectra are shown in figure 2. Figure 3 compares the cac of daptomycin in salt-free solution, and with molar ratios of 4:1 and 1:1 CaCl_2 added (based on previous reports [18]). The cac was found to be 0.02 wt%, with an error of 0.003 wt%, with no discernible differences between the three different solution types. This value of 0.02 wt% also correlates with another previously reported value through daptomycin auto fluorescence, in this case without CaCl_2 , using dynamic light scattering at pH4 (0.02 wt% in this case is equal to the 0.12 mM quoted in the reference) [4].

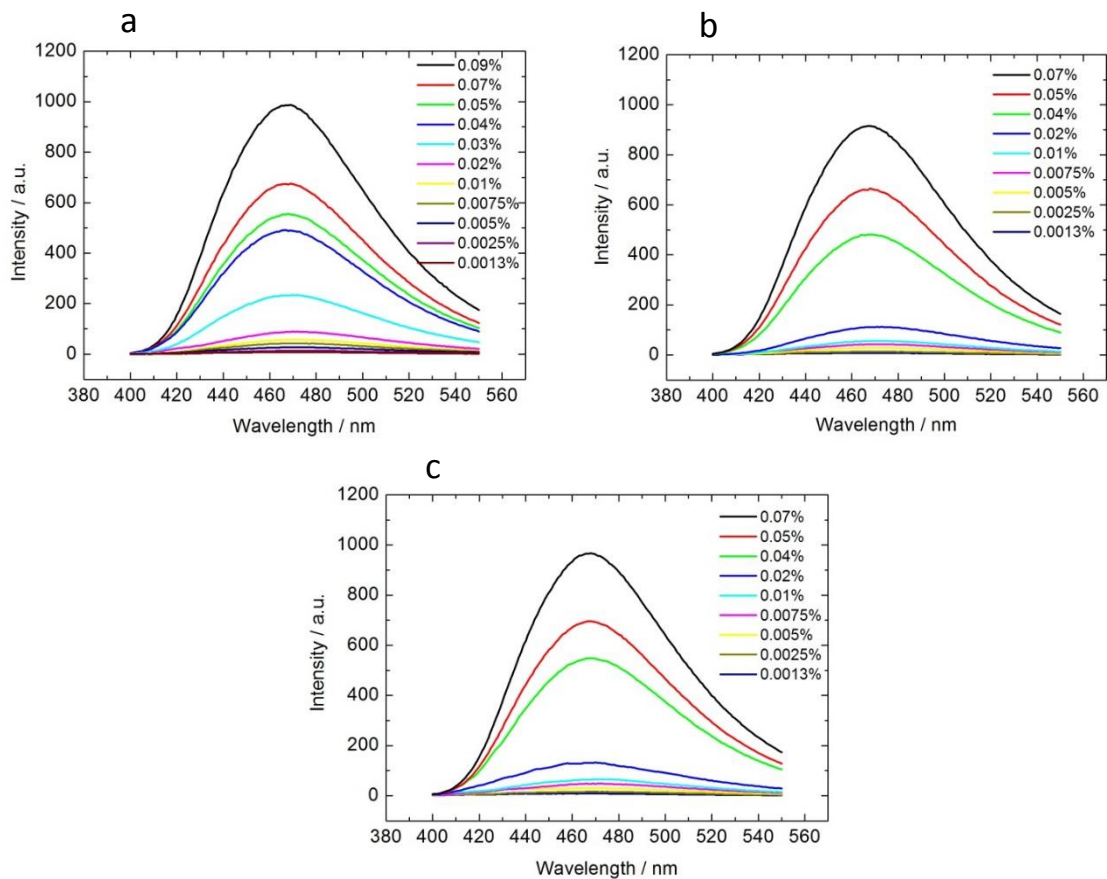


Figure 2 Fluorescence emission spectra for daptomycin solutions at various concentrations in 100 mM KCl. a) daptomycin with no CaCl_2 , b) with a daptomycin : CaCl_2 ratio of 4:1, and c) daptomycin : CaCl_2 ratio of 1:1.

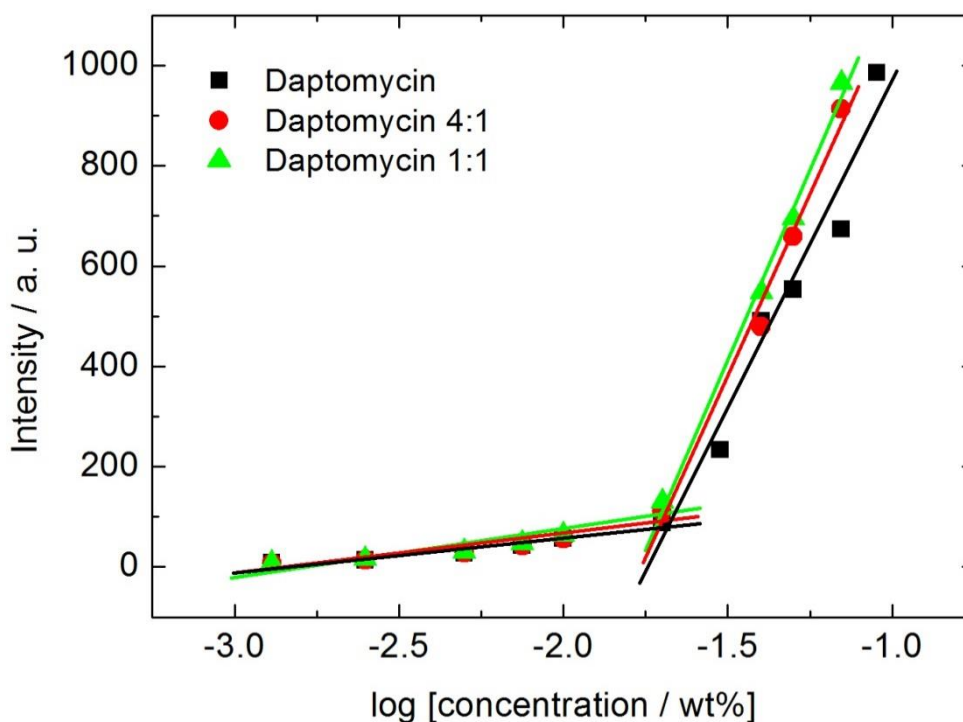


Figure 3 Critical aggregation concentration of daptomycin using the self-fluorescing emission peak at 466 nm, with cac indicated by the intersection of the lines. Daptomycin ratios are presented as a molar ratio between daptomycin and CaCl_2 .

The secondary structure of daptomycin was investigated through the use of CD and FTIR, both in the presence and absence of CaCl_2 , above the measured cac. Figure 4 shows CD spectra of daptomycin on its own, along with two solutions with the molar ratio to CaCl_2 as seen in the cac measurements at room temperature, and Figure 5 shows CD spectra taken over a range of successive temperatures. As with the cac measurements, there is no systematic difference seen between any of the spectra for a given sample as a function of temperature. The spectra are similar to those that have been seen before in the literature with daptomycin with CaCl_2 [17], including the very broad peak around 360 nm, as well as the prominent maximum peak around 231 nm. In this paper, the latter peak shifted from 233 nm to 231 nm upon addition of CaCl_2 , a change which was not observed in these experiments. The solution containing a 1:1 ratio of daptomycin to CaCl_2 did cause an increase in the maximum of the peak when

compared with daptomycin without CaCl_2 . A 4:1 ratio however causes the peak to become negative. Changes in the spectra around 231 nm have previously been associated with the presence of Trp [20], and so the peak seen in these experiments can tentatively be applied to this. The peak at 258 nm has previously been seen with absorption spectra of daptomycin and kynurenine, as well as the aforementioned broad peak around 360 nm [4,13].

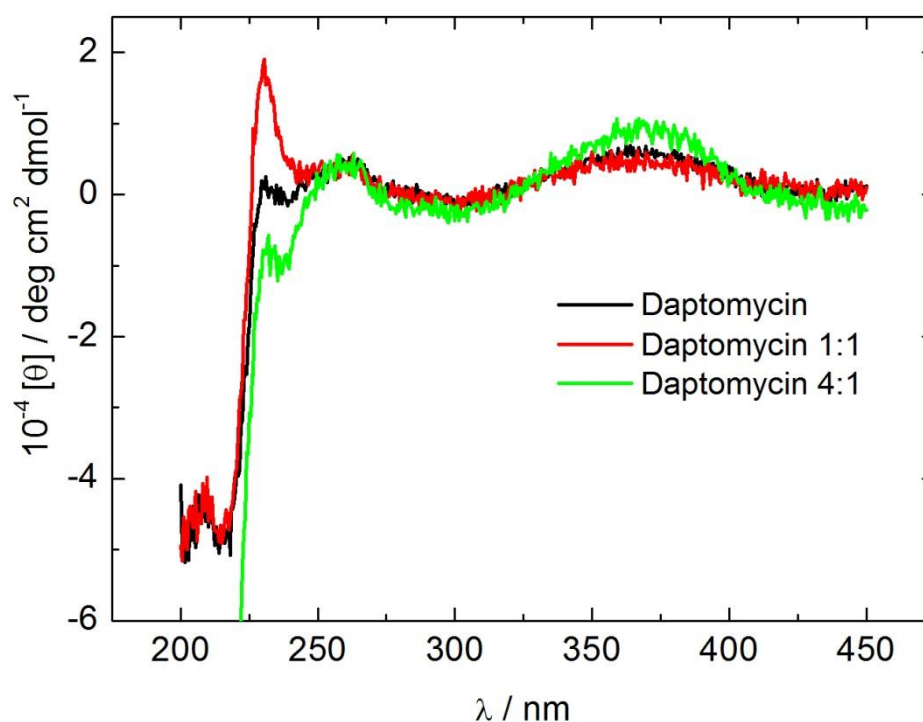


Figure 4 CD spectra for 0.1 wt% daptomycin solutions in 100 mM KCl with daptomycin to CaCl_2 ratios indicated.

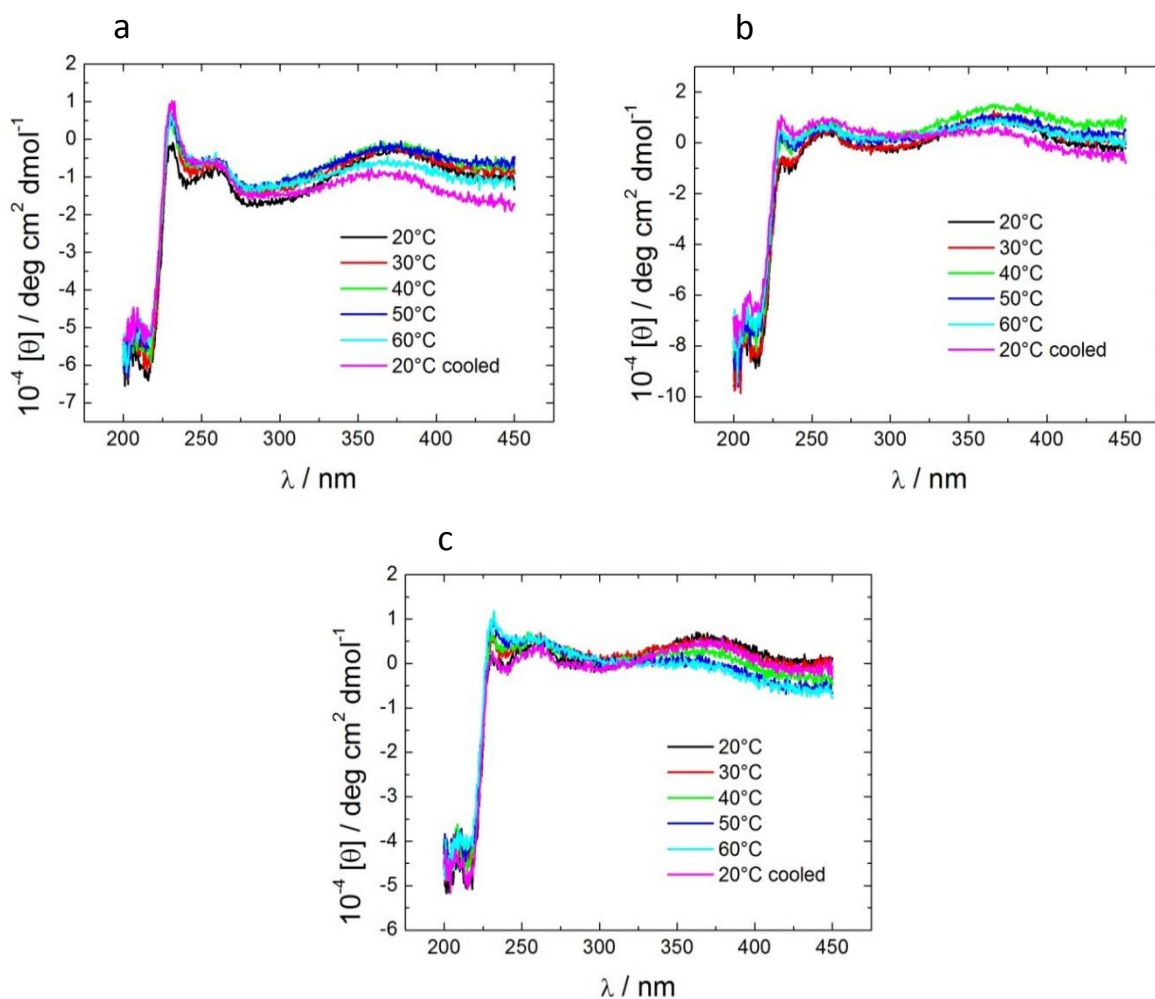


Figure 5 CD spectra for 0.1 wt% daptomycin solutions in 100 mM KCl with daptomycin to CaCl_2 ratios of a) 1:1, b) 4:1, c) no CaCl_2 .

Figure 6 shows the FTIR spectra for all three solutions tested. The spectra for the three are very similar in the range of $1250\text{-}2000\text{ cm}^{-1}$. The peak at 1454 cm^{-1} can be assigned to HDO stretching deformations, which is formed through H/D exchange between protons and D_2O [21]. However, this peak could also be due to a Trp side group deformation [22, 23]. The peak at 1648 cm^{-1} , in the amide I' band, is indicative of an unordered peptide conformation [22, 24], and the shoulder peak at 1720 cm^{-1} attached to it is assigned to carbonyl stretch [25]. The intensity of the broad peak at 3400 cm^{-1} is the only peak which significantly differs between the three spectra. Daptomycin with no CaCl_2 shows a very low intensity peak, followed by the

4:1 daptomycin to CaCl_2 solution having a more pronounced peak, and the 1:1 solution giving the highest intensity. This peak is assigned to $-\text{OH}$ stretch vibrations [25]. The increased intensity of the peak in CaCl_2 -containing solutions could be caused by the increased stabilisation of H-bonding between daptomycin molecules in the presence of salt.

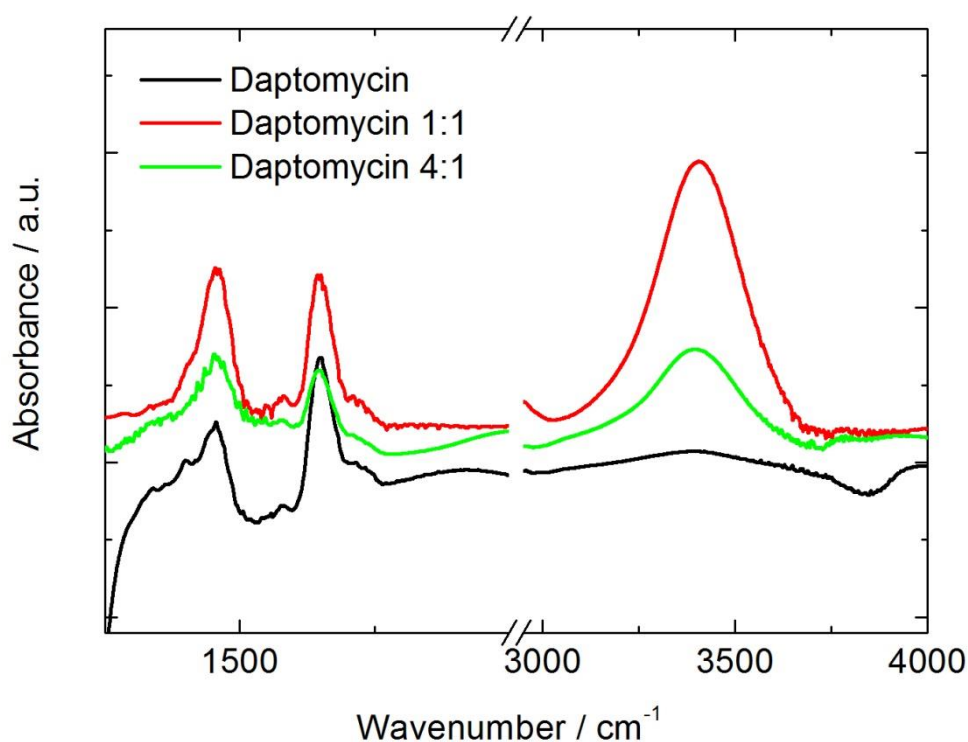


Figure 6 FTIR spectra for 1 wt% daptomycin solutions in 100 mM KCl solutions in D_2O . Daptomycin ratios are presented as a molar ratio between daptomycin and CaCl_2 .

Cryo-TEM images of daptomycin both in the presence and absence of CaCl_2 were obtained from our collaborators in Finland. Figure 7 reveals the presence of spherical micelles from all three different solutions, with the structures estimated to have a diameter of around 5 nm. This correlates with the lack of secondary structure seen in both the CD and FTIR results. This

lack of secondary structure combined with micelle formation has also been seen in the previous chapter [26], as well as in other papers by colleagues in our group [27].

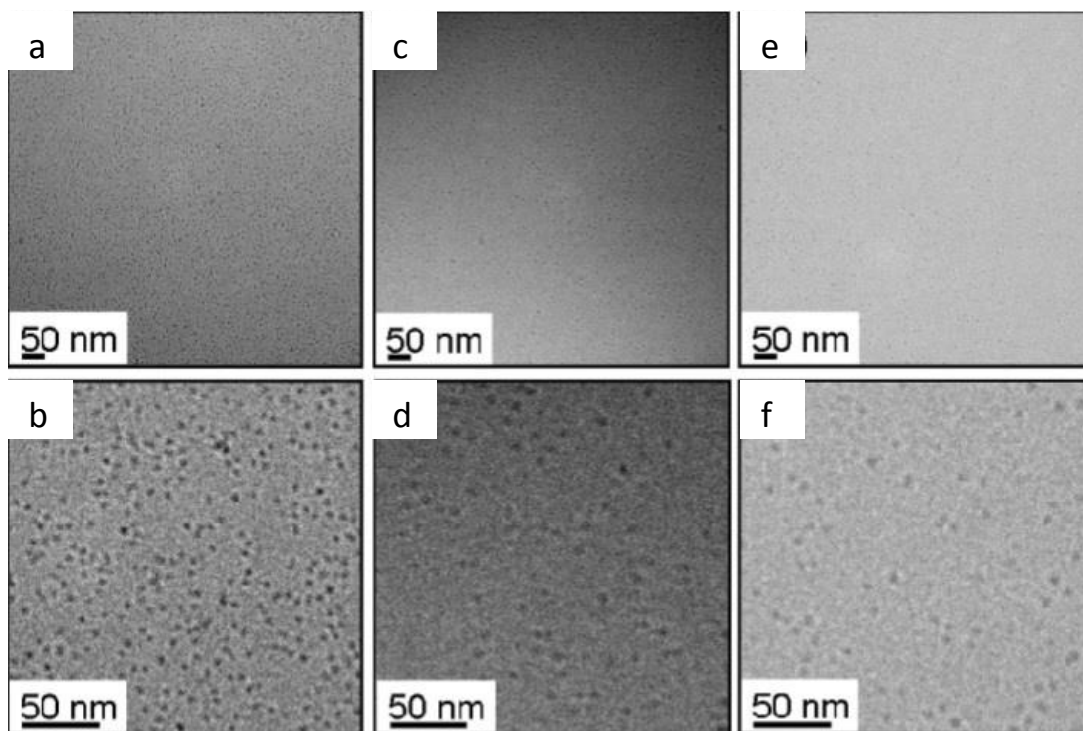


Figure 7 Representative cryo-TEM images of 0.5 wt% daptomycin solutions (a) and b)), with daptomycin:CaCl₂ ratio of 4:1 (in c) and d)), and 1:1 (in e) and f)).

SAXS was then used in order to determine the specific structural parameters and dimensions of the micelles. The data were fitted to a core-shell sphere model, with the data and fit of daptomycin with CaCl₂ shown in figure 8a, and without CaCl₂ in figure 8b. It was found that, despite changes in concentration and the presence/absence of CaCl₂, the radius of the micelles stayed constant at a radius of 27.2 Å with an error of 0.1 Å. The only parameters which changed included the scattering contrast of the shell and core, and the inner radius of the core. This is particularly shown at 2 wt% where the inner core radius value is higher and

the relative scattering contrast of the inner core is lower, which is indicative of an increased packing of hydrophobic units owing to these units having a negative scattering density relative to the solvent. The full list of specific parameters is presented in table 1 and 2.

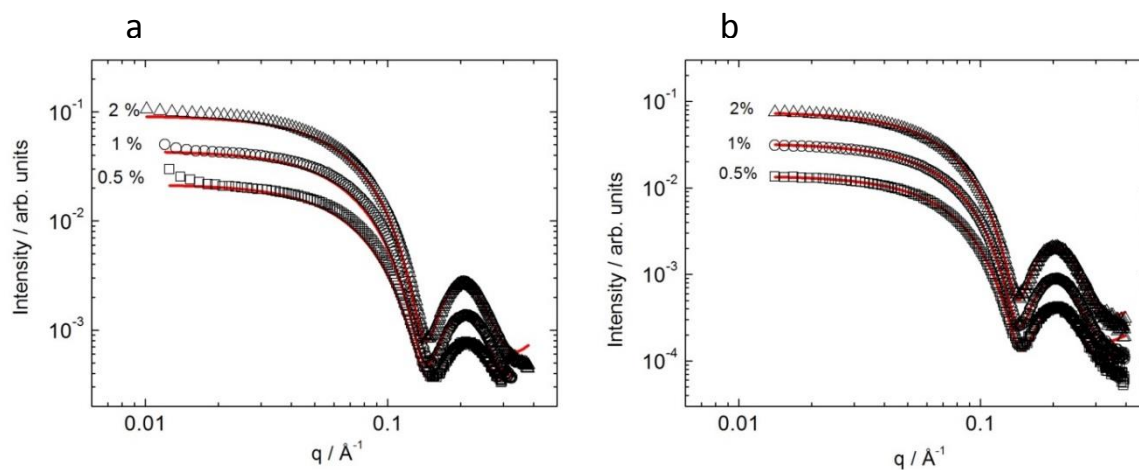


Figure 8 SAXS data of a range of concentrations of a) 1 wt% daptomycin with a 4:1 molar ratio with CaCl_2 , b) 1 wt% daptomycin with no CaCl_2 present.

Table 1 Fitting parameters for SAXS data using a core-shell sphere form factor. 1 wt% daptomycin 4:1 molar ratio to CaCl₂ (corresponding to figure 8a). Courtesy of I.W. Hamley.

| Daptomycin wt% | N ^a (x10 ⁻⁹) | σ ^b | R _o ^c (Å) | R _i ^d (Å) | μ ^e | η ^f | Background (x10 ⁻⁴) |
|----------------|-------------------------------------|----------------|---------------------------------|---------------------------------|----------------|----------------|---------------------------------|
| 0.5 | 2.06 | 2.08 | 27.21 | 7.61 | -2.49 | 0.04 | 3.2 |
| 1 | 2.88 | 2.54 | 27.27 | 7.61 | -2.98 | 0.05 | 3.5 |
| 2 | 5.11 | 2.9 | 27.1 | 7.39 | -3.74 | 0.05 | 4.8 |

Table 2 Fitting parameters for SAXS data using a core-shell sphere form factor. 1 wt% daptomycin (corresponding to figure 8b). Courtesy of I.W. Hamley.

| Daptomycin wt% | N ^a (x10 ⁻⁹) | σ ^b | R _o ^c (Å) | R _i ^d (Å) | μ ^e | η ^f | Background (x10 ⁻⁴) |
|----------------|-------------------------------------|----------------|---------------------------------|---------------------------------|----------------|----------------|---------------------------------|
| 0.5 | 0.90 | 2.08* | 27.21* | 7.61* | -2.49* | 0.05 | 1.1 |
| 1 | 1.72 | 2.54* | 27.27* | 7.61* | -2.98* | 0.05 | 1.6 |
| 2 | 4.11 | 2.9* | 27.1* | 7.39* | -3.74* | 0.05 | 0.25 |

SAXS form factor model fitting parameter definitions:

^a = Scale factor

^b = Gaussian polydispersity (of outer radius) parameter

^c = outer radius

^d = inner radius

^e = scattering contrast of inner core

^f = scattering contrast of shell

* = value constrained based on fits in table 1

In this chapter the self-assembly of daptomycin was explored, with two different molar ratios of the compound to CaCl₂, as well as in the absence of CaCl₂. Up to a molar ratio of 1:1, used in previous literature, we have shown that, in contrast to findings reported previously [15, 18, 28, 29], CaCl₂ is not required in order for daptomycin to self-assemble into micelles. Prior publications [15] have claimed that a 1:1 molar ratio of daptomycin : CaCl₂, one of the ratios also used in this research, is required in order for daptomycin to oligomerize into a micelle, consisting of 14-16 daptomycin monomers. This self-assembly has been characterised to show

formation of spherical micelles, largely unchanged in dimension with daptomycin concentration or addition of CaCl_2 up to a 1:1 molar equivalent. Molecular dynamics simulations by another group have also shown no dependence on calcium ions for micellization [30]. As they summarise at the end of the report, this implies that the role of calcium ions in daptomycin's mechanism of action is either in binding, membrane entry or stabilisation in the membrane, and not in its aggregation.

6.4 References

- [1] M. Debono, B. Abbott, R. Molloy, D. Fukuda, A. Hunt, V. Daupert, F. Counter, J. Ott, C. Carrell, L. Howard, L. Boeck and R. Hamill, "Enzymatic and chemical modifications of lipopeptide antibiotic A21978C: the synthesis and evaluation of daptomycin (LY146032)," *The Journal of Antibiotics*, vol. 41, no. 8, pp. 1093-1105, 1988.
- [2] J. Woodworth, E. Nyhart, G. Brier, J. Wolny and H. Black, "Single-dose pharmacokinetics and antibacterial activity of daptomycin, a new lipopeptide antibiotic, in healthy volunteers," *Antimicrobial Agents and Chemotherapy*, vol. 36, no. 2, pp. 318-325, 1992.
- [3] R. Baltz, V. Miao and S. Wrigley, "Natural products to drugs: daptomycin and related lipopeptide antibiotics," *Natural Product Reports*, vol. 22, no. 6, pp. 717-741, 2005.
- [4] J. Qiu and L. Kirsch, "Evaluation of lipopeptide (daptomycin) aggregation using fluorescence, light scattering, and nuclear magnetic resonance spectroscopy," *Journal of Pharmaceutical Sciences*, vol. 103, no. 3, pp. 853-861, 2014.
- [5] S. van Hal and D. Paterson, "New Gram-positive antibiotics: better than vancomycin?," *Current Opinion in Infectious Diseases*, vol. 24, no. 6, pp. 515-520, 2011.
- [6] M. Boaretti, P. Canepari, M. Lleo and G. Satta, "The activity of daptomycin on *Enterococcus faecium* protoplasts: indirect evidence supporting a novel mode of action on lipoteichoic acid synthesis," *The Journal of Antimicrobial Chemotherapy*, vol. 31, no. 2, pp. 227-235, 1993.
- [7] P. Canepari, M. Boaretti, M. Lleo and G. Satta, "Lipoteichoic acid as a new target for activity of antibiotics: mode of action of daptomycin (LY146032)," *Antimicrobial Agents and Chemotherapy*, vol. 34, no. 6, pp. 1220-1226, 1990.
- [8] V. Laganas, J. Alder and J. Silverman, "In vitro bactericidal activities of daptomycin against *Staphylococcus aureus* and *Enterococcus faecalis* are not mediated by inhibition of lipoteichoic acid biosynthesis," *Antimicrobial Agents and Chemotherapy*, vol. 47, no. 8, pp. 2682-2684, 2003.
- [9] Y. Chen, T. Sun, Y. Sun and H. Huang, "Interaction of daptomycin with lipid bilayers: a lipid extracting effect," *Biochemistry*, vol. 53, no. 33, pp. 5384-5392, 2014.
- [10] T. Zhang, J. Muraih, B. MacCormick, J. Silverman and M. Palmer, "Daptomycin forms cation- and size-selective pores in model membranes," *Biochimica et Biophysica Acta*, vol. 1838, no. 10, pp. 2425-2430, 2014.
- [11] J. Silverman, N. Perlmutter and H. Shapiro, "Correlation of daptomycin bactericidal activity and membrane depolarization in *Staphylococcus aureus*," *Antimicrobial Agents*

and Chemotherapy, vol. 47, no. 8, pp. 2538-2544, 2003.

- [12] G. Eliopoulos, C. Thauvin, B. Gerson and R. Moellering, "In vitro activity and mechanism of action of A21978C1, a novel cyclic lipopeptide antibiotic," *Antimicrobial Agents and Chemotherapy*, vol. 27, no. 3, pp. 357-362, 1985.
- [13] J. Lakey and M. Ptak, "Fluorescence indicates a calcium-dependent interaction between the lipopeptide antibiotic LY146032 and phospholipid membranes," *Biochemistry*, vol. 27, no. 13, pp. 4639-4645, 1988.
- [14] R. Hancock, "Mechanisms of action of newer antibiotics for Gram-positive pathogens," *The Lancet. Infectious Diseases*, vol. 5, no. 4, pp. 209-218, 2005.
- [15] W. Scott, S. Baek, D. Jung, R. Hancock and S. Straus, "NMR structural studies of the antibiotic lipopeptide daptomycin in DHPC micelles," *Biochimica et Biophysica Acta*, vol. 1768, no. 12, pp. 3116-3126, 2007.
- [16] A. Gonzalez-Ruiz, R. Seaton and K. Hamed, "Daptomycin: an evidence-based review of its role in the treatment of Gram-positive infections," *Infection and Drug Resistance*, vol. 9, pp. 47-58, 2016.
- [17] D. Jung, A. Rozek, M. Okon and R. Hancock, "Structural transitions as determinants of the action of the calcium-dependent antibiotic daptomycin," *Chemistry & Biology*, vol. 11, no. 7, pp. 949-957, 2004.
- [18] S. Ho, D. Jung, J. Calhoun, J. Lear, M. Okon, W. Scott, R. Hancock and S. Straus, "Effect of divalent cations on the structure of the antibiotic daptomycin," *European Biophysics Journal*, vol. 37, no. 4, pp. 421-433, 2008.
- [19] M. Steed, C. Vidailic, W. Rose, P. Winterfield, G. Kaatz and M. Rybak, "Characterizing vancomycin-resistant Enterococcus strains with various mechanisms of daptomycin resistance developed in an in vitro pharmacokinetic/pharmacodynamic model," *Antimicrobial Agents and Chemotherapy*, vol. 55, no. 10, pp. 4748-4754, 2011.
- [20] S. Vuilleumier, J. Sancho, R. Loewenthal and A. Fersht, "Circular dichroism studies of barnase and its mutants: characterization of the contribution of aromatic side chains," *Biochemistry*, vol. 32, no. 39, pp. 10303-10313, 1993.
- [21] Y. Marechal, "Infrared spectra of water. I. Effect of temperature and of H/D isotopic dilution," *The Journal of Chemical Physics*, vol. 95, pp. 5565-5573, 1991.
- [22] A. Barth and C. Zscherp, "What vibrations tell us about proteins," *Quarterly Reviews of Biophysics*, vol. 35, no. 4, pp. 369-430, 2002.
- [23] A. Barth, "The infrared absorption of amino acid side chains," *Progress in Biophysics and Molecular Biology*, vol. 74, no. 3-5, pp. 141-173, 2000.

- [24] B. Stuart, *Biological Applications of Infrared Spectroscopy*, Chichester: Wiley, 1997.
- [25] L. Bellamy, *The Infrared Spectra of Complex Molecules*, London: Springer Netherlands, 1980.
- [26] I. Hamley, S. Kirkham, A. Dehsorkhi, V. Castelletto, M. Reza and J. Ruokolainen, "Toll-like receptor agonist lipopeptides self-assemble into distinct nanostructures," *Chemical Communications*, vol. 50, no. 100, pp. 15948-15951, 2014.
- [27] A. Dehsorkhi, I. Hamley, J. Seitsonen and J. Ruokolainen, "Tuning self-assembled nanostructures through enzymatic degradation of a peptide amphiphile," *Langmuir*, vol. 29, no. 22, pp. 6665-6672, 2013.
- [28] K. Rotondi and L. Gierasch, "A well-defined amphipathic conformation for the calcium-free cyclic lipopeptide antibiotic, daptomycin, in aqueous solution," *Biopolymers*, vol. 80, no. 2-3, pp. 374-385, 2005.
- [29] L. Ball, C. Goult, J. Donarski, J. Micklefield and V. Ramesh, "NMR structure determination and calcium binding effects of lipopeptide antibiotic daptomycin," *Organic & Biomolecular Chemistry*, vol. 2, no. 13, pp. 1872-1878, 2004.
- [30] B. Liu and M. Karttunen, "Subtle balance of calcium ions, hydrogen bonding and charged lipids is the key to daptomycin's ability to destabilize bacterial membranes".

Chapter 7 - Self-assembly of custom-synthesised telechelic conjugates with PEO/poly(alanine) central blocks

7.1 Introduction

The combining of peptides with polymers in order to enable both components' properties is an interesting area of research in the production of biomaterials and can be used in a wide range of applications [1]. Polymer-peptide conjugates can be designed either to synergistically combine the two component properties when linked together, or to compensate for disadvantages one component may possess [2]. Addition of synthetic polymers to peptides has been shown to improve the stability, solubility and biocompatibility of the combined compound [3, 4], among other factors [5, 6]. From this, biomaterials with a range of applications in the medical, biotechnological and nanotechnological areas can be derived [1]. Based on these interesting characteristics, three samples were custom synthesised by a collaborator at the University of Athens, Greece, consisting of a central block polymer with short tyrosine end caps. Two of these had a central block consisting of polyethylene oxide/polyethylene glycol (PEO/PEG), but with different molar masses; 2000 g mol⁻¹ and 6000 g mol⁻¹. Both were capped at each end of the chain by pentameric tyrosine sequences. The other compound had a central block of poly(alanine), estimated to be 64 repeats, and trimeric tyrosine sequences capping either end.

The custom-synthesised compounds used in this research also possess another interesting dimension through their hydrophobic-hydrophilic-hydrophobic triblock sequence. There are a number of hydrophobicity scales for determining the classification of amino acids [7-11], which in general state tyrosine as being hydrophobic, and alanine as hydrophilic. Compounds with this triblock sequence are used in associating polymers, which are polymers with a small

number of hydrophobic groups attached to either side of the polymer backbone. This enables self-association in aqueous solution to reduce exposure to the solvent, similarly to micelles [12]. The rheological properties of associative polymers, specifically over the past five years, has been reviewed extensively elsewhere [13]. Briefly, these associative polymers are able to provide useful properties, including increased viscosity, gelation and shear-thinning and thickening. An example of associative polymers are reverse Pluronics, a type of reverse poloxamer which have a hydrophobic-hydrophilic-hydrophobic amphiphilic sequence through the copolymers PEO (hydrophilic) and poly(propylene oxide) (PPO) (hydrophobic) [14].

The compounds used in this work also present an interesting area as there is currently little research into the self-assembled properties of telechelic polymers. These are defined as polymers with the same reactive end groups on either side of a central block, able to further polymerise or enter into other reactions [15]. In the case of the three custom-synthesised polymers, these reactive groups are the tyrosine end-caps, although no reactions with tyrosine were performed in this research. Telechelic polymers have been reported to form networks when in high concentration, connected through PEO chains, and flower-like micelles at lower concentration, where both end groups arrange to become part of the hydrophobic core [16]. The Hamley group have investigated a similar compound consisting of a 1500 g mol^{-1} PEO centre block, capped with differing hydrophobic dipeptides [17]. When tyrosine dipeptides were present, β -sheet fibrillar structures were formed, which contrasted with those seen with diphenyl end caps which didn't show β -sheet formation. The tyrosine end-capped telechelic polymer was also shown to undergo a transition at $37 \text{ }^\circ\text{C}$ (physiologically relevant as it correlates with body temperature) causing a melting of the hydrogel. Another group used a PEO centre block of 3000 g mol^{-1} end-capped by desaminotyrosine (DAT) and desaminotyrosyltyrosine (DATT) [18], which were shown to display surfactant-like properties. Another triblock copolymer comprised of PEO with poly(L-leucine) end caps with a total molecular weight of 3500 Da was investigated [19]. It was found to self-assemble into micelles

with the peptide adopting an α -helical conformation which was shown to make it a good candidate as a delivery system for hydrophobic drugs.

Polymer-peptide conjugates can be used as novel materials in the creation of hydrogels (defined as a water phase immobilised by a scaffold [20]), in applications such as drug delivery [21, 22] and as artificial extracellular matrices (ECM) [23]. The hydrogel becomes the framework whereby reservoirs are present which components such as drugs can be released from [24]. Alginates are polysaccharides which are isolated from brown algae [25], commonly used in cell culturing experiments and which are relatively inexpensive [26-28]. When it was found later in the project that the compounds were unable to form a gel at higher concentrations in order to introduce to the cells on their own, incorporation of them into an alginate gel was proposed. The tyrosine component of the compounds represented an interesting area of research. Tyrosine kinases and phosphorylases, enzymes which add and remove phosphate groups respectively, affect upon tyrosine and are involved in many cellular processes [29].

7.2 Materials & Methods

Synthesis was performed in the group of Hermis Iatrou at the University of Athens, Greece, and can be found in full detail in the published paper [30].

7.2.1 NMR and FTIR Spectroscopy

^1H NMR spectroscopy (300 MHz) was performed by collaborators at the University of Reading using a Varian Unity Plus 300/54 spectrometer. The spectra of the polymers were measured either in deuterated DMSO (NCA and poly(L-tyrosine)-PEO-poly(L-tyrosine)) or in CF_3COOD (the Tyr₃-PAla-Tyr₃ copolyptide). FTIR measurements were also performed by collaborators at

the University of Reading with a PerkinElmer Spectrum One instrument, in KBr pellets at room temperature, with spectra being recorded over the range 450–4000 cm^{-1} .

7.2.2 Sample Preparation

The solubility of samples dissolved into water was found to be poor, but pH adjustment to 12 (above the pK_a of tyrosine [31]) using an NaOH solution led to satisfactory solubility. Therefore this was the pH value selected for all measurements for samples Tyr₅-PEO2k-Tyr₅ and Tyr₃-PAla-Tyr₃. Since sample Tyr₅-PEO6k-Tyr₅ was found to show good solubility in water, it was also studied at its native pH, pH 5.69.

7.2.3 Circular Dichroism (CD)

CD spectra were recorded using a Chirascan spectropolarimeter (Applied Photophysics, UK) in the wavelength range 190–320 nm. The samples, 0.5 wt% in water raised to pH 12 or native pH for Tyr₅-PEO6K-Tyr₅, were placed in a coverslip cuvette (0.1 mm thick), with spectra presented with absorbance $A < 2$ at any measured point with a 0.5 nm step, 1 nm bandwidth, and 1 s collection time per step. Samples were acclimatized at each increasing 10 °C temperature point for 5 min, and 30 min for the 60–20 °C change, before measurements were taken. The CD signal from the background was subtracted from the CD spectra of the sample solutions.

7.2.4 Fourier transform infrared spectroscopy (FTIR)

Spectra were recorded using a Thermo Scientific Nicolet IS5 and a Nexus-FTIR spectrometer, both equipped with a DTGS detector. A 40 μL drop of the sample (in D₂O) was sandwiched

between two CaF₂ plate windows, with a 0.006 mm thick Mylar spacer in a Specac GS20500 sample cell holder. Spectra were scanned 128 times over the range of 900–4000 cm⁻¹.

7.2.5 X-ray Diffraction (XRD)

X-ray diffraction was performed on a peptide stalk prepared by drawing a fiber of 1 wt% conjugate solution between the ends of wax-coated capillaries. After separation and drying a stalk was left on the end of one capillary. For some samples, the capillary was mounted vertically onto the four axis goniometer of a RAXIS IV++ X-ray diffractometer (Rigaku) equipped with a rotating anode generator (CuK_α radiation, wavelength $\lambda = 1.54 \text{ \AA}$). The XRD data was collected using a Saturn 992 CCD camera. The sample-to-detector distance was 50 mm. Other measurements were performed on stalks mounted (vertically) onto the goniometer of an Oxford Instruments Gemini X-ray diffractometer, equipped with a Sapphire 3 CCD detector. The sample to detector distance was 45 mm.

7.2.6 Cryo-Transmission electron microscopy (cryo-TEM)

Experiments were carried out by our collaborators at the University of Aalto, Finland using a field emission cryo-electron microscope (JEOL JEM-3200FSC) operating at 200 kV. Images were taken using bright-field mode and zero loss energy filtering (omega type) with a slit with 20 eV. Micrographs were recorded using a Gatan UltraScan 4000 CCD camera. The specimen temperature was maintained at -187 °C during the imaging. Vitrified specimens were prepared using an automated FEI Vitrobot device using Quantifoil 3.5/1 holey carbon copper grids with 3.5 μm hole sizes. Grids were cleaned using a Gatan Solarus 9500 plasma cleaner just prior to use and then transferred into an environmental chamber of FEI Vitrobot at room temperature and 100% humidity. Thereafter, 3 μl of each sample solution at 1 wt% was applied on the grid,

blotted once for 1 second and then vitrified in a 1/1 mixture of liquid ethane and propane at -180 °C. Grids with vitrified sample solutions were maintained in a liquid nitrogen atmosphere and then cryo-transferred into the microscope.

7.2.7 Small-Angle X-ray Scattering (SAXS)

For the solutions, experiments were performed on ID02 at the ESRF, Grenoble France. Samples were flowed through a quartz capillary. After the sample was injected in the capillary and reached the X-ray beam, the flow was stopped during the SAXS data acquisition. The sample–detector distance was 2 m (data were also obtained at 10 m). Data processing (background subtraction, radial averaging) was performed using the dedicated beamline software or SAXSutilities.

7.2.8 Alginate hydrogel protocol

As briefly mentioned in the introduction, the three custom-synthesised compounds were unable to form gels at high concentrations. Alginate hydrogels were therefore produced to incorporate the compounds into. Alginate hydrogels were prepared based on a protocol by Jang et al. [32]. Briefly, a final concentration of 2 wt% sodium alginate was dissolved in PBS/media, followed by addition of calcium carbonate powder to the solution in a final molarity of 144 mM. This solution was thoroughly mixed through vortexing and sonicating. Another solution of GdL in the same corresponding solvent was prepared, with a CaCO₃ to GdL molar ratio of 0.5 in order to keep the pH neutral. HeLa cells in a final concentration of 1x10⁷ cells/ml were added to the alginate/CaCO₃ solution. The GdL solution was then added to this and rapidly mixed, then added to dishes for incubation. In later experiments which introduced

peptide-polymer compound to the gels, Tyr₅-PEO6k-Tyr₅ was mixed into the GdL solution, and then added to the rest of the mix as the protocol states.

7.3 Results and discussion

The secondary structure of the compounds was investigated using CD and FTIR. As with previous chapters, the temperature effect on secondary structure was also performed using temperature-dependent CD. The results are shown in figure 1. There are β -sheet features seen in the Tyr₅-PEO6k-Tyr₅ at native pH, shown in figure 1c, due to the minimum at 218 nm, and the maximum near 200 nm [33, 34]. The extra positive peak at 228 nm has previously been seen with a similar compound, Tyr₂-PEO1.5k-Tyr₂ [17], as well as another compound containing dityrosine residues [35], and is attributed to tyrosine residue absorption. The adjacent spectra of Tyr₅-PEO6k-Tyr₅ at pH 12 (figure 1d) shows a similar shape to the one at native pH, but with lower molar ellipticity values, which points to a reduction in secondary structure formation. The change in pH also leads to a red-shift in peaks, with the 200 nm positive peak shifting to 211 nm, and the 228 nm peak shifting to 241 nm. This change has previously been described [36], and is attributed to the formation of the phenoxide form of tyrosine at high pH, as opposed to the carboxyl-end group protonated/special position of tyrosine also previously described elsewhere [37]. Red-shifted β -sheet formation can also be seen with the Tyr₅-PEO2k-Tyr₅ sample with the minimum at 220 nm and maximum at 244 nm. The same is true for Tyr₃-PAla-Tyr₃ which has a minimum at 226 nm, however the maximum is reduced, presumably due to overwhelming contribution from the alanine repeats. This spectrum is the only one which changes with temperature, with a progressive reduction in molar ellipticity, showing a reduction in self-assembled structure.

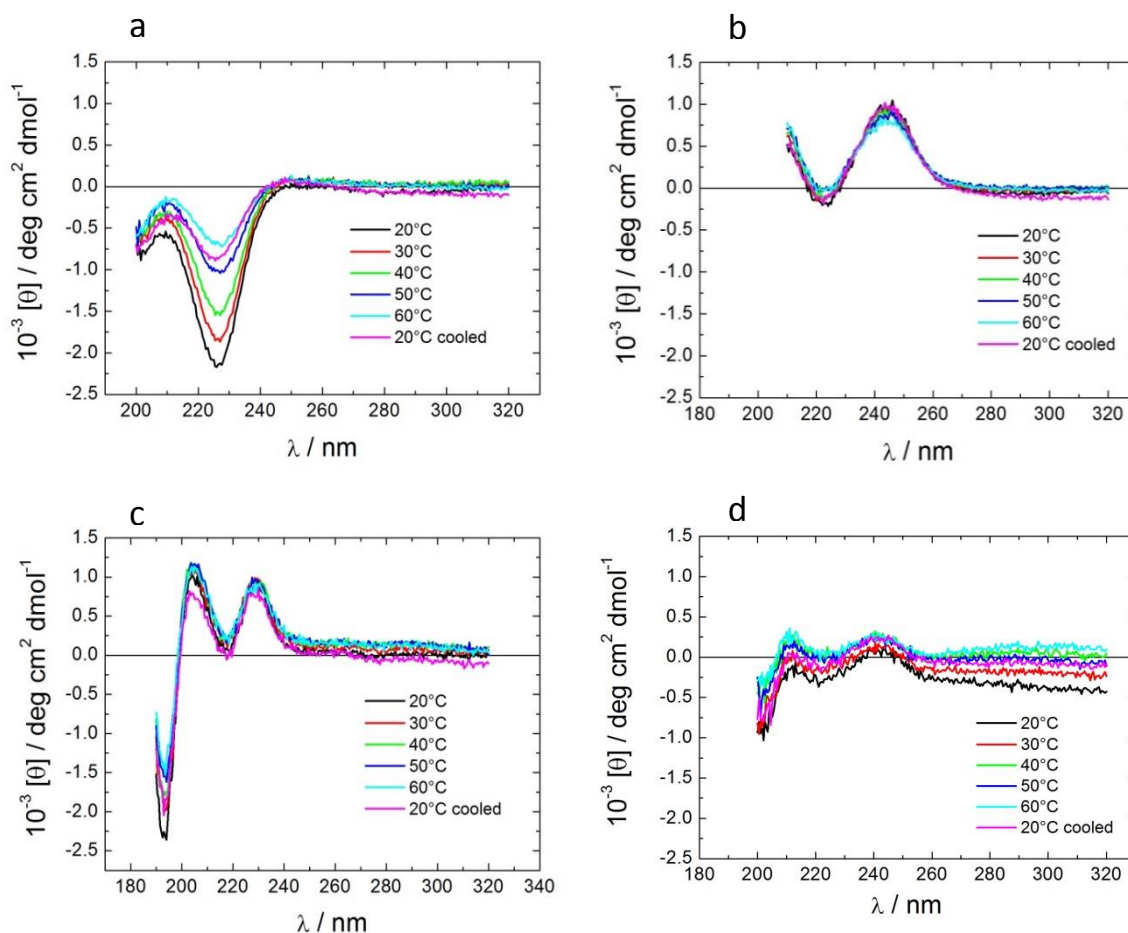


Figure 1 Temperature-dependent CD spectra of each sample at 0.1 wt% and pH 12 unless stated. a) Tyr₃-PAla-Tyr₃, b) Tyr₅-PEO2k-Tyr₅, c) Tyr₅-PEO6k-Tyr₅ at native pH = 5.69, d) Tyr₅-PEO6k-Tyr₅.

The four samples/conditions were then investigated through FTIR. All of the samples at all conditions show peaks in the 1500 cm⁻¹ range, the amide II' region, and show NH₂ deformations caused by the tyrosine residues. The amide I' region reveals the self-assembly properties of the samples. The 1623 cm⁻¹ peak seen with the Tyr₃-PAla-Tyr₃ spectrum has been correlated to formation of β-sheets [38], specifically for another alanine-rich peptide [39]. β-sheets were also shown with Tyr₅-PEO2k-Tyr₅ through the 1635 cm⁻¹ peak [38, 40]. The Tyr₅-PEO6k-Tyr₅ at both pHs tested did not reveal peaks in this area despite the observation of β-sheets in the CD data. This is believed to be due to the overwhelming absorption of the longer

PEO chain. The largest peak, seen with all samples/conditions, is at around 3400 cm^{-1} which has been discussed in the previous amphotericin B chapter [41], and is attributed to O-H stretch bonds, along with amine stretch [42]. The peak at 2930 cm^{-1} , along with the peak at 3400 cm^{-1} , have previously been seen with PEO compounds, with the former peak being attributed to PEO $-\text{CH}_2$ or poly(alanine) backbone $-\text{CH}$ deformation [43]. Temperature-dependent FTIR, as with CD, would have revealed more information, particularly with the PAla sample due to the changes already seen upon increase in temperature in the CD data. However, this line of experiments was unable to be undertaken due to constraints on sample quantity and time.

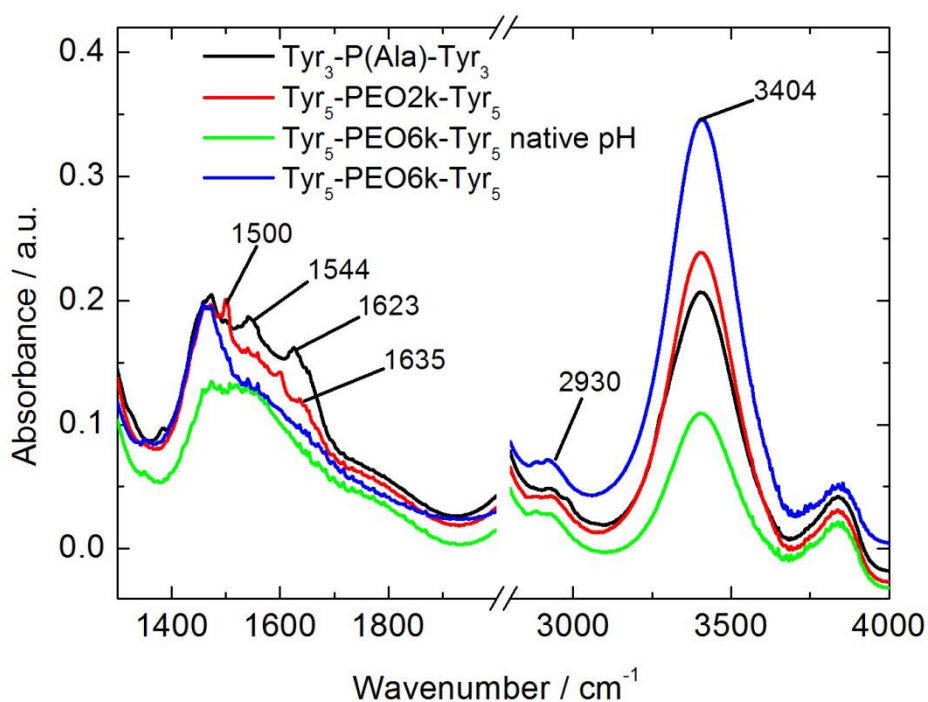


Figure 2 FTIR spectra for samples at 1 wt% and pH 12 unless stated.

From each solution condition, a stalk was produced in order to perform fiber XRD. It was found that Tyr₅-PEO6k-Tyr₅ at both native and pH 12 produced the same result, and so only the

native pH is shown for clarity. The results are shown in figure 3. The PAla sample gave peaks at 7.49, 5.27, 4.36 and 3.71 Å. Other peptides with oligo-alanine components have also been shown to give similar peaks, caused by the tightly packed β -sheets [39, 44-46]. The 4.36 Å peak has been previously assigned to the spacing between β -strands, and 5.27 Å to β -sheet spacing. The XRD data from Tyr₅-PEO6k-Tyr₅ shows the most prominent parts of the spectrum through peaks at 4.69 and 3.83 Å. The former peak has previously been associated with β -sheet content in fibril formation and corresponds to spacing between the peptide backbone [40, 47]. The others in the spectrum are assigned to a high degree of crystallisation of PEO. The crystallisation of PEO has previously been investigated through the use of XRD with expected d-spacings mapped out [48]. These are 7.89, 5.11, 4.63, 3.94, 3.86, 3.81, 3.79/3.78 Å. The Tyr₅-PEO2k-Tyr₅ sample does not have any peaks which can be assigned to β -sheet content. It does however have a large amorphous peak with small sharp peaks on top, which the broad peak can be assigned to semi-crystalline PEO. The shift is believed to be from the influence of the tyrosine end-caps. The differing levels of crystallinity in the PEO containing samples can be explained through previous studies into its influence and the influence of peptide end groups. The Hamley group has shown that PEO crystallisation is enhanced when a less actively fibril-forming peptide is linked to the same PEO centre block [49, 50]. A fibrilliser was also used bonded to a range of differing molar mass PEO centre blocks [51], and along with the results seen here suggest that a molar mass of 2000 g mol⁻¹ of PEO may be on the borderline for observation of crystallinity.

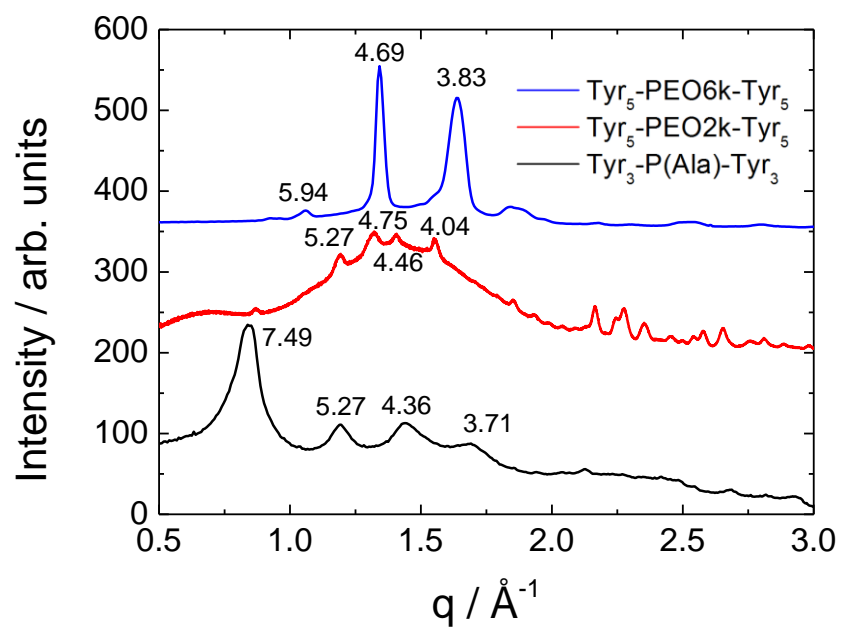


Figure 3 X-ray diffraction data obtained from stalks dried from 1 wt% solutions. Figure courtesy of I.W. Hamley.

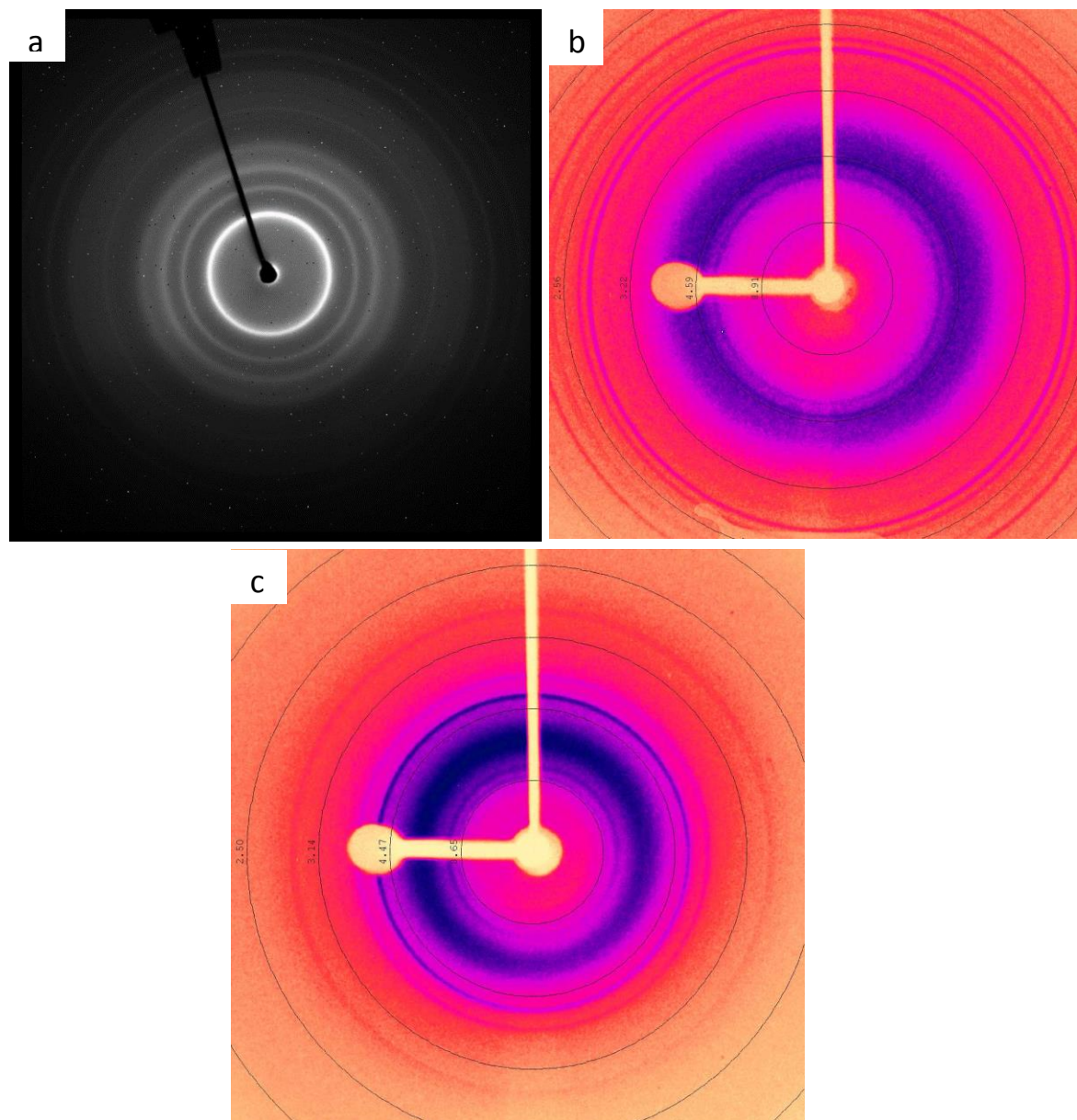


Figure 4 Corresponding 2D images of the X-ray diffraction data obtained from stalks dried from 1 wt% solutions of a) $\text{Tyr}_5\text{-PEO6k-Tyr}_5$, b) $\text{Tyr}_5\text{-PEO2k-Tyr}_5$, and c) $\text{Tyr}_3\text{-PALa-Tyr}_3$.

Cryo-TEM images of the samples are shown in figure 5. Both $\text{Tyr}_3\text{-PALa-Tyr}_3$ and $\text{Tyr}_5\text{-PEO2k-Tyr}_5$ (figures 6a and b) show similar short fibrillar structures. These are commonly seen with self-assembling compounds which have shown β -sheet formation, as revealed in the CD and FTIR results. $\text{Tyr}_5\text{-PEO6k-Tyr}_5$ (figure 6c) on the other hand shows straight fibrils estimated to

have a diameter of 5 nm interspersed with much shorter, spherical-like structures. These very straight short fibrils are likely an influence of the longer PEO chain, based on observations of similar structures in previous work by the Hamley group involving other hydrophobic residues (phenyl alanine) attached to 5k units long PEO polymers [52]. By contrast, when shorter PEO blocks (up to 1800 g mol⁻¹ tested [53]) are present, worm-like micelles, like those seen with Tyr₅-PEO2k-Tyr₅, are common [53].

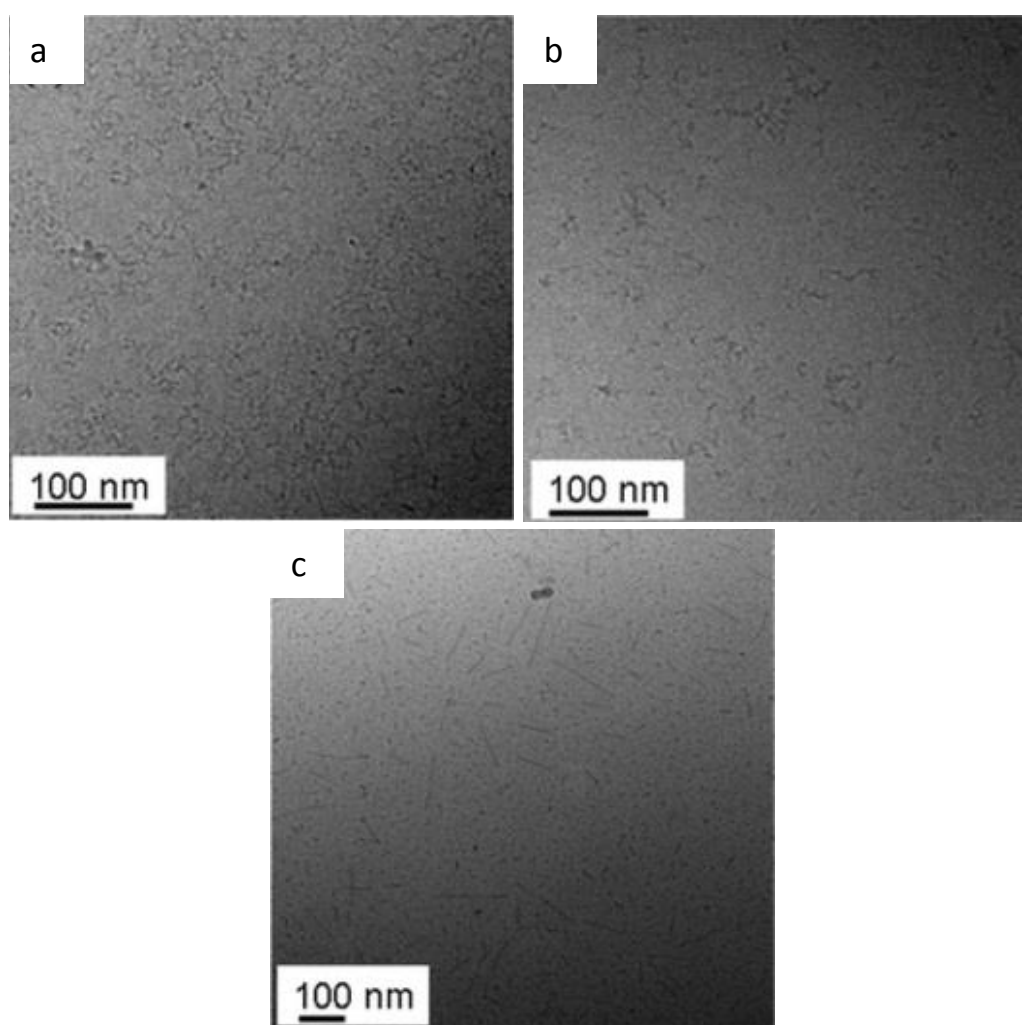


Figure 5 Representative cryo-TEM images of 1 wt% solutions at pH 12 unless otherwise stated of a) Tyr₃-PAL α -Tyr₃, b) Tyr₅-PEO2k-Tyr₅, and c) Tyr₅-PEO6k-Tyr₅ at native pH.

SAXS data was collected (shown in figure 6) of Tyr₅-PEO2k-Tyr₅ and Tyr₅-PEO6k-Tyr₅. The structures observed in the cryo-TEM images were used as an input to constrain the form factor fitting of the structural parameters. Due to time restraints, Tyr₃-PAla-Tyr₃ wasn't able to be done. Both of the samples were fitted to a cylindrical core-shell form factor, with specific parameters listed in table 1. The radius of the structures was found to be 1.03 nm for the Tyr₅-PEO2k-Tyr₅ sample, and 2.28 nm for Tyr₅-PEO6k-Tyr₅, with the latter correlating well with the estimated diameter from the cryo-TEM images of 5 nm.

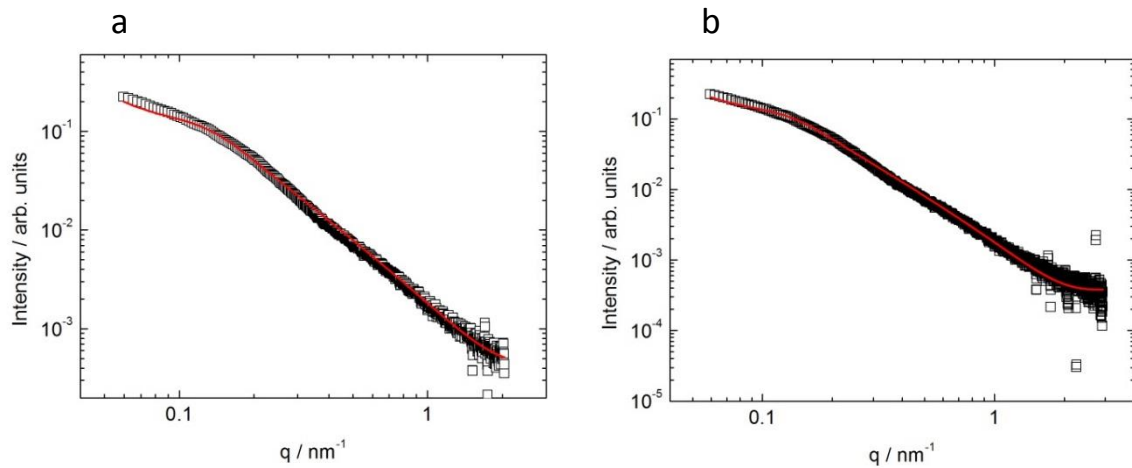


Figure 6 SAXS data obtained for 1 wt% solutions of a) Tyr₅-PEO2k-Tyr₅, and b) Tyr₅-PEO6k-Tyr₅. Black squares show data, red line shows form factor fitting.

| Sample | N | σ /nm | R/nm | ΔR /nm | L/nm | $\eta(\text{core})$ | $\eta(\text{shell})$ | $\eta(\text{solv})$ | BG |
|--------|-------|--------------|------|----------------|------|----------------------|----------------------|----------------------|----------------------|
| PEO2k | 0.06 | 2.48 | 1.03 | 1.92 | 50 | 1.6×10^{-5} | 7.1×10^{-4} | 2.4×10^{-4} | 1.3×10^{-4} |
| PEO6k | 0.015 | 2.66 | 2.28 | 2.20 | 50 | 4.1×10^{-4} | 1.7×10^{-3} | 1.0×10^{-4} | 3.0×10^{-4} |

Table 1 Parameters for SAXS fitting form factor models using SASfit software. Form factor was cylindrical shell for both samples.

N = scaling factor

σ = Gaussian polydispersity parameter

R = cylinder radius

ΔR = shell thickness

L = length of cylinder (fixed value)

$\eta(\text{core})$ = scattering length density of core

$\eta(\text{shell})$ = scattering length density of shell

$\eta(\text{solv})$ = scattering length density of solvent

BG = background (fixed value)

The samples were tested to determine whether they were able to form a gel by dissolving high weight % of the compounds. It was found that Tyr₃-PAla-Tyr₃ was unable to dissolve at higher concentrations, and Tyr₅-PEO2k-Tyr₅ and Tyr₅-PEO6k-Tyr₅ did not form a gel up to concentrations of 20 wt%. Rheological experiments on Tyr₅-PEO6k-Tyr₅ were performed by V. Castelletto, giving results indicating a largely fluid-like consistency. These are described in more detail in the published paper [30].

Another objective with the compounds was to introduce them into cell cultures to determine their effects on cells. This was proposed due to the known functions of tyrosine in cell signalling and enzyme-responsiveness, described in more detail in the introduction. Another

reason was PEO spacers, when linked to peptides, having shown to improve stability and circulation time, with applications including gene delivery [54] and cell signalling [55]. Therefore the two combined into one molecule posed an interesting compound to investigate their effects in cell culture. Due to the lack of gel formation by the three telechelic compounds, even at higher concentration, integration of them into an alginate-based hydrogel was proposed. The suitability of alginate gels being used for this purpose was described in more detail in the introduction. An already established protocol by Jang et al [32] was used as the basis for the alginate gel experiments, which manipulated cross-linking through addition of CaCO_3 to sodium alginate, with GdL added to maintain neutral pH. This protocol was tested multiple times before introducing the polymer/peptide conjugates. During attempts to prepare the hydrogels and test out this protocol however, the pH was found to be around 6.09, rather than neutral. This was understood to be unsuitable for cell culture experiments. The concentration of GdL used was then adjusted, which did lead to a more favourable pH, but also a much more fluid gel not suitable for the intended purpose. However, as the protocol [32] had been shown to be suitable for cell culturing previously, despite the observed pH being low, by a number of different groups [56, 57], this protocol was taken forward and used in further experiments.

Assays, initially investigating the gels with no added polymer/peptide compound, were performed to determine the state and positioning of the cells with NucBlue staining, which binds to DNA and which stains nuclei. Imaging of cells in the gel in general proved to be difficult, due in part to the different planes of cells throughout the gel. Comparisons between a control (cells grown in media without gel present), gel made up in PBS, and gel made up in media after being left for 24 hours are shown in figure 7. The figures show a clear difference in cell confluence between the control in media, and the two gel samples, with the two samples leading to a much lower cell count versus the control. There is also a difference between the two gels, with PBS having a larger number cell count than the media gel.

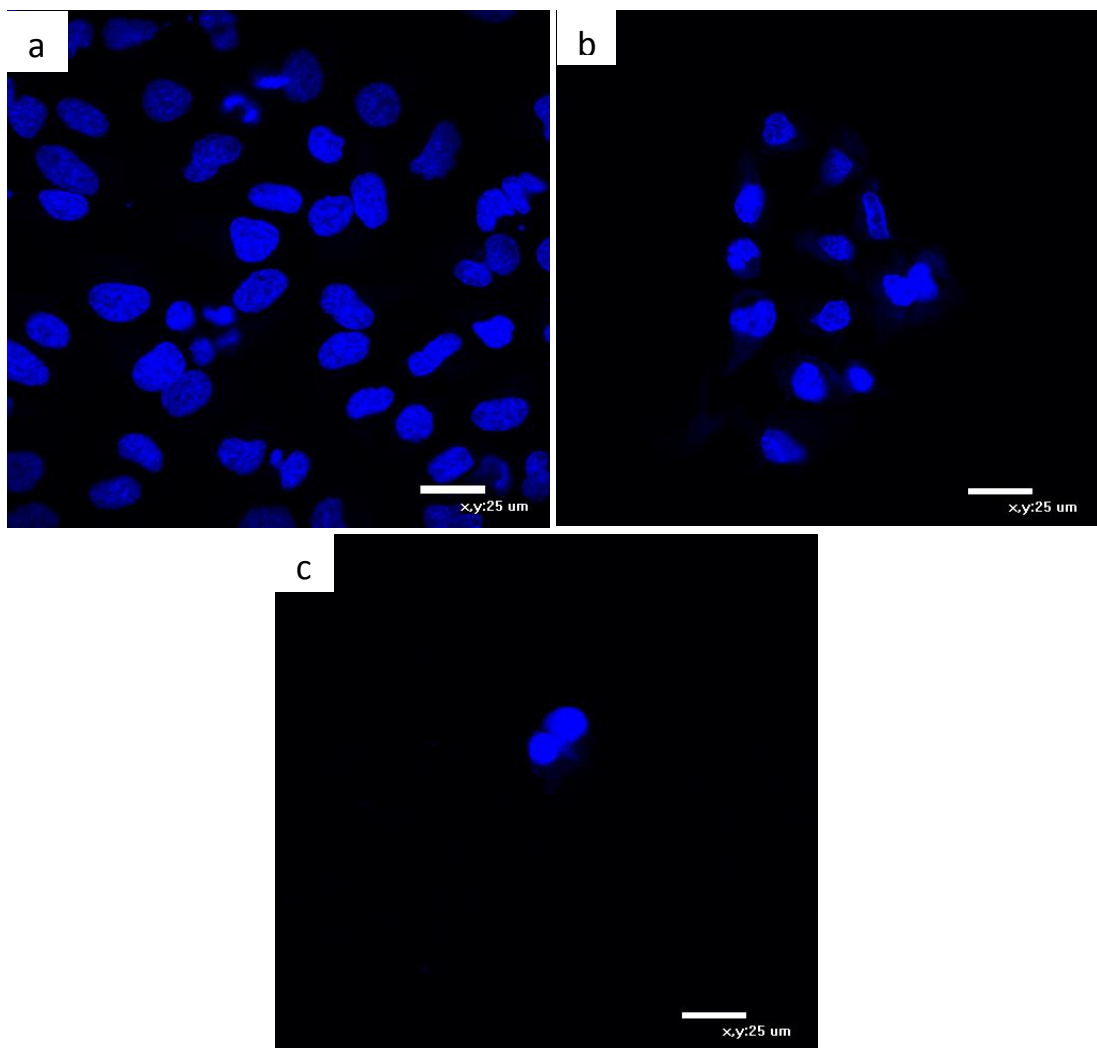


Figure 7 Cells incubated for 24 hours, then with NucBlue staining added. a) As a control, b) with PBS-based hydrogel, c) media-based hydrogel.

After this relatively successful result, the alginate gel made up in PBS was chosen to be used in subsequent experiments. In order to conserve compound stock, only one of the peptide-polymer conjugates was tested initially. Tyr₅-PEO6k-Tyr₅ was chosen and introduced into the PBS gel in the next portion of experiments along with cells at a final concentration of 1 wt%. The results are shown in figure 8 with a control of cells in media compared with cells in gel with and without Tyr₅-PEO6k-Tyr₅. The results show an aggregation of cells in both of the gel samples, compared with the confluence of cells seen in the control sample. However, the

compound caused the gel to become lumpy and fluid when compared with the PBS gel without the compound, shown in the photographs of figure 9. Due to time constraints and lack of polymer/peptide samples, this study had to be left incomplete.

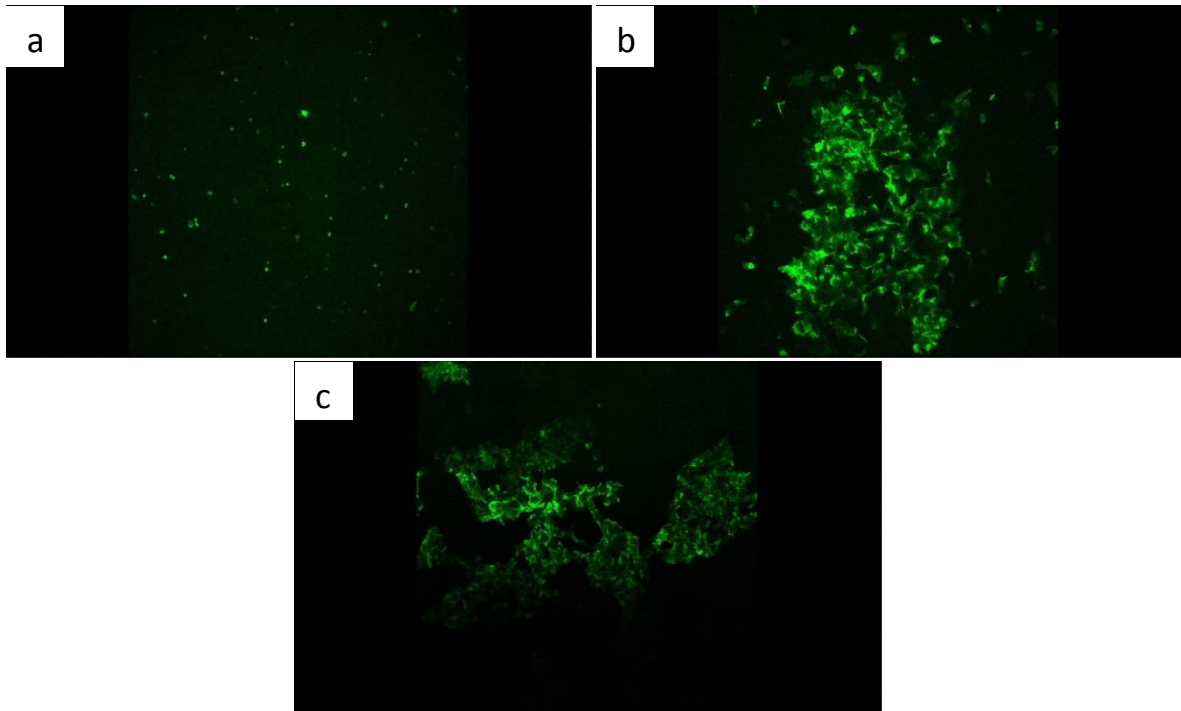


Figure 8 Cells incubated for 24 hours, then with ActinGreen staining added. Images taken 24 hours after gels added/not added. a) is a control, b) with PBS-based hydrogel, c) PBS-based hydrogel + 1 wt% Tyr₅-PEO6k-Tyr₅.

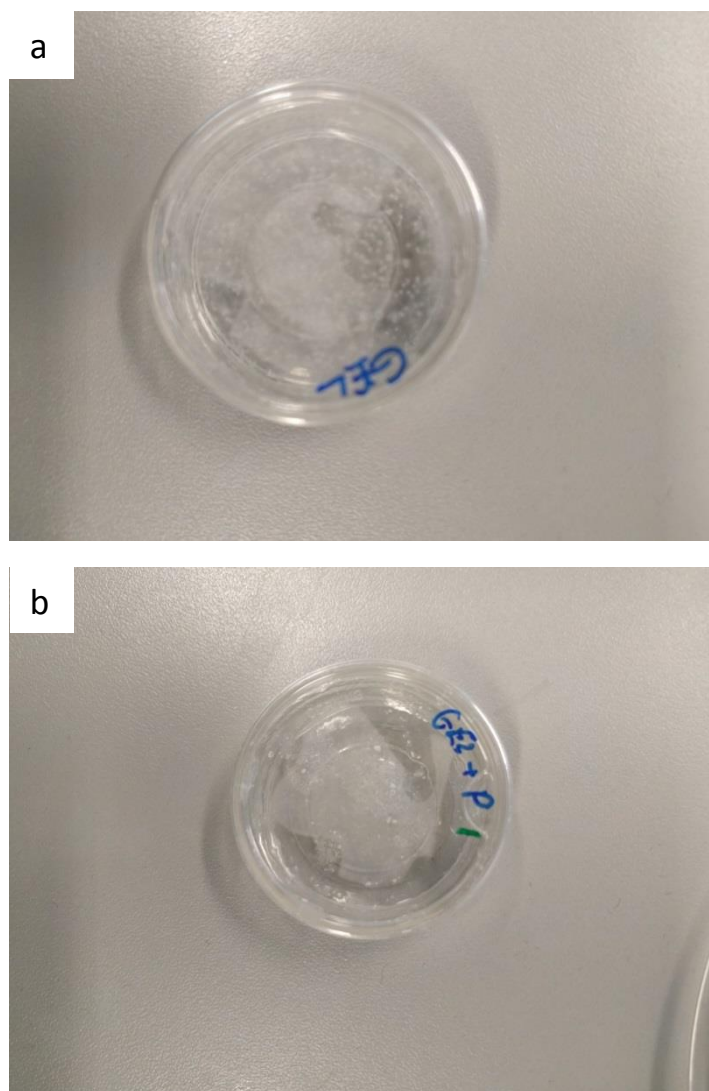


Figure 9 Photographs of a) gel, and b) gel + 1 wt% Tyr₅-PEO6k-Tyr₅

In this chapter, the self-assembling properties of three different custom-synthesised triblock copolymers consisting of oligotyrosine end-caps and hydrophilic centre blocks were investigated. All three were shown to form fibrils, and the influence of tyrosine on self-assembly was shown by the presence of even a short sequence containing only three tyrosines causing the formation of fibrils. There are some interesting observations of the differences between the three compounds. The polyalanine sample was shown to form very tightly-packed β -sheets when compared with the PEO samples. During early sample preparation it was found that the Tyr₅-PEO6k-Tyr₅ sample, in contrast to the Tyr₅-PEO2k-Tyr₅ sample, did not

need water alkalised to pH 12 in order for it to dissolve. The Tyr₅-PEO6k-Tyr₅ sample also formed incredibly straight fibers, in contrast to the more worm-like fibers of Tyr₅-PEO2k-Tyr₅, and exhibited PEO crystallinity unlike the semi-crystallinity observed for Tyr₅-PEO2k-Tyr₅. Unfortunately due to time constraints, the cytocompatibility of the compounds was not able to be investigated. This remains an interesting area for research owing to the role tyrosine plays in affecting cellular signalling etc., and the added effects PEO polymers bound to peptides can have, described in the introduction.

7.4 References

- [1] K. Heredia and H. Maynard, "Synthesis of protein-polymer conjugates," *Organic & Biomolecular Chemistry*, vol. 5, no. 1, pp. 45-53, 2007.
- [2] L. Canalle, D. Lowik and J. van Hest, "Polypeptide-polymer bioconjugates," *Chemical Society Reviews*, vol. 39, pp. 329-353, 2010.
- [3] P. Calceti and F. Veronese, "Pharmacokinetic and biodistribution properties of poly(ethylene glycol)-protein conjugates," *Advanced Drug Delivery Reviews*, vol. 55, no. 10, pp. 1261-1277, 2003.
- [4] A. Rosler, G. Vandermeulen and H. Klok, "Advanced drug delivery devices via self-assembly of amphiphilic block copolymers," *Advanced Drug Delivery Reviews*, vol. 53, no. 1, pp. 95-108, 2001.
- [5] J. Nicolas, G. Mantovani and D. Haddleton, "Living radical polymerization as a tool for the synthesis of polymer-protein/peptide bioconjugates," *Macromolecular Rapid Communications*, vol. 28, no. 10, pp. 1083-1111, 2007.
- [6] P. Bailon and W. Berthold, "Polyethylene glycol-conjugated pharmaceutical proteins," *Pharmaceutical Science & Technology Today*, vol. 1, no. 8, pp. 352-356, 1998.
- [7] W. Wimley and S. White, "Experimentally determined hydrophobicity scale for proteins at membrane interfaces," *Nature Structural Biology*, vol. 3, no. 10, pp. 842-848, 1996.
- [8] T. Hessa, H. Kim, K. Bihlmaier, C. Lundin, J. Boekel, H. Andersson, I. Nilsson, S. White and G. von Heijne, "Recognition of transmembrane helices by the endoplasmic reticulum translocon," *Nature*, vol. 433, no. 7024, pp. 377-381, 2005.
- [9] J. Kyte and R. Doolittle, "A simple method for displaying the hydropathic character of a protein," *Journal of Molecular Biology*, vol. 157, no. 1, pp. 105-132, 1982.
- [10] C. Moon and K. Fleming, "Side-chain hydrophobicity scale derived from transmembrane protein folding into lipid bilayers," *Proceedings of the National Academy of Sciences of the United States of America*, vol. 108, no. 25, pp. 10174-10177, 2011.
- [11] S. White and W. Wimley, "Membrane protein folding and stability: physical principles," *Annual Review of Biophysics and Biomolecular Structures*, vol. 28, pp. 319-365, 1999.
- [12] K. Taylor and H. Naser-El-Din, "Water-soluble hydrophobically associating polymers for improved oil recovery: A literature review," *Journal of Petroleum Science and Engineering*, vol. 19, no. 3-4, pp. 265-280, 1998.
- [13] C. Chassenieux, T. Nicolai and L. Benyahia, "Rheology of associative polymer solutions," *Current Opinion in Colloid & Interface Science*, vol. 16, no. 1, pp. 18-26, 2011.
- [14] E. Larraneta and J. Isasi, "Phase behavior of reverse poloxamers and poloxamines in water," *Langmuir*, vol. 29, no. 4, pp. 1045-1053, 2013.

- [15] A. McNaught and A. Wilkinson, "IUPAC," in *Compendium of Chemical Terminology, 2nd ed. (the "Gold Book")*, Oxford, Blackwell Scientific Publications, 1997.
- [16] I. Hamley, *Block Copolymers in Solution*, Chichester: Wiley, 2005.
- [17] I. Hamley, G. Cheng and V. Castelletto, "A thermoresponsive hydrogel based on telechelic PEG end-capped with hydrophobic dipeptides," *Macromolecular Bioscience*, vol. 11, no. 8, pp. 1068-1078, 2011.
- [18] K. Julich-Gruner, A. Neffe and A. Lendlein, "Synthesis and characterization of oligo(ethylene glycol)s functionalized with desaminotyrosine or desaminotyrosyltyrosine," *Journal of Applied Biomaterials & Functional Materials*, vol. 10, no. 3, pp. 170-176, 2012.
- [19] S. Hua, Y. Li, Y. Liu, W. Xiao, C. Li, F. Huang, X. Zhang and R. Zhuo, "Self-assembled micelles based on PEG-polypeptide hybrid copolymers for drug delivery," *Macromolecular Rapid Communications*, vol. 31, no. 1, pp. 81-86, 2010.
- [20] D. Adams and P. Topham, "Peptide conjugate hydrogelators," *Soft Matter*, vol. 6, pp. 3707-3721, 2010.
- [21] J. Shu, B. Panganiban and T. Xu, "Peptide-polymer conjugates: from fundamental science to application," *Annual Review of Physical Chemistry*, vol. 64, pp. 631-657, 2013.
- [22] A. Sodhi, D. Campbell and P. Topham, "Polymer-peptide conjugate hydrogels; towards controlled drug delivery," *Chiang Mai Journal of Science*, vol. 39, no. 3, pp. 351-372, 2012.
- [23] M. Lutolf and J. Hubbell, "Synthetic biomaterials as instructive extracellular microenvironments for morphogenesis in tissue engineering," *Nature Biotechnology*, vol. 23, no. 1, pp. 47-55, 2005.
- [24] Y. Nagai, L. Unsworth, S. Koutsopoulos and S. Zhang, "Slow release of molecules in self-assembling peptide nanofiber scaffold," *Journal of Controlled Release*, vol. 115, no. 1, pp. 18-25, 2006.
- [25] A. Augst, H. Kong and D. Mooney, "Alginate hydrogels as biomaterials," *Macromolecular Bioscience*, vol. 6, no. 8, pp. 623-633, 2006.
- [26] K. Lee and D. Mooney, "Alginate: properties and biomedical applications," *Progress in Polymer Science*, vol. 37, no. 1, pp. 106-126, 2012.
- [27] T. Andersen, P. Auk-Emblem and M. Dornish, "3D Cell Culture in Alginate Hydrogels," *Microarrays*, vol. 4, no. 2, pp. 133-161, 2015.
- [28] G. Palazzolo, N. Broguiere, O. Cenciarelli, H. Dermutz and M. Zenobi-Wong, "Ultrasoft alginate hydrogels support long-term three-dimensional functional neuronal networks," *Tissue Engineering. Part A.*, vol. 21, no. 15-16, pp. 2177-2185, 2015.
- [29] M. Lemmon and J. Schlessinger, "Cell signaling by receptor tyrosine kinases," *Cell*, vol. 141, no. 7, pp. 1117-1134, 2010.
- [30] S. Kirkham, V. Castelletto, I. Hamley, M. Reza, J. Ruokolainen, D. Hermida-Merino, P. Bilalis and H. Iatrou, "Self-Assembly of Telechelic Tyrosine End-Capped PEO and

- Poly(alanine) Polymers in Aqueous Solution," *Biomacromolecules*, vol. 17, no. 3, pp. 1186-1197, 2016.
- [31] T. Creighton, *Proteins: Structures and Molecular Properties*, New York: W.H.Freeman, 1993.
- [32] J. Jang, Y. Seol, H. Kim, J. Kundu, S. Kim and D. Cho, "Effects of alginate hydrogel cross-linking density on mechanical and biological behaviors for tissue engineering," *Journal of the Mechanical Behaviour of Biomedical Materials*, vol. 37, pp. 69-77, 2014.
- [33] C. Toniolo, F. Formaggio and R. Woody, "Electronic Circular Dichroism of Peptides," in *Comprehensive Chiroptical Spectroscopy: Applications in Stereochemical Analysis of Synthetic Compounds, Natural Products, and Biomolecules, Volume 2*, New York, Wiley-Blackwell, 2012.
- [34] B. Norden, A. Rodger and T. Dafforn, *Linear Dichroism and Circular Dichroism: A Textbook on Polarized-Light Spectroscopy*, Royal Society of Chemistry, 2010.
- [35] I. Hamley, V. Castelletto, C. Moulton, D. Myatt, G. Siligardi, C. Oliveira, J. Pederson, I. Abutbul and D. Danino, "Self-assembly of a modified amyloid peptide fragment: pH-responsiveness and nematic phase formation," *Macromolecular Bioscience*, vol. 10, no. 1, pp. 40-48, 2010.
- [36] G. Siligardi, M. Campbell, W. Gibbons and A. Drake, "Conformational analysis of the melanin-concentrating hormone core by circular dichroic spectroscopy. Disulphide bridge and tyrosine contributions," *European Journal of Biochemistry*, vol. 206, no. 1, pp. 23-29, 1992.
- [37] D. Brown, M. Campbell, R. Kinsman, P. White, C. Moss, D. Osguthorpe, P. Paul and B. Baker, "Melanin-concentrating hormone: a structural and conformational study based on synthesis, biological activity, high-field NMR, and molecular modeling techniques," *Biopolymers*, vol. 29, no. 3, pp. 609-622, 1990.
- [38] A. Adochitei and G. Drochioiu, "Rapid characterization of peptide secondary structure by FTIR spectroscopy," *Academia Romana*, vol. 56, no. 8, pp. 783-791, 2011.
- [39] I. Hamley, A. Dehsorkhi, V. Castelletto, J. Seitsonen, J. Ruokolainen and H. Iatrou, "Self-assembly of a model amphiphilic oligopeptide incorporating an arginine headgroup," *Soft Matter*, vol. 9, no. 19, pp. 4794-4801, 2013.
- [40] I. Hamley, "Peptide fibrillisation," *Angewandte Chemie*, vol. 46, no. 43, pp. 8128-8147, 2007.
- [41] I. Hamley, S. Kirkham, R. Kowalczyk, V. Castelletto, M. Reza and J. Ruokolainen, "Self-assembly of the anti-fungal polyene amphotericin B into giant helically-twisted nanotapes," *Chemical Communications*, vol. 51, no. 100, pp. 17680-17683, 2015.
- [42] L. Bellamy, *The Infrared Spectra of Complex Molecules*, London: Springer Netherlands, 1980.
- [43] A. Dehsorkhi, V. Castelletto, I. Hamley and P. Harris, "Multiple hydrogen bonds induce formation of nanoparticles with internal microemulsion structure by an amphiphilic

- copolymer," *Soft Matter*, vol. 7, no. 21, pp. 10116-10121, 2011.
- [44] I. Hamley, A. Dehsorkhi and V. Castelletto, "Self-assembled arginine-coated peptide nanosheets in water," *Chemical Communications*, vol. 49, no. 18, pp. 1850-1852, 2013.
- [45] D. Middleton, J. Madine, V. Castelletto and I. Hamley, "Insights into the Molecular Architecture of a Peptide Nanotube Using FTIR and Solid-State NMR Spectroscopic Measurements on an Aligned Sample," *Angewandte Chemie*, vol. 52, no. 40, pp. 10537-10540, 2013.
- [46] I. Hamley, S. Kirkham, A. Dehsorkhi and V. Castelletto, "Self-assembly of a model peptide incorporating a hexa-histidine sequence attached to an oligo-alanine sequence, and binding to gold NTA/nickel nanoparticles," *Biomacromolecules*, vol. 15, no. 9, pp. 3412-3420, 2014.
- [47] L. Serpell, "Alzheimer's amyloid fibrils: structure and assembly," *Biochimica et Biophysica Acta*, vol. 1502, no. 1, pp. 16-30, 2000.
- [48] Y. Takahashi and H. Tadokoro, "Structural studies of polyethers, $-(\text{CH}_2)_m\text{-O-})_n\text{-X}$. Crystal structure of poly(ethylene oxide)," *Macromolecules*, vol. 6, pp. 672-675, 1973.
- [49] I. Hamley and M. Krysmann, "Effect of PEG crystallization on the self-assembly of PEG/peptide copolymers containing amyloid peptide fragments," *Langmuir*, vol. 24, no. 15, pp. 8210-8214, 2008.
- [50] M. Krysmann, S. Funari, E. Canetta and I. Hamley, "The effect of PEG crystallization on the morphology of PEG/peptide block copolymers containing amyloid beta-peptide fragments," *Macromolecular Chemistry and Physics*, vol. 209, no. 9, pp. 883-889, 2008.
- [51] V. Castelletto, G. Newby, Z. Zhu, I. Hamley and L. Noirez, "Self-assembly of PEGylated peptide conjugates containing a modified amyloid beta-peptide fragment," *Langmuir*, vol. 26, no. 12, pp. 9986-9996, 2010.
- [52] V. Castelletto and I. Hamley, "Self assembly of a model amphiphilic phenylalanine peptide/polyethylene glycol block copolymer in aqueous solution," *Biophysical Chemistry*, vol. 141, no. 2-3, pp. 169-174, 2009.
- [53] N. Tzokova, C. Fernyhought, M. Butler, S. Armes, A. Ryan, P. Topham and D. Adams, "The effect of PEO length on the self-assembly of poly(ethylene oxide)-tetrapeptide conjugates prepared by "click" chemistry," *Langmuir*, vol. 25, no. 18, pp. 11082-11089, 2009.
- [54] M. Pilkington-Miksa, S. Sarkar, M. Writer, S. Barker, P. Shamlou, S. Hart, H. Hailes and A. Tabor, "Synthesis of bifunctional integrin-binding peptides containing PEG spacers of defined length for non-viral gene delivery," *European Journal of Organic Chemistry*, vol. 2008, no. 17, pp. 2900-2914, 2008.
- [55] F. Dekker, N. de Mol, J. van Ameijde, M. Fischer, R. Ruijtenbeek, F. Redegeld and R. Liskamp, "Replacement of the intervening amino acid sequence of a Syk-binding diphosphopeptide by a nonpeptide spacer with preservation of high affinity," *Chembiochem*, vol. 3, no. 2-3, pp. 238-242, 2002.

- [56] A. Travan, F. Scognamiglio, M. Borgogna, E. Marsich, I. Donati, L. Tarusha, M. Grassi and S. Paoletti, "Hyaluronan delivery by polymer demixing in polysaccharide-based hydrogels and membranes for biomedical applications," *Carbohydrate Polymers*, vol. 150, no. 5, pp. 408-418, 2016.
- [57] F. You, X. Wu, N. Zhu, M. Lei, B. Eames and X. Chen, "3D printing of porous cell-laden hydrogel constructs for potential applications in cartilage tissue engineering," *ACS Biomaterials Science and Engineering*, vol. 2, no. 7, pp. 1200-1210, 2016.

Chapter 8 - General conclusions and future work

Throughout these six chapters, the self-assembly properties of a range of compounds has been investigated, including commercially available antimicrobial and antifungal compounds, TLR-agonists, and novel, custom-synthesised peptide-based molecules.

In chapter 2, three different TLR agonist lipopeptides were investigated consisting of a peptide sequence, CSK₄, with one, two, or three attached palmitoyl chains. It was found that the self-assembly properties were similar when one and two lipid chains were attached; showing disordered secondary structure which wasn't modified by temperature change, and spherical micelle formation. This contrasted with the three lipid chain Pam₃CSK₄, which showed β -sheet secondary structure partially reversibly transitioning into disordered conformation upon heating, along with worm-like micelle formation. Differences between the three were also noted in terms of the cac values, which decreased with increasing lipid chain number. These differences in self-assembly based on number of attached lipid chains may relate to bioactivity.

Future work could investigate whether there is any interaction of the self-assembled structures with the TLRs, and the mechanism by which this occurs if so. This would likely involve a ligand binding assay to firstly detect the quantity of binding at the concentration used in this work at which these nanostructures form. When the Pam_nCSK₄ are bound to the TLRs, microscopy using labelling techniques may be able to shed more light on the nature of the interaction of the nanostructures with the receptors, if indeed there is any.

The work in chapter 2 influenced the research in chapter 3, which investigated the self-assembly and effect the attached lipid chains had on another TLR agonist; MALP-2. Here, the differences between the self-assembly of MALP-2 and its constituent peptide

(GNNDESNISFKEK) were investigated. There were notable differences in cryo-TEM images, where twisted tapes were seen with the peptide, contrasted with more organised raft-like structures of MALP-2, which appeared to be composed of laterally bound tape-like fibers. These raft-like structures are interesting as they have not been reported before for lipopeptides as far as we are aware. These results clearly show the strong influence lipid chains are able to have on self-assembly, particularly in the case of MALP-2.

One of the questions for the future of this specific research would be to discover the kinetics and mechanisms of the formation of the raft-like structures. The samples used in cryo-TEM experimentation in the chapter were left for several days before being imaged. Therefore imaging at various time points starting from when the compound was first dissolved may give insight into the structure formation steps. It would also be interesting to determine whether the higher concentrations used in this study would affect the bioactivity of the compound, and if so, in what way. Relevant bioassays have already been used to determine the bioactivity at lower concentrations [1, 2].

Chapter 4 consisted of an investigation into a peptide conjugate comprising a dileucine motif attached to a bulky aromatic fluorophore; fluorescein isothiocyanate (FITC). The determination of the cac of the compound was interesting as it was shown to self-assemble above a cac using its own self-fluorescing properties, until a point at which self-quenching occurs. This was believed to be due to the formation of large extended nanosheets, seen through cryo-TEM images, which had not previously been observed for this group of compound. The secondary structure data showed apparent inconsistencies, with FTIR data showing potential β -sheet formation which wasn't seen in the CD data. This could however be explained through formation of the large sheets, or UV absorbance effects. Experimentation of the compound incubated in cell culture showed that it was not cytotoxic, and was readily taken up into cells when compared with FITC on its own. This showed the ability of the

dileucine motif to enable transport into the cells. Further experimentation showed specific localisation in peri-nuclear regions. The mechanism by which FITC-LL is uptaken poses an interesting question for future research, as the dileucine motif seems too short to relate to any transporter sequence.

In chapter 5, the self-assembling properties of a commercial antifungal drug, amphotericin B, were explored. A time-dependent change in secondary structure was shown to occur through a change in CD signal over a 24 hour time period. A novel CD peak was seen at 326 nm in a spectrum not previously observed for this compound. As the concentration used was over the experimentally determined cac, this leads to the belief that aggregated forms of amphotericin B evolve over time to form a different aggregated conformation. Fluorescence-lifetime imaging microscopy (FLIM) experimentation disputed previous reports, including by the Starzyk group [3], that amphotericin B can be present in two different dimer forms; parallel and antiparallel based on observed differing lifetimes. In their work, this was shown through the use of different solvents. The FLIM data in this chapter showed that different lifetimes could be seen by just changing the excitation wavelength. As this was only preliminary data, full conclusions could not be drawn, but it poses questions for future work. A model of the twisted tapes observed for amphotericin B in pH 11/12 solutions has been tentatively proposed by I.W. Hamley in the published paper [4]. A more in-depth study of these novel nanostructures would be interesting for future work, paired with computer simulations, to further characterise them.

Chapter 6 described an investigation into the self-assembly of another commercially available drug; daptomycin, a lipopeptide used against infection by gram-positive bacteria. It had been believed that calcium ions are required in order for self-assembly to occur, which is linked to the mechanism of action of the drug. Cac measurements showed that the compound aggregated at the same concentration whether in the presence of calcium ions or not. Cryo-

TEM images also showed the formation of spherical micelles in the presence and absence of calcium ions. Secondary structure studies were performed, with CD showing no systematic differences in spectra between the different sample conditions. FTIR showed similarities in the 1250-2000 cm^{-1} region, but differences in peak intensity relating to $-\text{OH}$ stretch vibrations, potentially explained through increased H-bond stabilisation in the presence of higher calcium ions. These results together suggest that daptomycin self-assembly does not require the presence of calcium ions.

The final chapter, chapter 7, concerned three different custom-synthesised compounds containing a repeating hydrophilic centre block (either PEO or poly alanine), with short hydrophobic tyrosine end-caps. The self-assembly of the compounds was investigated using the methods employed in the other chapters. All three compounds ($\text{Tyr}_3\text{-PAla-Tyr}_3$, $\text{Tyr}_5\text{-PEO}2\text{k-Tyr}_5$ and $\text{Tyr}_5\text{-PEO}6\text{k-Tyr}_5$) were shown to form fibrils through cryo-TEM, although the $\text{Tyr}_5\text{-PEO}6\text{k-Tyr}_5$ sample differed from the other two, forming very straight fibers compared with worm-like micelles. All samples showed some β -sheet formation, and in the case of the poly alanine compound, very tightly-packed β -sheets. These tightly packed sheets were also shown through XRD, which showed little or no PEO crystallinity in the case of the PEO2k sample, and a high degree of crystallinity in the PEO6k sample. In addition to the self-assembling properties, some preliminary experiments were also conducted into the cytocompatibility of the compounds. As the compounds were shown to be unable to form into gels at high concentrations, they were incorporated into an alginate-based hydrogel. Due to time constraints and lack of compound, these experiments remained incomplete and inconclusive.

Future work would involve continuing on with cytocompatibility tests of the compounds when introduced into alginate gels, or potentially other gels. The addition of adhesion motifs (RGD) in order to increase the binding and growth of cells in the gel would alleviate some of the

difficulties experienced in the chapter. Tyrosine reactivity of the end caps of these compounds was not a focus of this work, but could pose questions for future studies. Tyrosine residues can for example be induced through kinases, which are important reactions in cell signalling. It would also be interesting to attempt to induce gelation of the compounds through alteration of pH.

8.1 References

- [1] P. Muhlradt, M. Kiess, H. Meyer, R. Sussmuth and G. Jung, "Isolation, structure elucidation, and synthesis of a macrophage stimulatory lipopeptide from *Mycoplasma fermentans* acting at picomolar concentration," *Journal of Experimental Medicine*, vol. 185, no. 11, pp. 1951-1958, 1997.
- [2] M. Morr, O. Takeuchi, S. Akira, M. Simon and P. Muhlradt, "Differential recognition of structural details of bacterial lipopeptides by toll-like receptors," *European Journal of Immunology*, vol. 32, no. 12, pp. 3337-3347, 2002.
- [3] J. Starzyk, M. Gruszecki, K. Tutaj, R. Luchowski, R. Szlajak, P. Wasko, W. Grudzinski, J. Czub and W. Gruszecki, "Self-association of amphotericin B: spontaneous formation of molecular structures responsible for the toxic side effects of the antibiotic," *The Journal of Physical Chemistry B*, vol. 118, no. 48, pp. 13821-13832, 2014.
- [4] I. Hamley, S. Kirkham, R. Kowalczyk, V. Castelletto, M. Reza and J. Ruokolainen, "Self-assembly of the anti-fungal polyene amphotericin B into giant helically-twisted nanotapes," *Chemical Communications*, vol. 51, no. 100, pp. 17680-17683, 2015.
- [5] M. Jin, S. Kim, J. Heo, M. Lee, H. Kim, S. Paik, H. Lee and J. Lee, "Crystal structure of the TLR1-TLR2 heterodimer induced by binding of a tri-acylated lipopeptide," *Cell*, vol. 130, no. 6, pp. 1071-1082, 2007.

List of publications

I.W. Hamley, **S. Kirkham**, A. Dehsorkhi, V. Castelletto, J. Adamcik, R. Mezzenga, J. Ruokolainen, C. Mazzuca, E. Gatto, M. Venanzi, E. Placidi, P. Bilalis, H. Iatrou (2014). Self-assembly of a model peptide incorporating a hexa-histidine sequence attached to an oligo-alanine sequence, and binding to gold NTA/nickel nanoparticles. *Biomacromolecules*, 15 (9), 3412-3420.

I.W. Hamley, **S. Kirkham**, A. Dehsorkhi, V. Castelletto, M. Reza, J. Ruokolainen (2014). Toll-like receptor agonist lipopeptides self-assemble into distinct nanostructures. *Chemical Communications*, 50 (100), 15948-15951.

I.W. Hamley, **S. Kirkham**, R.M. Kowalczyk, V. Castelletto, M. Reza, J. Ruokolainen (2015). Self-assembly of the anti-fungal polyene amphotericin B into giant helically-twisted nanotapes. *Chemical Communications*, 51 (100), 17680-17683.

S. Kirkham, I.W. Hamley, A.M. Smith, R.M. Gouveia, C.J. Connon, M. Reza, J. Ruokolainen (2016). A self-assembling fluorescent dipeptide conjugate for cell labelling. *Colloids and Surfaces. B, Biointerfaces*, 137, 104-108.

V. Castelletto, **S. Kirkham**, I.W. Hamley, R. Kowalczyk, M. Rabe, M. Reza, J. Ruokolainen (2016). Self-Assembly of the Toll-Like Receptor Agonist Macrophage-Activating Lipopeptide MALP-2 and of Its Constituent Peptide. *Biomacromolecules*, 17 (2), 631-640.

S. Kirkham, V. Castelletto, I.W. Hamley, M. Reza, J. Ruokolainen, D. Hermida-Merino, P. Bilalis, H. Iatrou (2016). Self-Assembly of Telechelic Tyrosine End-Capped PEO and Poly(alanine) Polymers in Aqueous Solution. *Biomacromolecules*, 17 (3), 1186-1197.

S. Kirkham, V. Castelletto, I.W. Hamley, K. Inoue, R. Rambo, M. Reza, J. Ruokolainen (2016). Self-Assembly of the Cyclic Lipopeptide Daptomycin: Spherical Micelle Formation Does Not Depend on the Presence of Calcium Chloride. *Chemphyschem*, 17 (14), 2118-2122.

I.W. Hamley, J. Hutchinson, **S. Kirkham**, V. Castelletto, A. Kaur, M. Reza, J. Ruokolainen (2016). Nanosheet Formation by an Anionic Surfactant-like Peptide and Modulation of Self-Assembly through Ionic Complexation. *Langmuir*, 32 (40), 10387-10393.

“Two-component fluorescent semiconducting hydrogel from NDI-appended peptide with long chain amines: Variation of thermal and mechanical strength of gels” – currently under peer-review approval.